Spring 5-2022

A Preventive Medicine Framework for Wearable Abiotic Glucose Detection System

Saikat Banerjee
Old Dominion University, saikat3banerjee@gmail.com

A PREVENTIVE MEDICINE FRAMEWORK FOR WEARABLE ABIOTIC GLUCOSE DETECTION SYSTEM

by

Saikat Banerjee
B.E. August 2016, Nagpur University, India
M.S. August 2019, University of Maryland, Baltimore County

A Dissertation Submitted to the Faculty of
Old Dominion University in Partial Fulfillment of the
Requirements for the Degree of

DOCTOR OF PHILOSOPHY

ENGINEERING - ELECTRICAL AND COMPUTER

OLD DOMINION UNIVERSITY
May 2022

Approved by:

Gymama Slaughter (Director)

Chungsheng Xin (Member)

Barbara Hargrave (Member)

Nancy Xu (Member)

ABSTRACT

A PREVENTIVE MEDICINE FRAMEWORK FOR WEARABLE ABIOTIC GLUCOSE DETECTION SYSTEM

Saikat Banerjee
Old Dominion University, 2022
Director: Dr. Gymama Slaughter

In this work, we present a novel abiotic glucose fuel cell with battery-less remote access. In the presence of a glucose analyte, we characterized the power generation and biosensing capabilities. This system is developed on a flexible substrate in bacterial nanocellulose with gold nanoparticles used as a conductive ink for piezoelectric deposition-based printing. The abiotic glucose fuel cell is constructed using colloidal platinum on gold (Au-co-Pt) and a composite of silver oxide nanoparticles and carbon nanotubes as the anodic and cathodic materials. At a concentration of 20 mM glucose, the glucose fuel cell produced a maximum open circuit voltage of 0.57 V and supplied a maximum short circuit current density of 0.581 mA/cm^2 with a peak power density of 0.087 mW/cm^2. The system was characterized by testing its performance using electrochemical techniques like linear sweep voltammetry, cyclic voltammetry, chronoamperometry in the presence of various glucose level at the physiological temperatures. An open circuit voltage (Voc) of 0.43 V, short circuit current density (Isc) of 0.405 mA/cm^2, and maximum power density (Pmax) of 0.055 mW/cm^2 at 0.23 V were achieved in the presence of 5 mM physiologic glucose. The results indicate that glucose fuel cells can be employed for the development of a self-powered glucose sensor. The glucose monitoring device demonstrated sensitivity of 1.87 $uA/mM\text{-}cm^2$ and a linear dynamic range of 1 mM to 45 mM with a correlation coefficient of 0.989 when utilized as a self-powered glucose sensor. For wireless communication, the incoming voltage from the abiotic fuel cell was fed to a low power microcontroller that enables battery-less communication using NFC technology. The voltage translates to the NFC module as the

digital signals, which are displayed on a custom-built android application. The digital signals are converted to respective glucose concentration using a correlation algorithm that allows data to be processed and recorded for further analysis. The android application is designed to record the time, date stamp, and other independent features (e.g. age, height, weight) with the glucose measurement to allow the end-user to keep track of their glucose levels regularly. Analytics based on in-vitro testing were conducted to build a machine learning model that enables future glucose prediction for 15, 30 or 60 minutes.

This thesis is dedicated to my parents Pinaki and Sadhana Banerjee, and my sister Swaralipi.

ACKNOWLEDGMENTS

I would like to thank my esteemed advisor, Dr. Gymama Slaughter for her invaluable supervision, support, and tutelage during the course of my PhD degree. My gratitude extends to her immense knowledge and extensive experience that have encouraged me in all the time of my academic research and daily life. Additionally, I would like to express gratitude to Dr. Meimei Lai, Dr. Thakshila Lingaye, Dr. Faruk Hossain and Dr. Ahmad Qamar for their treasured support which was influential in shaping my experiment methods and critiquing my results. I would also like to thank my committee members Dr. Barbara Hargrave, Dr. Nancy Xu and Dr. Chenshung Xin for their insightful and encouraging comments. My heartiest appreciation goes out to my family; they were the pillars of my academic life that allowed me to pursue my interest and passions. This dissertation is my letter of love and appreciation towards my family for their sacrifices and constant support. Also, I would like to thank my friends Harshita Batra, Ankit Baingane, Kunal Bendey, Prasad Akmar, Priyanka Annamalai, Jayashree Yalamanchili and lab mates Yash Patel, Mathew Nguyen, Stephanie McCracken, for a cherished time spent together in the lab and in social settings.

TABLE OF CONTENTS

Page

Chapter Page

LIST OF TABLES

LIST OF FIGURES

Figure Page

Figure Page

CHAPTER I

INTRODUCTION

Background

Diabetes is a dangerous disorder caused by the body's inability to manage the amount of sugar in the bloodstream. The human body's tissues and cells require sustenance to survive. The nourishment that cells consume is a form of sugar known as glucose. Without sufficient glucose, the body's cells would eventually perish. Humans consume food, and as part of the natural digestive process, the food is converted into glucose [1].

Glucose enters the bloodstream, thereby raising the quantity of dissolved glucose in the blood. The dissolved glucose is subsequently carried by the bloodstream to the body's numerous tissues and cells. The amount and kind of meals consumed influence the levels of glucose in the bloodstream at any given time. Refined carbs, candies, and sweets are simple to convert to glucose [2]. As a result, blood glucose levels rise fast after eating such items. In contrast, blood sugar levels increase gradually and steadily after consuming more complex, unprocessed carbs (oatmeal, apples, baked potatoes, etc.) that need more digestive processes before glucose can be produced. When blood glucose levels get too high, diabetes or prediabetes can develop [3]. Having too much glucose in the blood might lead to health concerns over time.

According to the WHO's 10 November 2021 report, diabetes mellitus was the cause of 1.5 million fatalities in 2019. Before the age of 70, the existence of high blood sugar was responsible for about half of all fatalities. According to the WHO, diabetes was the tenth biggest cause of death in 2019 [4]. In the United States, 34.2 million individuals of all ages – roughly one in ten – have diabetes, while 7.3 million adults aged 18 and older (almost one in

5) are unaware that they have diabetes (just under 3 percent of all U.S. adults). The number of people who are diagnosed with diabetes increases with age. More than 26% of adults aged 65 and older (about 1 in 4) have diabetes [4]. Diabetes affects an increasing number of people as they become older. Major issues with blood vessels, the heart, nerves, kidneys, the mouth and feet develop over time. These issues may necessitate the amputation of a limb. Diabetes's most significant complication is heart disease [5]. Diabetes makes a person more than twice as likely as a non-diabetic to experience heart disease or a stroke. Diabetes might cause a person to miss out on the common signs and symptoms of a heart attack. Diabetes is divided into three types: type 1, type 2, and gestational diabetes.

Type 1 Diabetes.

Type 1 diabetes is an autoimmune illness in which the body's immune system assaults and destroys insulin-producing cells in the pancreas. As a result, the affected individual is unable to generate insulin naturally. Type 1 diabetes, often known as juvenile diabetes, frequently develops in childhood. It is rather uncommon, accounting for just around 5% of all diabetes cases. It would be a fatal condition if it weren't for the fact that insulin manufactured outside the body can be manually administered to replace what the body lacks [2,3]. Although type 1 diabetes is also known as Insulin Dependent Diabetes Mellitus, the term ‘insulin dependent’ is a misnomer because both type 1 and type 2 diabetes can require insulin therapy.

Type 2 Diabetes.

Type 2 diabetes differs from Type 1 diabetes in that it begins with a progressive loss in the body's capacity to respond to insulin (a condition known as "Insulin Resistance") rather

than an abrupt cessation of insulin production. Insulin resistance develops when the body is regularly exposed to high insulin levels in the bloodstream. After a period, the cells no longer respond to insulin as fiercely as they previously did. At this stage, it requires more insulin to deliver the same quantity of glucose to cells.

Gestational Diabetes.

Gestational diabetes occurs in the latter stages of pregnancy, is quite uncommon, and usually resolves with the end of the pregnancy. It is similar to type 2 diabetes. Women who have had gestational diabetes are at a higher risk of having type 2 diabetes later in life.

Diabetes causes vary depending on the kind of diabetes. Type 1 diabetes is an autoimmune illness whose specific origins are unknown at this time. Variables linked with type 1 diabetes risk include genetic susceptibility and exposure to one or more environmental factors, which may include viral exposure [5]. In contrast to the mystery surrounding type 1 diabetes, there are well-established risk factors for type 2 diabetes:

- growing Older - As people get older, they are more likely to acquire type 2 diabetes. While type 2 diabetes can arise at any age, it is far more frequent in those over the age of 40.
- ethnicity and race - Certain ethnic groups are more likely to develop type 2 diabetes than others. African Americans, Native Americans, Hispanic Americans, Pacific Islanders, and Asian Americans are more likely than Caucasians to develop the disease.
- diabetes in the family - Persons who have close blood relatives (siblings or parents) with diabetes are more likely to develop the condition themselves than people who do not have a blood relative with the disease.

• pre-diabetes - Pre-diabetes, often known as "impaired glucose tolerance," is a condition that precedes type 2 diabetes. Blood sugar levels in a pre-diabetic person are higher than usual but not yet as high as required for a diabetes diagnosis.

• a sedentary lifestyle - Persons with sedentary, inactive lifestyles (e.g., working at a desk job and then watching a lot of TV) are more likely to acquire diabetes than persons with more active lifestyles (e.g., who have built regular exercise into their daily routines).

• obesity and Diet - the majority of Type 2 diabetes patients are overweight individuals.

In diabetics and non-diabetics blood glucose levels will increase and decrease normally during the day. For example, after a meal, they will rise, but after activity, they will decline. Blood glucose levels can be low, normal, or elevated. A normal glucose level varies depending on how long someone has had diabetes, their age, and other health issues. The American Diabetes Association, on the other hand, maintains standard blood glucose recommendations for diabetics:

Prior to meals:

- between 80 and 130 mg/dL

1 to 2 hours after meals:

- 180 mg/dL or less

Hypoglycemia, or low blood sugar, is described as having a glucose level of less than 70 mg/dL or slightly higher, and hyperglycemia, or high blood sugar, is defined as having a glucose level of more than 125 mg/dL while fasting (not eating for at least eight hours) [7]. Diabetes is defined as a fasting blood glucose level more than 125 mg/dL, whereas prediabetes is defined as a fasting blood glucose level between 100 mg/dL and 125 mg/dL. While

everyone's blood glucose levels differ, some people are predisposed to hyperglycemia or hypoglycemia. Hyperglycemia is more likely in persons who:

- have a family history of type 2 diabetes;
- are African American, Native American, Hispanic, or Asian American;
- are overweight;
- have high blood pressure or cholesterol;
- have polycystic ovary syndrome; and
- have a history of gestational diabetes (diabetes during pregnancy).

Hypoglycemia, on the other hand, is most frequent among diabetics and occurs quite rarely in persons who do not have the disease. It can occur if diet, exercise, and diabetes medicines are out of balance.

Usual pitfalls for people with diabetes include:

- being more active than normal
- drinking alcohol without eating
- eating late or missing meals
- not balancing meals by incorporating fat, protein, and fiber
- not eating enough carbs
- not timing insulin and carb intake appropriately (for example, waiting too long to eat a meal after taking insulin for the meal)

Hypoglycemia can also occur when a diabetic uses the incorrect insulin, consumes too much of it, or injects it inappropriately.

Continuously testing and documenting blood glucose levels can aid in the monitoring and management of diabetes. If the blood glucose level is too high or too low, the person may require a change in food, physical exercise, or medicine to live a healthy lifestyle. The following are the most generally accessible techniques for a diabetic to monitor and maintain

appropriate blood glucose levels: Continuous Glucose Monitoring (CGM) system, finger prick test using a test strip and a glucometer [8].

Figure 1. Finger prick test for individual with diabetes to monitor and most widely available glucose detection system [8].

As depicted in Figure 1, the finger prick test involves pricking the finger with a lancet and extracting a blood drop with a disposable glucose test strip, which is then inserted in the glucometer to determine the blood glucose level. A glucose specific enzyme, such as glucose oxidase, is used in the disposable test strip. The glucose specific enzyme oxidizes the glucose in the blood, releasing electrons and producing gluconic acid. These released electrons are proportional to the concentration of glucose, which is transformed into varied voltages using analog to digital converters. The level is then shown in mg/dl or mmol/l units by the meter. The test strips used in a glucometer are costly. Manufacturers frequently supply meters for little or no cost in order to generate demand for the profitable test strips. Due to the dynamics of insulin adjustment, people with type 1 diabetes may test up to 10 times per day, although those with type 2 often test less frequently, especially when insulin is not part of the treatment [7,8]. External elements such as humidity, temperature, and altitude also have an impact on these strips. The glucometer must be calibrated for different batches of test strips. Furthermore,

blood glucose readings can vary by as much as 4 mmol/dL or 72 mg/dL, which can be fatal in blood glucose monitoring [7,8,9].

Figure 2. External data recorder with implanted sensor as a continuous glucose monitoring system [9].

Continuous glucose monitoring devices (CGMs) were created to minimize the frequency of finger pricking. As illustrated in Figure 2, CGMs can consist of a disposable sensor inserted beneath the skin, a transmitter attached to the sensor, and a reader that receives and displays the results [10,11]. Before it must be replaced, the sensor can be utilized for many days [11-13]. The proposed wearable device is fueled by an external power source, such as a battery, making the device large. Companies like Medtronic and Dexcom are at the forefront of glucose monitoring research since it is a lucrative market for them. However, the CGM devices produced by both Medtronic and Dexcom have a huge receiver, making them a bulky device that cannot be miniaturized. In addition, for reliable blood glucose readings, the receiver must be calibrated, which takes approximately 2 hours and has a maximum lifetime of just one week [12-13].

Research on wearable healthcare devices has mostly focused on device miniaturization and wireless operation (e.g., Bluetooth and near-field communication (NFC)) [14–15].

Although the wearable device has mostly used Bluetooth technology, its large size and weight may affect wearability [14]. Ali et al. [15] propose an implanted glucose monitoring device using Bluetooth low energy (BLE). Glucose data from the system is transferred over BLE to a PDA (smartphone or Ipad), which displays the data in text form. The technology has some success in lowering the power consumption of an external power unit and an implanted unit. Rasyid et al. [16] presented a wireless body area network-based blood glucose level monitoring system for diabetes detection. A glucometer sensor, an Arduino Uno, and a Zigbee module are used to construct the system. A doctor or caregiver can use a website to remotely check a patient's glucose levels. However, due to the high power consumption of the Arduino Uno board and the Zigbee module, the system is not energy efficient. Mortello et al. [17] used an external transmitter that connects with and charges the sensor wirelessly, and it also has Bluetooth functionality for interacting with a Smartphone application. Over the course of 28 days and six in-clinic appointments, the accuracy of 19 implanted sensors was assessed by comparing CGM glucose levels to venous blood glucose measurements collected every 15 minutes. It is critical to have a closed loop system that is minimally intrusive, versatile, and simple to use, with data that is easily available to end users and service providers. To address this issue, much research has been conducted to make these monitoring devices as non-invasive and compact as feasible and without a battery.

To have a truly battery-less system, a fuel cell with dual functionality of acting as a battery and a sensor is needed. General Electric's Neidrach and Grubb developed the first conventional fuel cell for NASA [16]. Platinum served as a noble metal electrocatalyst in the fuel cell, oxidizing hydrogen and reducing oxygen. Hydrogen oxidation generates protons and electrons, which flow via the external circuit. The generation of electricity is caused by the passage of electrons in the system. When the electron in the system recombines with the oxygen existing in the system, oxygen is reduced at the cathode. Water is produced as a byproduct of

this process. Because of its efficacy in oxidizing hydrogen, a platinum metal catalyst is utilized. Furthermore, hydrogen fuel is prone to carbon contamination, and a constant supply of hydrogen fuel is required to provide electrical power.

A glucose (bio-)fuel cell has been considered as a potential source of power for implanted bioelectronic devices. The fundamental impetus for the substantial study in the field of glucose fuel cell technology is the hunt for a cost-effective alternative sustainable fuel source that can fulfill rising global energy demands, as well as recent breakthroughs in microelectronics [17]. Many researchers are striving to power implantable bioelectronic devices with glucose fuel cells. A conventional fuel cell assembly is made up of an anode, a cathode, and an electrolyte, and it works by converting chemical energy into electrical energy. In a fuel cell, two sorts of processes take place: 1) oxidation and 2) reduction. The entire process is referred to as a redox reaction. The anode undergoes the oxidation reaction, whereas the cathode undergoes the reduction reaction. They are environmentally friendly, biocompatible, small in form factor, and their use as analytical devices has increased because of their capability to serve as diagnostic tools [18–19].

A key advantage of glucose fuel cells is that at ambient temperature and neutral pH conditions, they demonstrate high conversion efficiency and have been demonstrated to generate adequate bioelectricity to power small electronic devices [20]. The two types of commonly developed glucose fuel cells are the enzymatic biofuel cell and the non-enzymatic fuel cell. The enzymatic biofuel cell uses complex enzyme immobilization strategies to immobilize enzymes to the surface of electrode material. The enzyme stability is widely affected by pH and temperature, which can result in enzyme denaturation if the microenvironment conditions are not optimal. To address the current limitations associated with enzymatic glucose biofuel cells, conductive materials such as carbon nanotubes [21,22], metal oxides [23,24], nanostructured materials [25,26], and graphene [27] are being explored

as an alternative sensing material for glucose and molecular oxidation and reduction of oxygen, respectively.

Noble metal nanoparticles such as gold, platinum, and silver have received a lot of attention due to their unique electrocatalytic capabilities [28,29]. When utilized as a sensing material, these nanoparticles have been found to increase direct electron transfer, signal transduction, and sensor efficiency. Platinum nanoparticles (PtNPs) and nanocomposites have been demonstrated to electro-oxidize glucose directly in the absence of enzymes and mediators [30,31]. Nanoparticles, notably colloidal platinum in biofuel cells, have a huge surface area, making them appealing for the creation of glucose sensors [32,33].

Flexible electronics that incorporate tiny components to create analytical devices on conformal substrates are in high demand. Because of its great mechanical strength and flexibility, bacterial nanocellulose (BNC) thin film has attracted interest in biomedical, flexible electronics, separation, and waste purification research [34]. When compared to native cellulose, BNC has transferrable tattoo-like qualities such as strong form preservation, high water-binding capacity, and greater surface area [35,36]. These distinct qualities enable the use of BNC in the production of a variety of goods, including membranes, high-grade paper, speaker diaphragms, diet food, and textiles.

The inclusion of inorganic and/or organic nanomaterials to give antibacterial, optical, electrical, magnetic, and catalytic capabilities for application in biomedical research is the focus of current BNC research [37]. Using screen printing and inkjet printing technologies, BNC might be used as a substrate or sensing material in the creation of transferable tattoo-like biosensors and bioelectronics. These technologies have various benefits over cleanroom microfabrication strategies, including lower processing costs, faster processing rates, less waste creation, and lower contamination [38,39]. Inkjet printing allows for the reliable large-scale fabrication of conductive material arrays. Materials ranging from nanoparticles to proteins that

can be printed using inkjet printers provide a method for mass producing functional components for biofuel cells. Inkjet printing of conductive and non-conductive materials allows for the production of ultra-thin and compact analytical devices, which have the potential to revolutionize wearable and implantable devices in terms of cost, efficiency, and repeatability [40,41,42].

Problem statement

The purpose of this research is to create a unique abiotic continuous glucose monitoring system that can obtain and monitor data wirelessly from anywhere. The created technology will operate without an external battery source and under physiological settings on a flexible substrate. The system is intended to have a wide linear range as well as good sensitivity and selectivity toward the analyte glucose. It can also serve as a power supply for small electrical equipment if necessary. Using an NFC based circuit allows for a battery-less instantaneous reading using a custom-built smartphone application. The collected data will be recorded into the database to monitor glucose levels and enable the user to make lifestyle changes to improve health outcomes. The data can be given to doctors or health care providers to be maintained in a patient's medical record and to determine the appropriate treatment strategy. The constructed system includes a flexible wireless battery-less data access and monitoring system as illustrated in Figure 3.

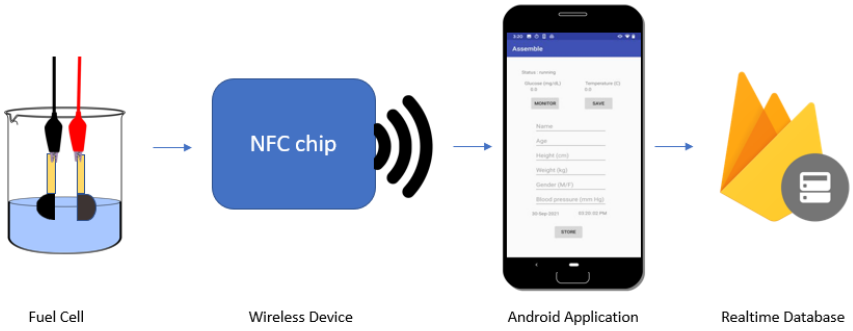

Figure 3. Schematic of a continuous glucose monitoring system with wireless module and application interface.

Dissertation contribution

In this dissertation, we developed a novel abiotic glucose fuel cell consisting of an anode made up of conductive gold nanoparticles ink with electrodeposited colloidal platinum and a cathode made up of a composite of silver oxide nanoparticles and carbon nanotubes on flexible biocompatible bacterial nanocellulose substrate. The morphology of the electrode materials was characterized using scanning electron microscopy (SEM), and the electrochemical characterization was achieved via linear sweep voltammetry (LSV) and cyclic voltammetry (CV). This combination of anodic and cathodic sensing materials enables the direct oxidation of glucose at the anode and reduction of Ag_2O at the cathode to generate bioelectricity. Amperometry was also carried out to further study the performance of the biosensor.

The power output of the biofuel cell is directly proportional to the glucose concentration level. This abiotic fuel can then be used to act as an input for the 13NFC based circuit. The NFC based circuit consist of a low power microcontroller which enables analog to digital

conversion (ADC) of the input signal which is directly proportional to the power produced by a biofuel cell. By incorporating a wireless NFC based circuit, a complete glucose sensing system was realized. An android application was designed, which uses a custom-built algorithm that correlates the input signal from 14-bit ADC values to a glucose concentration. This data is recorded in the application with other independent parameters which then can be stored onto a Realtime database for data processing.

For diabetes management, a machine learning algorithm is developed to provide insight on the future level prediction for the respective user over a period of continuous data collection.

Scope of dissertation

The purpose of chapter 2 is to provide context for the thesis and to expose the reader to the electrical and bioelectrical concepts that regulate the operation of a basic fuel cell and biofuel cells. The chapter also discusses the various electron transfer mechanisms utilized in biofuel cells, which are responsible for current flow in a sensing system.

Chapter 3 focuses on the glucose biosensor. This chapter discusses the many types and generations of glucose biosensors. It also discusses continuous glucose monitoring technologies and current research and development trends.

Chapter 4 focuses on the Near-field communication based wireless circuit and its operating principle. This chapter provides a detailed explanation of the RF430frl152h and general operation.

Chapter 5 describes the custom-built android application for data processing with NFC based modules. This chapter provides insight on the machine learning based analytics used to predict future glucose levels.

Chapter 6 focuses on the different electrochemical characterization methods used.

Chapter 7 focuses on the discussion of the fabricated abiotic glucose sensing system. The manufacturing methods and materials used in the preparation of the bioelectrodes are explained.

Chapter 8 describes all the experimental data, the characterization methods, stabilization studies, and results obtained by the glucose monitoring system.

Chapter 9 summarizes the studies performed. The result and path forward of the novel glucose sensing system are also discussed.

CHAPTER II

FUEL CELL

A fuel cell is an electrochemical device that directly transforms a fuel's chemical energy into electrical energy. This one-step process from chemical to electrical energy as opposed to the multi-step (e.g., from chemical to thermal to mechanical to electrical energy) characteristics involved in combustion-based heat engines, has numerous distinct benefits [43]. Current combustion-based energy generating methods, for example, are extremely damaging to the environment and are primarily contributing to many global issues, such as climate change, ozone layer depletion, acidic rains, and consequently a continual loss in plant cover. Furthermore, these technologies rely on the world's finite and declining supply of fossil fuels. Fuel cells, on the other hand, provide an efficient and clean energy conversion method. Furthermore, fuel cells are compatible with renewable energy sources and contemporary energy carriers (such as hydrogen) for long-term development and energy security. As a result, they are viewed as the future of energy conversion devices. Because fuel cells are static, they operate quietly and without vibration, and their inherent modularity allows for easy assembly and a wide range of applications in portable, fixed, and transportation power production.

A thorough grasp of the operations of fuel cells and the fuel cell industry, are critical for overcoming existing difficulties and advancing fuel cell technology in general [43,44]. Despite this, constructing a fuel cell requires a thorough understanding of electrochemistry, thermodynamics, engineering economics, material science and engineering, and electrical engineering, making this a challenging undertaking. A fuel cell is made up of three active components: a fuel electrode (anode), an oxidant electrode (cathode), and an electrolyte in between. The electrodes are made of a porous substance with a coating of catalyst on top. The

essential operational mechanisms within a typical hydrocarbon cell are depicted in Figure 4. A typical fuel cell functions by transferring hydrogen through the anode and oxygen via the cathode. A catalyst at the anode site separates hydrogen molecules into electrons and protons. Protons travel through the porous electrolyte membrane, while electrons are driven through a circuit, resulting in an electric current and surplus heat. Protons, electrons, and oxygen mix at the cathode to form water molecules.

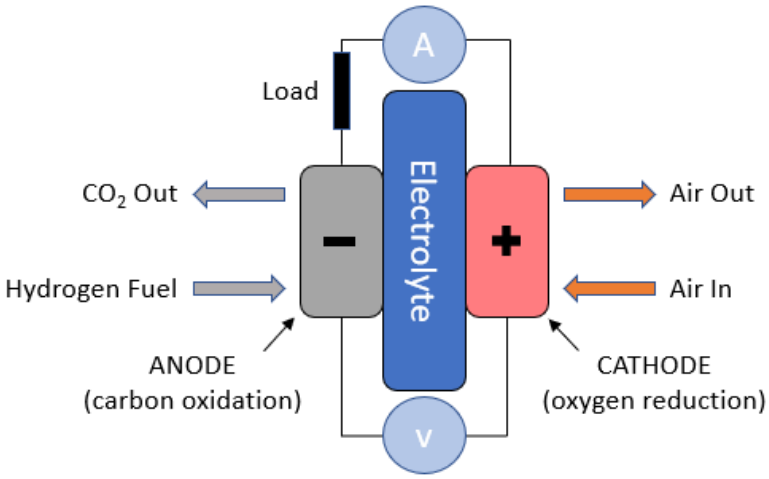

Figure 4. Hydrocarbon Fuel Cell Representation.

In order to sustain continuous isothermal operation for optimal electric power generation, heat and water byproducts must be continually eliminated. As a result, water and temperature management are critical components in the effective design and operation of fuel cells. Fuel cells and batteries are quite similar in that they are both electrochemical cells made up of an electrolyte sandwiched between two electrodes. Both employ internal oxidation–reduction processes to convert a fuel's chemical energy content to direct current power. The composition and function of the electrodes, on the other hand, change dramatically between the two energy devices. A battery's electrodes are often metals (such as zinc, lead, or lithium) submerged in mild acids [43]. The electrodes (catalytic layer and gas diffusion layer) in fuel cells are generally made up of a proton-conducting medium, a carbon-supported catalyst, and

electron-conducting fibers. Batteries are used for both energy storage and conversion, whereas fuel cells are exclusively utilized for energy conversion. The chemical energy stored in a battery's electrodes is used to power the electrochemical processes that produce electricity at a certain potential difference. As a result, a battery has a finite lifespan and can only work as long as the electrode material is not exhausted. As a result, an operational fuel cell system must have a fuel storage mechanism as well as an oxidant supply mechanism. Furthermore, when the battery is inactive, electrochemical processes that damage the battery occur slowly, decreasing the battery's lifetime [44].

Many technological difficulties restrict the usage of rechargeable batteries, including power storage and retrieval potential, depth of charge, and number of charge/discharge cycles [4]. Acids, alcohol, oxides, and hydrogen are employed as fuel sources in laboratories and commercial settings [45]. The fuel must be easily available inside the human body in the case of portable and implanted devices. In this case, a regular fuel cell cannot be used. Abiotic fuel cells (AFC) and biofuel cells (BFCs) might be viewed as the optimal power source for portable and implantable devices to overcome this challenge. The human body has more than 100 W of power as chemical energy on average. AFC and BFC convert chemical energy from molecules in living organisms into electrical energy. The distinction between biofuel cells and batteries is that in both AFCs and BFCs, the reactant content is constantly re-established by bodily fluids. The permanent presence and availability of fuel straight from the body eliminates the need for external recharging systems or replacement, and theoretically allows for endless operation if there is a steady supply of fuel.

Biofuel cell

The benefits of these fuel cells are typically obscured by one or more of the aforementioned problems, namely high temperatures, expensive costs, and, in some circumstances, very corrosive medium. BFCs are appealing in this regard because they operate under mild reaction conditions, namely ambient operational temperature, and pressure, use neutral or circumneutral electrolytes, and use inexpensive catalysts and anodic fuel, which can range from simple organic molecules like glucose or acetate to complex organic waste, such as waste waters and urine [47]. Depending on the catalysts utilized in the oxidation and reduction processes, biofuel cells can be enzymatic, microbial, or mammalian in nature. BFCs are devices that may convert chemical energy to electrical energy via electrochemical processes involving biological pathways. The former employs selected enzymes to carry out redox reactions that generate current, whilst the latter employs electroactive microorganisms to breakdown organics and generate power. Because of the quantity and sustainability of these fuels, biofuel cells are a renewable energy source, albeit it has recently been demonstrated that biofuel cells can even run-on JP-8 airplane fuel [48]. The key parameters influencing the power generation of a biofuel cell are the electrodes and biocatalysts used, the operational component in described in Figure 5. Driving the recent ascendance of biofuel cells are the aspects of biocatalysis that are unmatched by conventional low-temperature oxidation-reduction catalysts, namely, activity at near-room temperatures and neutral pH and, more importantly, selective catalytic activity.

Microbes have benefits over enzymes because they can catalyze biofuel oxidation. It is also less susceptible to poisoning and activity loss under normal working conditions, making it a good candidate for usage in biofuel cells [48,49]. One of the most significant shortcomings is the use of the electrons generated during the process that occurs inside the cell. One possible

solution is to employ mediators, which must otherwise satisfy many characteristics, including (a) passage across the membrane of the microorganism's cell and (b) not be harmful. Organelles, on the other hand, are in their infancy compared to their enzymatic and microbiological counterparts. As a result, they lack the power output of enzymatic biofuel cells as well as the stability of microbial biofuel cells. Organelles, such as mitochondria, may be separated from live cells and connected directly to an electrode [50]. Mitochondria include a number of membrane-bound enzymes that create an electron transport chain that can connect directly to an electrode. Because the enzymes are membrane-bound, they should be more stable than in an enzymatic biofuel cell, and because the mitochondria are not surrounded by cellular walls, they should transport electrons faster than a microbial fuel cell. Fuel cells have the ability to deal with miniaturization because of their simple manufacturing design, which includes no moving parts. Non-biological miniature fuel cells consisting of methanol and air, with an active area of 0.25 cm^2, employs polymer electrolytes instead of a solution and achieves power densities comparable to big cells [51].

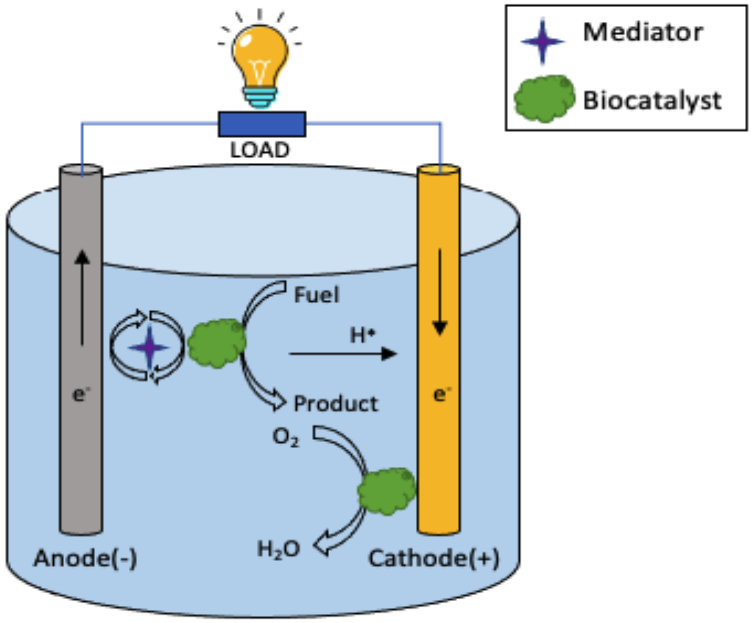

Figure 5. Biofuel cell consisting of its major components and basic operational components.

Enzymatic biofuel cells are composed of enzyme catalysts derived from biological sources and applied to the anode, cathode, or both electrodes as shown in Figure 6. Because the enzymes have been separated from their natural environment, they may be able to communicate directly with mediators or electrodes, resulting in higher power density than microbial or organelle biofuel cells. Enzymes have higher electrochemical catalytic activity than microorganisms in general, but they are less sustainable. Because of their unique characteristics, such as high turnover rates, which results in a high bio-catalysis rate, researchers are constantly thinking about biofuel cells that use enzymes. The requirement to transfer electrons to the electrode is one of the primary issues with such biofuels. Extensive study of new advances in enzyme immobilization on the surface of an electrode using a variety of methods results in higher transfer rates, making them an appealing option [51,52].

Although most attention has been focused on anode reactions, study of the reduction of oxygen at the cathode may also be undertaken utilizing biological moieties, which was proposed as an alternative to the usage of platinum [53]. Enzymes offer several advantages over chemical catalysts, including biocompatibility, higher trans-formation efficiency, activity at mild conditions, and most crucially, increased specific selectivity. These characteristics enable BFCs to function without a separation membrane, allowing for miniaturization and potential use in wearable and implantable devices [54].

Unfortunately, enzyme lifetime is limited, and it is significantly reduced when interfering analytes are present [55]. One of the challenges of an Enzymatic biofuel cell (EFC) is the use of mediators, which has been overcome by the development of mediatorless enzyme-based biocathodes and bioanodes. Encapsulating immobilized enzymes in micellar polymers has been shown to limit enzyme denaturation and offer a biocompatible hydrophobic and pH-buffered environment [56].

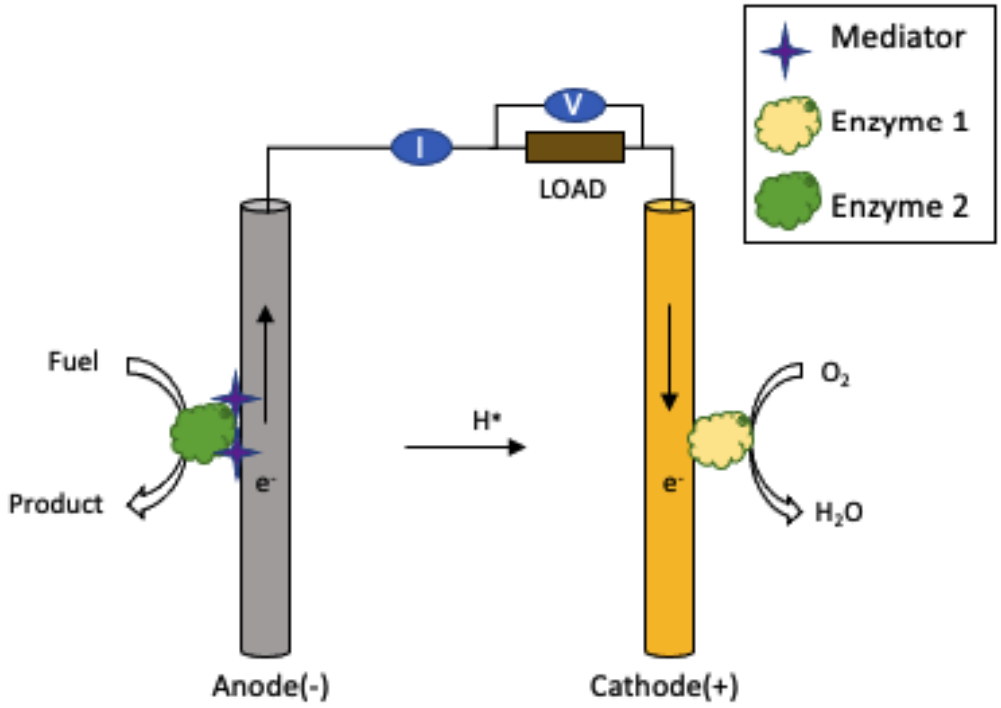

Figure 6. Model representation of enzymatic biofuel cell.

Enzyme biocatalyst assemblies on electrode surfaces typically do not accomplish considerable electron transfer communication between the redox center and the conductive support, owing to the surrounding protein matrix's electrical insulation of the biocatalytic site. Several strategies have been presented and researched in the field of bioelectrochemical technology during the last four decades in an effort to establish effective electrical communication between biocatalysts and electrodes. In general, electron transfer is divided into two mechanisms: mediated electron transfer (MET) and direct electron transfer (DET) (DET) [54]. A low-molecular-weight, redox-active molecule known as a mediator is used in MET to shuttle electrons between the enzyme active site and the electrode. In this situation, the enzyme catalyzes the redox mediator's oxidation or reduction. On the electrode surface, the mediator undergoes a reverse transition (regeneration). The main properties of mediator-

assisted electron transfer are that (i) the mediator functions as a co-substrate for the enzymatic process and (ii) the mediator's electrochemical transformation on the electrode must be reversible. The catalytic process in these systems involves enzymatic changes of both the first substrate (fuel or oxidant) and the second substrate (mediator).

At the electrode surface, the mediator is renewed, ideally at a modest overvoltage. The enzymatic reaction and the electrode response can be thought of as independent but linked processes. Direct (mediatorless) electron transfer links the enzymatic and electrode processes in DET. The electron is transmitted straight from the electrode to the substrate molecule (or vice versa) via the enzyme's active site in this situation [57]. The coupled overall process in such a system is the redox transformation of the substrate(s), which may be thought of as an enzyme-catalyzed electrode process. According to this mechanism, the electrode surface serves as an enzyme substrate, and the enzymatic and electrode reactions are not distinct; rather, they are formal steps of the bioelectrocatalytic reaction process [58].

Sensors and biofuel cells have considerable overlap in technological criteria, such as chemical and mechanical stability, selectivity, and material cost. However, these two technologies differ in terms of energy supply, as sensors are often energy-consuming cells, whereas biofuel cells, by definition, are energy providers. Because of this large variation, in the areas of current density and cell potential, sensors driven by cells often function at cell potentials larger than an open circuit [59]. Also, cell current must be kept to a minimum in order to reduce power consumption. Usually the power consumption for biofuel cells are in mW and for biosensor in uW as compared to other energy production methods as shown in Figure 7. Sensors are often built with currents in the nanoampere to microampere range, resulting in very low power consumption even at cell potentials around 1 V. To avoid unwanted side effects, cell potential in a sensor is frequently reduced.

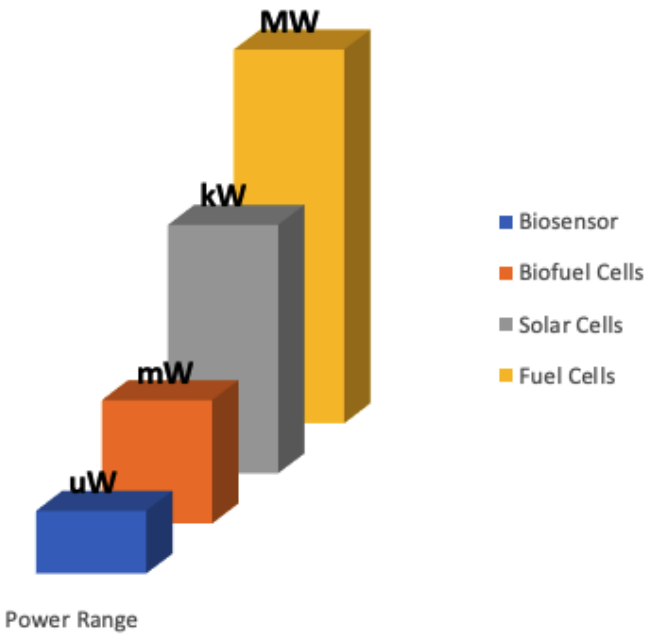

Figure 7. Visualization for reference of power range by some of the alternative energy production methods.

An ideal enzymatic fuel cell, on the other hand, creates maximum power as an energy-producing cell, implying both high current and high potential. Overpotentials owing to kinetics, ohmic resistance, and mass transfer must be reduced, while current density, particularly in terms of current per unit volume, must be optimized. Although these difficulties are more difficult in the context of biocatalyzed fuel cells, they are nevertheless ubiquitous in traditional fuel cell design. Indeed, since William Grove's pioneering tests in 1839, fuel cells have been stacked, or connected in series, to obtain larger total system voltage by increasing individual cell voltage.

Stability is another factor that separates biofuel cells from sensors. Because biocatalyzed electrochemical sensors are frequently cheap enough to be disposable, long-term stability is not required. If stability is essential, encapsulating the biocatalytic species in a low-porosity hydrophilic medium, such as silica gel, is one option [60]. Hydroxides on the gel surface interact with enzyme shell sugars to "cage" the enzyme, limiting translational motion

and decreasing enzyme denaturation. Caging of the molecule might result in diminished activity depending on the enzyme. Such gels also limit the mobility of reactants and products, limiting mass transfer in the electrode. In an amperometric sensor, where mass-transfer-limited signals are frequently linearly proportional to reactant concentration, this may be a desired result.

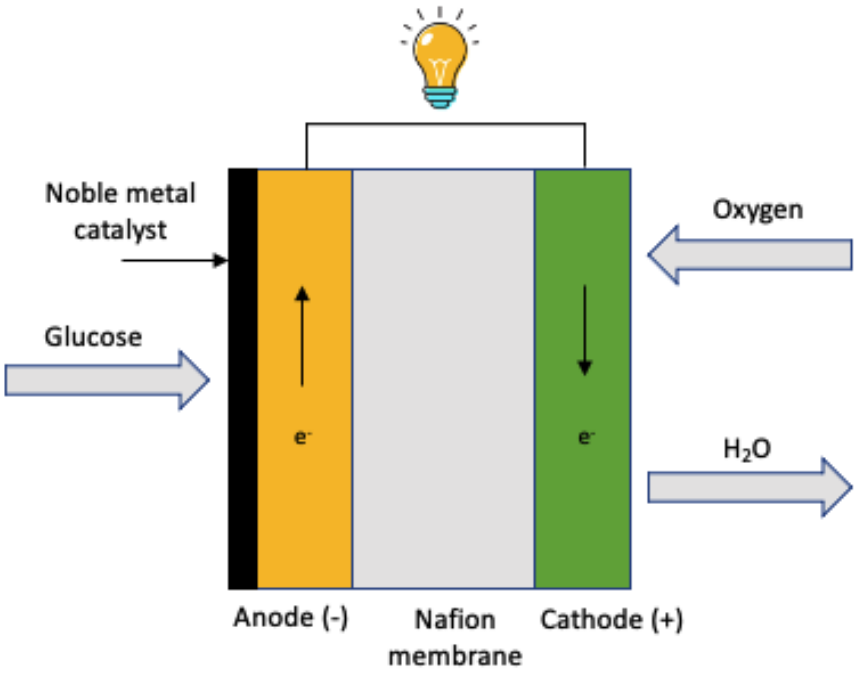

Figure 8. A model representing a non- enzymatic biofuel cell.

An abiotic glucose fuel cell uses noble metals as catalysts to transform the chemical energy of glucose and oxygen into electric power. An abiotic fuel cell's general electrode reactions involve the oxidation of glucose to gluconic acid at a platinum-based anode catalyst and the reduction of oxygen to water at the cathode as seen in Figure 8. Protons are released and pass from the anode to the cathode via a proton-conducting membrane or electrolyte, generating electric power. Glucose, methanol, and ethanol are examples of biofuels [60]. Abiotic cells also provide the prospect of long-term stability under operational and physiological settings. Furthermore, abiotic fuel cells may operate better at normal glucose

concentrations [60]. When compared to EBFC, an abiotic glucose fuel cell has superior stability and a longer life cycle.

Abiotic fuel cells might be viewed as an alternative to traditional fuel cells based on metal catalysts due to increased research and development in the field of biofuel cells. These devices create a system capable of directly converting chemical energy into electricity. The link between biology and electricity, as well as the notion of a biofuel cell, has been recognized since 1911, when MC Potter discovered that a culture of the bacteria E. coli produced electricity in half-cell investigations using platinum electrodes [61]. Glucose is more typically employed as a biofuel. Though enzymatic, microbial, and whole cell/organism-based bio-fuel cells have received a lot of interest in recent decades for implantable devices, abiotic fuel cells have several benefits over biotic biofuel cells. Even though using noble catalysts results in a more expensive biofuel cell system, abiotic fuel cells offer endurance to high temperatures during steam sterilization or a wide range of pH values.

For the electro-oxidation of glucose in neutral fluids, a variety of noble metals and alloys, including platinum–ruthenium alloys, rhodium, and iridium, have been proposed [61]. The persistent non-selectivity towards oxygen or glucose, as well as the electrocatalytic activity of metal-based catalysts at neutral pH, continue to motivate research to reach satisfying power output for the supply of electronic devices under physiological conditions. The primary benefits of AFCs and BFCs are the employment of environmentally friendly catalysts, the capacity to work at low temperatures (20-40 °C) and physiological pH levels, and the ability to utilize several fuels. These benefits point to an economically feasible method, as seen by the rising research in this sector throughout the world.

CHAPTER III

GLUCOSE BIOSENSOR

A biosensor is a device that monitors biological or chemical processes by producing signals proportional to an analyte concentration in the reaction. Biosensors are used in applications such as illness monitoring, drug discovery, and the detection of contaminants, disease-causing microorganisms, and disease markers in physiological fluids (blood, urine, saliva, sweat). A bioreceptor is a molecule that recognizes the analyte specifically. Bioreceptors include enzymes, cells, aptamers, deoxyribonucleic acid (DNA), and antibodies. Bio-recognition refers to the process of generating a signal (in the form of light, heat, pH, charge or mass shift, etc.) as a result of the interaction of the bioreceptor with the analyte [63, 64]. A transducer is a component that transforms one type of energy to another. The transducer in a biosensor converts the bio-recognition event into a quantifiable signal. This energy conversion process is called signalization. The majority of transducers provide optical or electrical signals that are proportional to the number of analyte–bioreceptor interactions.

Electrochemical, optical, thermometric, piezoelectric, and magnetic transducers are the five major types of transducers [65]. The bulk of modern glucose biosensors are electrochemical in nature, owing to their higher sensitivity, repeatability, ease of maintenance, and low cost. Potentiometric, amperometric, and conductometric electrochemical sensors are available [66-67]. Enzymatic amperometric glucose biosensors are the most prevalent commercially available devices, and they have been extensively researched over the previous few decades. Amperometric sensors measure currents that are created when electrons are transferred directly or indirectly between a biological system and an electrode [68,69]. A glucose biosensor is a device that detects the presence of glucose in a complicated mixture. A

blood glucose sensor monitors the concentration of glucose in the blood by using a glucose specific enzyme to break down glucose molecules and create electrons. When glucose is completely oxidized, the current created corresponds to the glucose concentration. Thus, the biorecognition enzyme element is immobilized on a transducer, which converts the chemical signal into an electrical signal that a read-out circuit can read. The glucose analyte is the chemical ingredient of interest in this investigation, and it is usually detected using the amperometric detection technique. Glucose biosensors have been created to offer diagnostic information about a patient's health status. Multiple laboratory tests are used to diagnose and treat diabetic individuals. The blood glucose concentration is a helpful parameter for patient monitoring and is the primary diagnostic criteria for diabetes with HbA1c level [69].

Self-monitoring of blood glucose (SMBG) has been proven to be an effective technique in the management of diabetes. The purpose of SMBG is to assist the patient in achieving and maintaining normal blood glucose concentrations, therefore delaying, or even preventing the advancement of microvascular (retinopathy, nephropathy, and neuropathy) and macrovascular problems (stroke and coronary artery disease). Furthermore, it may be used to identify hypoglycemia and provide real-time information for altering medicines, dietary recommendations, and physical activity to accomplish glycemic targets [69].

Blood – Glucose monitoring

Regular blood glucose measurements may give information for optimizing and/or altering patient treatment options. Blood-glucose concentrations in healthy persons are typically in the 4.9–6.9 mM range, increasing to up to 40 mM in diabetics after glucose injection [66–72]. Glucose concentrations are determined by interactions with one of three enzymes: hexokinase, glucose oxidase (GOx), or glucose-1-dehydrogenase (GDH) [68]. In

many clinical laboratories, the hexokinase assay is the gold standard for detecting glucose using spectrophotometry [69]. GOx and GDH enzyme families are commonly used in glucose biosensors for SMBG. These enzymes differ in terms of redox potential, cofactors, turnover rate, and glucose selectivity [70]. The usual enzyme for biosensors is GOx, which has a greater selectivity for glucose. GOx is simple to acquire, inexpensive, and can survive larger pH, ionic strength, and temperature fluctuations than many other enzymes, allowing for less demanding production conditions and comparatively flexible storage regulations for use by lay biosensor users [73,74]. The essential idea behind the glucose biosensor is that immobilized GOx catalyzes the oxidation of D-glucose by molecular oxygen, resulting in gluconic acid and hydrogen peroxide and water as byproducts as seen in Figure 9 [75].

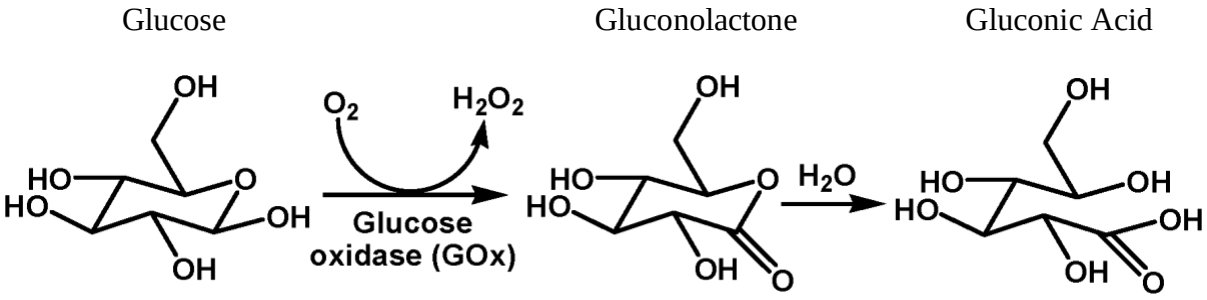

Figure 9.Glucose conversion to gluconic acid using mediator glucose oxidase [78].

For the electrochemical sensing of glucose, three broad methodologies are used: monitoring oxygen consumption, detecting the quantity of hydrogen peroxide created by the enzyme activity, or utilizing a diffusible or immobilized mediator to transfer electrons from the GOx to the electrode. The quantity and variety of GDH-based amperometric biosensors has lately increased. GDH-pyrroquinolinequinone (PQQ) [68-79] and GDH-nicotinamide-adenine dinucleotide (NAD) [80] are members of the GDH family. GDH's enzymatic process is not affected by dissolved oxygen. PQQ is used as a cofactor by the quinoprotein GDH recognition element. Clark and Lyons of the Children's Hospital of Cincinnati presented the concept of the biosensor for detecting glucose levels in 1962 [82]. An oxygen electrode with an inner oxygen

semipermeable membrane, a thin layer of GOx, and an outside dialysis membrane made up this glucose biosensor. To create an enzyme electrode, enzymes might be immobilized at an electrochemical detector. A reduction in measured oxygen concentration is proportionate to the concentration of glucose. The Yellow Springs Instrument Company analyzer (Model 23A YSI analyzer) [83] for the direct measurement of glucose, which is based on the amperometric detection of hydrogen peroxide, was the first commercially viable glucose biosensor employing Clark's method in 1975. This analyzer was almost entirely employed in clinical settings. The usual commercially employed methods are shown in Figure 10 illustrating the development.

The first generation of biosensors were improved by substituting oxygen with non-physiological electron acceptors known as redox mediators, which were capable of transporting electrons from the enzyme to the surface of the working electrode [84]. Instead of hydrogen peroxide, a reduced mediator is generated and subsequently re-oxidized at the electrode, delivering an amperometric signal and renewing the oxidized form of the mediator [85]. To increase sensor performance, a range of electron mediators such as ferrocene, ferricyanide, quinines, tetrathialfulvalene (TTF), tetracyanoquinodimethane (TCNQ), thionine, methylene blue, and methyl viologen were utilized [86-90].

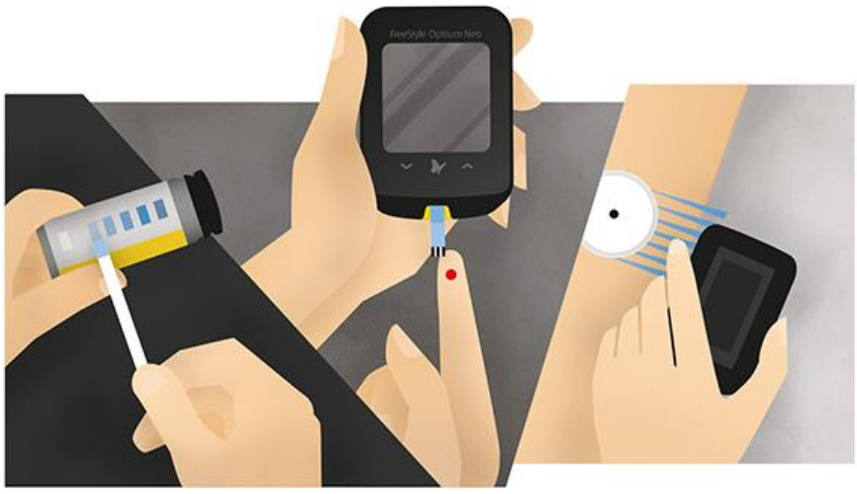

Figure 10.Illustration of a Urine glucose testing, finger prick glucometer and continuous glucose monitoring (CGM) from left to right.

Continuous ex vivo monitoring of blood glucose was proposed in 1974 [91] and Shichiri et al. [92] performed in-vivo glucose monitoring in 1982. CGMS is designed to enhance diabetes control by giving real-time data from an internal insulin release mechanism. There are two types of continuous glucose monitoring devices in use today: continuous subcutaneous glucose monitors and continuous blood glucose monitors. However, because of surface contamination of the electrode by proteins and coagulation factors, as well as the danger of thromboembolism, most CGMSs do not directly monitor blood glucose. As a result, subcutaneously implanted needle-type electrodes sensing glucose concentrations in interstitial fluid and reflecting blood glucose levels have been created [93-97]. Minimed was the first company to launch a needle-type glucose biosensor (Sylmar, CA, USA). It did not, however, give real-time data; nevertheless, the results of 72-hour monitoring could be retrieved in a physician's office [98]. The most extensively used CGMS devices on the market are FDA-approved needle-type CGMS devices such as the Minimed Guardian, REAL-Time system by Medtronic (Minneapolis, MN, USA), SEVEN by Dexcom (San Diego, CA, USA), and Freestyle Navigator by Abbott (Abbott Park, IL, USA). These glucose monitors display real-time glucose concentrations that are updated every one to five minutes and the disposable sensor has a three to seven-day lifespan [99-102].

Sweat - Glucose Monitoring

A continuous glucose monitoring device that can quantify glucose concentrations without frequent calibration is in great demand among consumers. Although blood is still the most researched bodily fluid for such assessments, other more accessible biological fluids such

as interstitial fluid, ocular fluid, perspiration, breath, saliva, or urine have been examined as alternative sample media for noninvasive continuous monitoring [103].

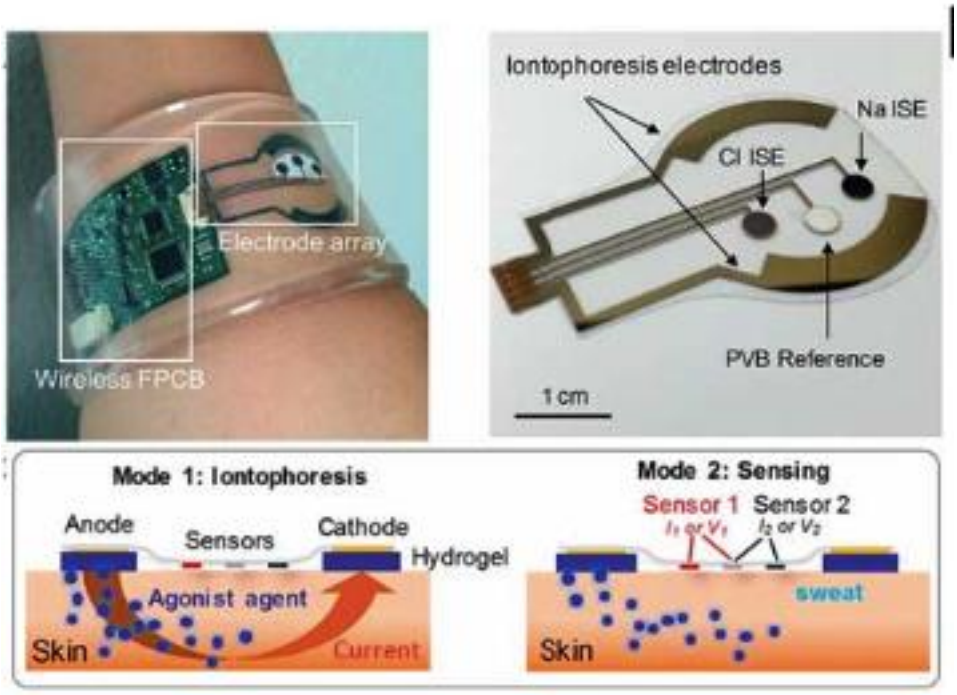

Figure 11.Integrated sweat extraction-based glucose monitoring system. Monitoring of sweat (intophoresis) on a stretchable and transparent nanowire heater for wearable electronics applications [103].

To date, two primary types of wearable glucose biosensors have been identified: enzymatic and non-enzymatic sensors. Colorimetric and electrochemical biosensing are both possible with enzymatic biosensors. Non-enzymatic sensors, on the other hand, can only be used for electrochemical sensing since glucose detection necessitates redox processes. For starters, wearable electrochemical and optical glucose biosensors based on the enzyme glucose oxidase (GOx) are extremely sensitive to changes in the sweat environment, such as temperature, pH, and ionic strength, which cannot be adjusted in situ [104]. Enzymes cannot restore their features after denaturation due to acidic pH, high temperature, or strong ionic strength. Second, in addition to enzyme degradation over time, low stability is an issue. Even if the GOx is highly glycated and therefore stable, its catalytic activity will gradually decline over time, reducing its shelf life and long-term wearable monitoring capabilities (increase in

skin temperature during exercise, normal body temperature: 36.5–37.5 C) [105]. Third, frequent mechanical friction and skin deformation may result in delamination of the mounted enzyme layer from the biosensor interface. These constraints reduce the sensors' long-term storage stability and continued utility in real-time monitoring. Fourth, enzyme immobilization on the transducer surface involves procedures like covalent attachment, cross-linking polymerization, or sol-gel entrapment on the working electrode surface. This not only lowers enzyme activity but also immobilizes electrode reagents, delaying electron transfer and decreasing detection sensitivity [106]. Fifth, commercially available enzymes are expensive and are often bio-sourced agents suited for in vitro analysis only, making them unsuitable for wearable biosensing. Sixth, wearable sweat-based biosensors with a closed air gap to avoid sweat evaporation have just a two-phase solid–liquid interface, with oxygen communicated through the liquid phase (excreted sweat) with a low diffusion coefficient compared to oxygen in the air. By utilizing iontophoresis to create perspiration, the body temperature would stay steady at 37 degrees Celsius at rest, allowing for optimum enzyme activity to detect glucose as shown in Figure 11. Due to the brief contact period between acidic sweat and immobilized GOx enzyme, the enzyme would not be destroyed until submerged in acidic sweat continuously in the absence of a microfluidic system. A thin, soft, and flexible outer cover sheet will also preserve the enzyme and prevent delamination from the biosensing interface by preventing sweat evaporation [107]. The exterior, isolating cover layer is constructed of soft silicone rubber with strategically placed air holes. As a result, oxygen may easily travel from the air to the active biosensing interface. For a long time, non-enzymatic electrochemical sensors have been used to detect glucose [108]. These sensors employ electrocatalytic materials capable of rapidly and efficiently oxidizing glucose (such as bulk metal, metal oxide, alloys, metal nanoparticles, and carbon nanocomposites). If the study is performed at the physiological pH of sweat (pH 7.2–7.3), electrochemical responses are reduced or even completely lost. The

linear range of non-enzymatic transition-metal sensors is insufficient for diagnosing blood glucose (2–40 mM) or sweat glucose (sweat glucose level: 0.2– 1 mM) as shown in Table 1.

Table 1. Biomarker – Glucose in physiological fluids for healthy and diabetic patients in mM.

Sr. No	Physiological Fluid	Concentration for Healthy Patients'	Sampling techniques	pH	Concentration among Diabetic Patients'
1	Blood	4.9-6.9 mM	Needle, lancet	7.35-7.45	2-40 mM
2	Sweat	0.06-0.11 mM	Swab, tattoo	4.5-7	0.01-1 mM
3	Urine	2.78-5.55 mM	Passive collection or catheter	4.5-8	>5.55 mM
4	Interstitial Fluid	3.9-6.6 mM	Tape-strip, iontophoresis, micro dialysis, microneedle array	7.2-7.4	1.99-22.2mM
5	Saliva	0.23–0.38 mM	Swab	6.2-7.6	0.55-1.77 mM
6	Tear Fluid	0.05-0.5mM	Swab, contact lens	6.5-7.6	0.5-5 mM

The fuel cell for energy harvesting and conversion and flexible and secure rechargeable batteries (e.g., Zn-MnO_2) are seen as intermediate energy storage devices for non-invasive, real-time, and continuous monitoring of sweat glucose levels. An iontophoretic system with a well-controlled sweat production rate has been implemented for autonomous on-demand sweat extraction (at least 100 nL/min/cm^2) [109]. A microfluidic system can be used for collecting and storing sweat and when coupled with electrochemical/colorimetric biosensing platform with functioning electrodes can convert sweat glucose concentrations into electrical/optical signals. As a controlling module, a flexible printed circuit board (PCB) drives the iontophoretic process and allows in-situ data analysis (e.g., processing, calibration, and easy read-out signal transmission), and there is preferably a digital screen for direct and real-time glucose tracking,

removing transmitting systems [110]. Furthermore, the electronic display module should ideally provide a steady display without the need for constant power, ultra-low power consumption, a broad viewing angle, great visibility, and strong contrast. However, without additional data storage and download capabilities, this architecture prohibits data storage or distribution of the data to health care providers and is thus less appealing for integrated health-monitoring systems [111, 112]. Therefore, it is critical to monitor sweat glucose levels continuously for at least 24 hours. The capacity to do so is obviously commercially useful, with the sole drawback being the limited downsizing of the entire system.

Other Physiological Fluids

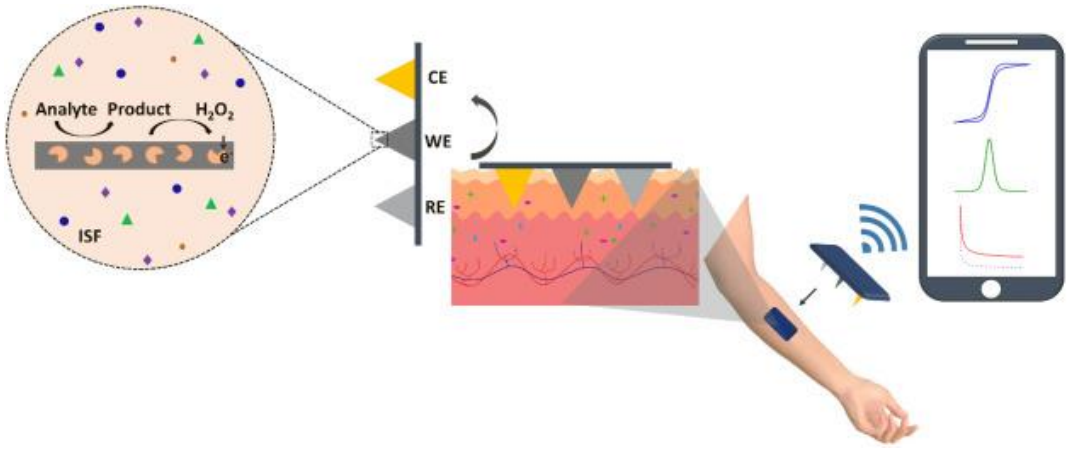

Figure 12. Concept for solid microneedle device with the representation of oxidase- enzyme electrochemical reaction at the microneedle interface with data recording to a phone [113].

The extracellular fluid that surrounds tissue cells is known as interstitial fluid. It has tremendous promise for medical diagnostics since it has a comparable composition to blood in terms of numerous clinically relevant indicators [113,114]. By diffusion with the interstitial fluid, blood and surrounding vascularized tissue exchange biological analytes and tiny compounds [114]. As a result, interstitial fluid can provide vital information about a patient's

health and has been used to determine hereditary metabolic illnesses, organ failure, and treatment efficacy in a minimally intrusive manner. Sode et al. have created the BioRadioTransmitter, a self-powered implanted continuous monitoring device for use in an artificial pancreas [115]. In this case, the device is made up of a capacitor, a radio transmitter, and a receiver. The BioRadioTransmitter device's capacitor discharges a radio signal in the presence of glucose, which is received and amplified by the radio receiver. The variation in transmission frequency is thus proportional to the concentration of glucose [116].

Several minimally invasive or invasive approaches have been developed to detect glucose in interstitial fluid, with many of these techniques used in animal and human (with and without diabetes) investigations under varied settings (e.g., glucose infusion, glucose plus insulin infusion, oral glucose tolerance test) with an example shown in Figure 12. These investigations have shown a broad range of accuracy, which might be attributed to variances in experimental settings, methodologies procedures, species, and subject characteristics [117]. In general, fluctuations in interstitial fluid (IF) and plasma glucose were assessed under two conditions: steady state and non–steady state. Under steady-state circumstances, IF glucose typically corresponded with blood glucose, with a reported lag time ranging from 0 to 45 minutes, with an average lag of 8–10 minutes. When plasma glucose levels are rising, boosting blood flow to the interstitial glucose sampling location with regulated pressure has been found to reduce the lag time between blood and interstitial glucose [118-120]. The observed gradient in interstitial and plasma glucose concentrations ranged from 20% to 110%. Interstitial glucose may decline ahead of plasma glucose and reach the lowest values that are lower than comparable venous glucose levels during a period of declining glucose. Interstitial glucose levels have been demonstrated to stay lower than plasma glucose concentrations for extended periods of time after insulin-induced hypoglycemia has been corrected.

Clinical studies representing the benefit of using CGM as an adjunct to detect glucose trends for various patient populations with and without diabetes are likely to broaden CGM use in medicine [121]. Sensors have been used successfully to detect abnormal glucose levels in the intensive care setting despite confounding factors like edema, hypothermia, or multiple medication use. Outpatient studies including the use of CGM for diagnosing gestational diabetes documents the need for a self-powered glucose biosensing microsystem that would reduce the need for batteries as a power source, glucometers, and CGM devices, therefore enhancing the standard of living of patients.

CHAPTER IV

NEAR FIELD COMMUNICATION BASED WIRELESS SYSTEM

Near Field Communication (NFC) technology is gaining attention in the implementation of current wireless technologies. It opens many new possibilities for designing innovative wireless systems including interaction between two NFC-enabled devices or between a device and an NFC tag. The communication method is quite easy; all that is required is to bring the device or specific label (tag) in proximity to the reader to begin signal transmission. NXP Semiconductors, created by Philips, is a co-inventor of NFC technology. In 2004, the corporation, along with Sony and Nokia, established the NFC Forum [126], a non-profit organization dedicated to the advancement of this technology [127]. As previously stated, NFC is not a new technology but an advancement of current RFID technology. It operates across a distance restricted by a fraction of a wavelength of the carrier frequency, as well as the size of the antenna in relation to the wavelength [127]. In practice, this means that NFC connection is only available within 4 centimeters of the Google Pixel 3a smartphone. Therefore, a mobile phone must get quite close to the NFC tag to power it, connect to it, and query its content.

A popular use-case is to have an NFC buscard for payment, with part of the leather/cloth wallet and the user's hand in between the card and the reader when held against the active reader. In this payment use-case, the distance and RF attenuation are near to the maximum feasible with the proximity-card specification and card-sized antenna diameter utilized, which is advantageous in terms of security and anti-collision. Another typical application is the use of proximity cards to get access to ski lifts. In contrast to vicinity cards, which have a minimum field strength of 1500 mA/m [126], proximity cards may function with a minimum field strength of 150 mA/m [127]. In reality, this equates to a communication distance of up to 1.5

meters for proximity cards if the reading antenna(s) are large enough to allow the reading of a card placed in the clothes of a person walking between two fixed antennae. NFC is intended to function between two nodes, one of which must be active. By feeding the antenna with power at the prescribed frequency, an active device generates an RF field surrounding its NFC-antenna. NFC is a subset of RFID that works in the high frequency band at 13.56 MHz utilizing three RFID protocols: ISO 14443-Type A and Type B [ISO08] and FeliCa. At a distance of 5-10 cm, the highest transmission speed can be 106 Kbit/s, 212 Kbit/s, or 424 Kbit/s. Table 2 showcases the different technologies with the comparison of attributes based on range, set up time and useability which is indirectly suitable for the application.

Table 2. Comparison between NFC and related technologies [131].

	NFC	**RFID (UHF)**	**IrDA**	**Bluetooth**
Set-up time	<0.1ms	<0.1ms	0.5sec	6sec
Range	Up to 10cm	Up to 3m	Up to 5m	Up to 30m
Usability	Easy, fast	Item centric, Easy	Data centric, Easy	Data centric, Medium
Consumer Experience	Touch, wave	Get Information	Easy	Configuration Needed

Near and far field

The near and far field operates on the fundamentals when an antenna emits RF energy at a specific frequency, *f*, the electromagnetic field around the antenna varies at different distances from the antenna. To begin, the distance from the antenna may be separated into two regions: near-field and far-field [126].

If the antenna length is half or less of the wavelength, the border between the near-field and the transition to the far-field is around one wavelength distance from the antenna. An electromagnetically short antenna is one that has a length that is less than half the wavelength. In the case of Nfc, for example, $f = 13.56[\text{MHz}]\ \lambda \approx 22.1[\text{m}]$. Second, the near field is separated into two parts: a reactive zone close to the antenna and a radiative region that extends out to one wavelength. The extent of the reactive near field is determined by the antenna's parameters, such as its size in relation to the wavelength. The near field of an antenna is inductive, which means it may induce a current (transfer electrical power) into properly designed antennas within this area. As seen in Figure 13, a load (resistance) on antenna B, existing in antenna A's reactive near-field, feeds back, generates a higher load on antenna A. In other words, antenna A can create an electromagnetic field while taking a specific amount of power from its power source, and the load on antenna A's power supply will rise only when antenna B, in the reactive near field, puts (or increases) a load on its antenna [126]. Near-field communication is based on the inductive characteristic of the near-field area for powering passive tags and the feedback characteristic of the reactive near-field region for signaling back to the reading device using load modulation by adjusting the load on its antenna.

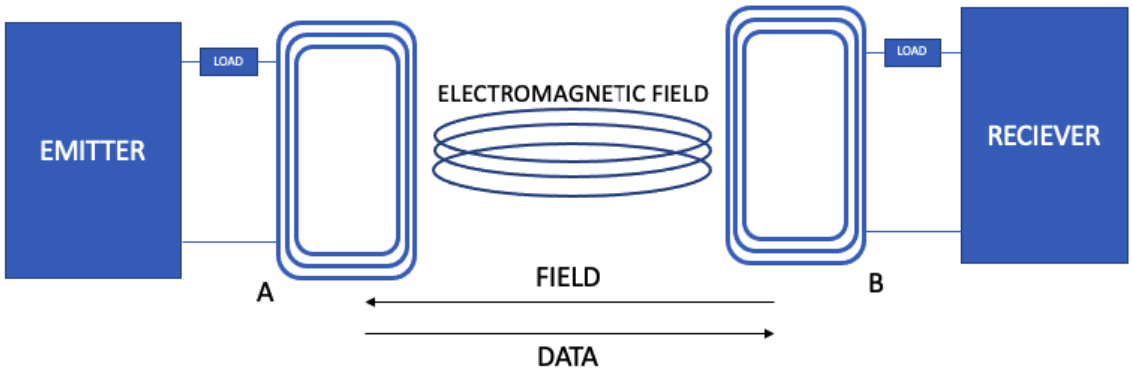

Figure 13.NFC based antenna communication mechanism between emitter and receiver.

ISO-15693 Vicinity cards

For this work the standard ISO-15693 “Contactless integrated circuit(s) cards - Vicinity cards” specify contactless cards are used which operates at a distance up to 1.5 meters [126]. The realistic read-distances of NFC and RFID-type technology differ significantly. RFID systems provide data back to the active reader using the same concepts of power induction into passive tags and load modulation on the reader's field [127]. Many RFID standards employ frequencies other than 13.56 MHz, which has additional properties such as a longer near-field and/or a higher allowable field strength, resulting in greater read-distances [128].

NFC supports three communication modes:

Reader/Writer Mode: This mode is most typically used for data exchange for reading the information contained on the tag (label) using an NFC-enabled device. The tag itself does not have a power source, but it is powered by an NFC-enabled smartphone (reader or writer). NFC Forum specifies four types of tags that can be used together with NFC [128]:

• Type 1 and Type 2:

– based on the ISO/IEC 14443 Type A standard

– small capacity (1 or 2 KB)

– cheap to produce

– transfer speed is limited to 106 Kbit/s

• Type 3:

– based on the FeliCa standard

– higher capacity (1 MB)

– higher price

– transfer speed is limited to 212 Kbit/s

• Type 4:

– based on both Type A and Type B ISO/IEC 14443 standards

– capacity of 32KB

– transfer speed between 106 Kbit/s and 424 Kbit/s

Card Emulation Mode: In this case, it is a reverse process. The NFC device acts as a tag and works in a passive mode. The device can emulate an unlimited number of smart cards which are read by an external NFC reader. It is mainly used as a method of payment or for identification.

Peer-to-peer mode: For this communication mode, two NFC-enabled devices are needed. It is used for direct data exchange between the devices.

The NFC Data Send Format (NDEF) message is a data format established by the NFC Forum and used to exchange data between two NFC devices or between two NFC devices and a tag. Each NDEF message can be made up of an infinite number of NDEF records, each of which provides a description of the sort of information it contains, and its length as shown in Figure 14 [141]. Record Type Definition (RTD) defines this information. According to NFC Forum [129], [132], commonly used RTD types are NFC Text RTD used for exchange of simple text string, whereas NFC URI RTD employs Uniform Resource Identifiers (URIs), which are used to describe resources on the Internet. They are compressed into a 1-byte field of the NDEF header. Smart Poster RTD allows the combination of multiple text and URI NDEF records, creating a self-describing ‘smart object’. The NFC Generic Control RTD contains a request for an NFC device to perform an action, such as start application, store data, modify

tag, etc. The NFC Signature RTD defines a format which is used to secure NDEF records and includes information about signature algorithms and certificates.

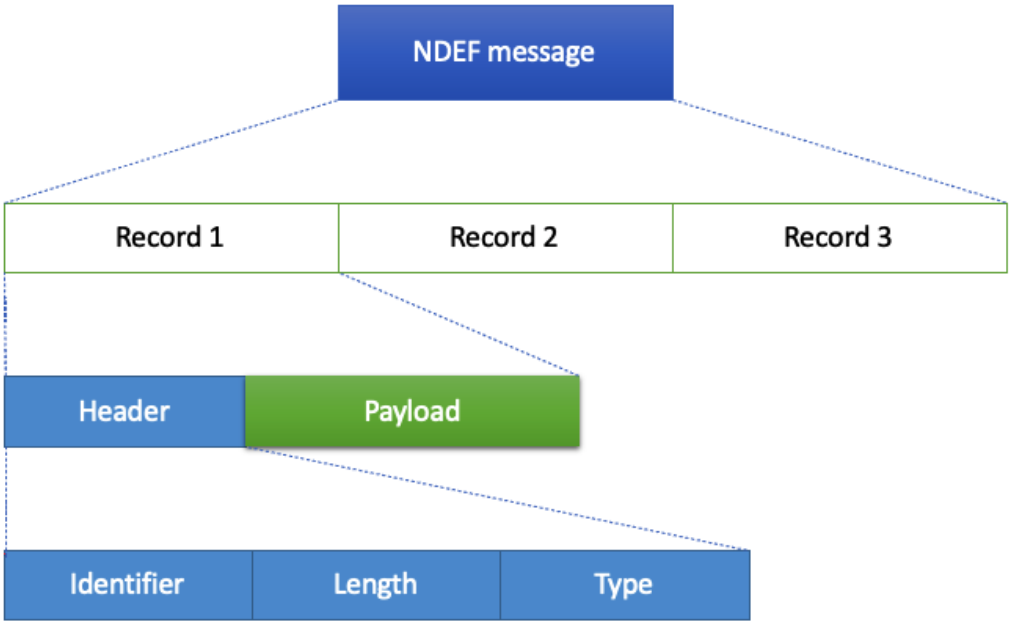

Figure 14.NDEF message consisting of record and its parts.

Android NFC-enabled smart phones are equipped with the Google Wallet1 application. This application enables customers to use their smartphones as payment (credit) cards instead of traditional payment (credit) cards. The smart phone emulates credit cards by employing the NFC card emulation mode. To complete the transaction, the user just places the smart phone near the NFC capable payment terminal. Aside from security features in communication between the smart phone and the payment terminal, the user must enter the password to approve the payment transaction. By placing the Android NFC-enabled smart phone upon the tag, the information is read from the tag. Depending on the type of tagged device and the read information, the Touch & Connect Android applications can be started on the Android NFC-enabled smart phone [129]. This application takes advantage of NFC to obtain Wi-Fi connection settings and a password from a tagged badge. Visitors to conferences throughout

the world are given badges as they enter the venue. The NFC tag connected to the badge carries all of the information needed by users to connect to a router through Wi-Fi. When a user scans the badge with an Android NFC-enabled phone the program instantly establishes a Wi-Fi connection.

RF430FRL152H NFC ISO/IEC 15693 Sensor Transponder

In this work we employ the RF430FRL15xH line of devices because it incorporates a programmable 16-bit MSP430 core that is linked to an analog front end (AFE) to provide a one chip solution. This allows for the connection of a large number of analog or digital sensors, as well as the transfer of sensor data using short-range wireless NFC technology. The integrated MSP430 core features 2KB of FRAM and 4KB of SRAM for programming and data storage. It supports SPI and I2C connection and has a 3-channel 14-bit sigma-delta ADC [143]. The device has a clock rate of 2 MHz. The RF430FRL15xH devices run at 1.5-V, making them suitable for use with low-voltage coin cell batteries as described in the block diagram in Figure 15 with the coin like shape and its components. It is even possible to passively power the device by drawing energy from the RF field of any reader connected to an RF430FRL15xH [131]. The RF430FRL15xH portfolio is divided into three components: the RF430FRL152H, the RF430FRL153H, and the RF430FRL154H. The 152H supports all of the hardware specifications stated above. The 153H, on the other hand, lacks SPI and I2C connections, and the 154H lacks the sigma-delta ADC.

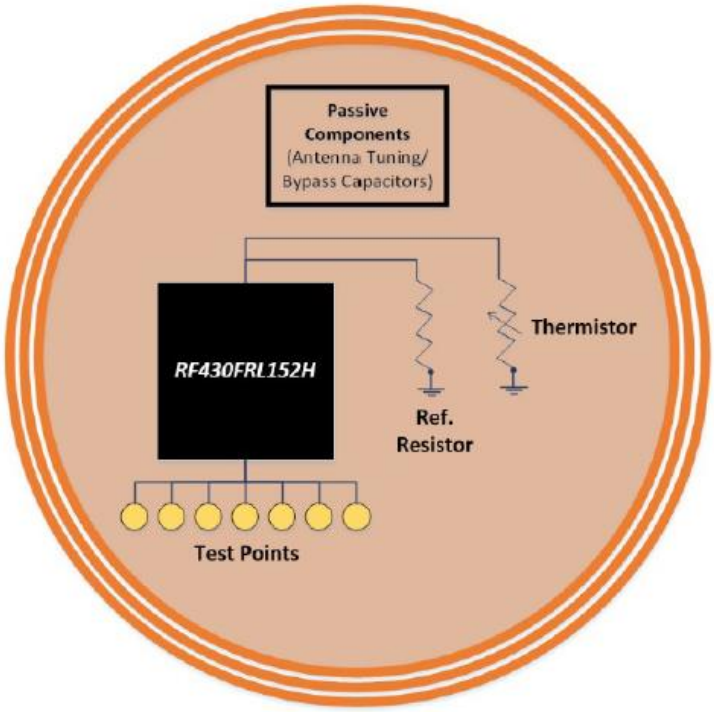

Figure 15. Block diagram for RF430FRL152H Sensor tag [147].

The RF430FRL15xH includes a Sensor Application ROM, which enables the simultaneous operation of multiple sensors by simply declaring a set of registers. Features that support the Sensor Application include:

- number of measurement cycles
- skipping of specific sensor measurements based on the cycle count
- measurement frequency (either predefined time steps or a custom time steps)
- format in which samples are stored (all, first, last, highest, lowest, or average)
- sensor configurations
  - gain
  - filter Type (CIC or Moving Average)
  - oversampling Rate

• monitor and Alarm Conditions

The features described above are handled by the ROM code and can be enabled, disabled, and configured with simple register writes that can be part of the FRAM firmware or done over the air with NFC technology [130].

The RF430FRL152H may be interfaced with up to three analog sensors via the 14-bit sigma-delta ADC. The ADC additionally contains two channels (ADC1 and ADC2) that can detect resistance, allowing thermistors to be used. The sigma-delta ADC is a slow-acquisition ADC with extremely low-power input current, offset, and noise thresholds. This allows users to reduce the amount of electricity necessary to take samples using the gadget. Because of the way sigma-delta ADCs work, getting high-accuracy samples takes longer. A full 14-bit conversion, for example, takes around 2 seconds. Much quicker samples can be collected at the expense of precision [130].

The sensor patch contains an RF430FRL152H IC chip, passive components needed to link the RF430FRL152H pins to power and ground, and thermistor circuitry including a reference resistor. The RFID antenna is built into the PCB on the patch's outside rim and surrounds it entirely. It is a three-turn coil that is adjusted by two capacitors. There is also a variety of test points that are used to program the RF430FRL152H with software, link the device through SPI or I2C lines, or attach a battery to the patch.

A technique for coping with tag collisions is specified in the ISO/IEC 15693 standard. When there are numerous NFC/RFID tags in the RF region, the ISO/IEC 15693 anti-collision procedure provides a robust solution to the difficulty of recognizing and communicating with a single NFC/RFID tag. When presented to an ISO/IEC 15693 compatible NFC/RFID reader, a single slot Inventory command may be used to initiate communication with a single ISO/IEC 15693 tag. The tag answers by providing its Unique Identifier (UID) and Identified Data Storage Format (IDSF) (DSFID). A collision occurs when many ISO/IEC 15693 tags are

shown at the same time because each tag is attempting to react to the same command. To overcome the collision of numerous ISO/IEC 15693 tags, a 16-slot Inventory command is supplied [131, 132].

One of the main components used in this module is the MSP430FR41xx ultra-low-power (ULP) microcontroller series designed for low-cost LCD applications that need an integrated 10-bit ADC, such as remote controls, thermostats, smart meters, blood glucose monitors, and blood pressure monitors. The MCUs include a strong 16-bit RISC CPU, 16-bit registers, and constant generators for optimal code efficiency. The digitally controlled oscillator (DCO) enables the device to go from low power to active mode in fewer than 10 seconds [132]. The architecture, paired with a wide range of low-power modes, is designed to maximize battery life in portable measurement applications. FRAM technology combines low-energy rapid writing speeds with flexibility and endurance of RAM with the nonvolatile behavior of flash. The MSP430 family mixed signal microcontrollers are particularly well known for their low cost and low power consumption with functional block diagram shown in Figure 16. Furthermore, they provide many peripherals and other hardware features. General characteristics and features of this microcontroller are:

- five power modes
- 16-bit RISC architecture
- fast wake up from standby mode
- 16KB flash storage
- 512B SRAM
- clock frequency scalable up to 16 MHz
- two 16-Bit Timers with capture/compare registers
- 16 GPIO pins
- universal Serial Communication Interface (USCI) module

• analog-to-digital converter

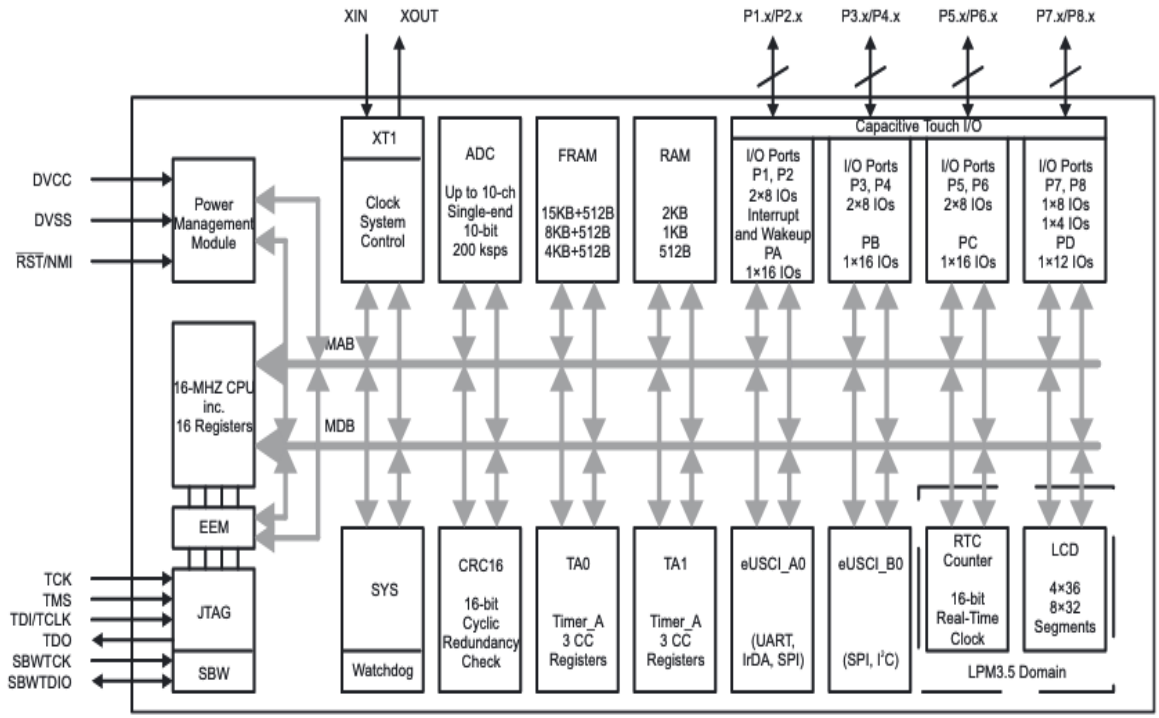

Figure 16. Functional Block Diagram of MSP430 microcontroller [132].

The most important features of the MSP430 which are essential for the realization of the project are described here. A sigma-delta modulator is provided for high resolution analog-to-digital conversion of quasi-dc voltages that uses first-order integrator, 1-bit comparator, 1-bit DAC, a sampling frequency of up to 2 kHz and is fully differential.

One advantage of this architecture as shown in Figure 17 is that the device does not require firmware to be configured. This design makes use of the ROM features included within the RF430FRL152H. The NFC/RFID Reader/Writer device that writes the configuration registers initializes the device "over the air." It is crucial to note that with this arrangement, each sample takes 128 ms to acquire [132].

Given that each ISO/IEC 15693 tag has its unique UID and that most applications interact with a large number of tags, it is typically not possible to utilize the UID just to identify a single ISO/IEC 15693 tag. Any NFC/RFID reader may identify a tag as an RF430FRL152H by combining the Get System Information answer with the tag UID. The first two UID bytes are the obligatory 0xE0 byte (needed for all ISO/IEC 15693 compliant tags) and the manufacturer identification byte, which is 0x07 for Texas Instruments devices. If the UID is supplied, this is referred to as an addressed read, and only the tag with that particular UID responds. Addressed reads can be used to verify that the data received is solely from the RF430FRL152H tag by first identifying it.

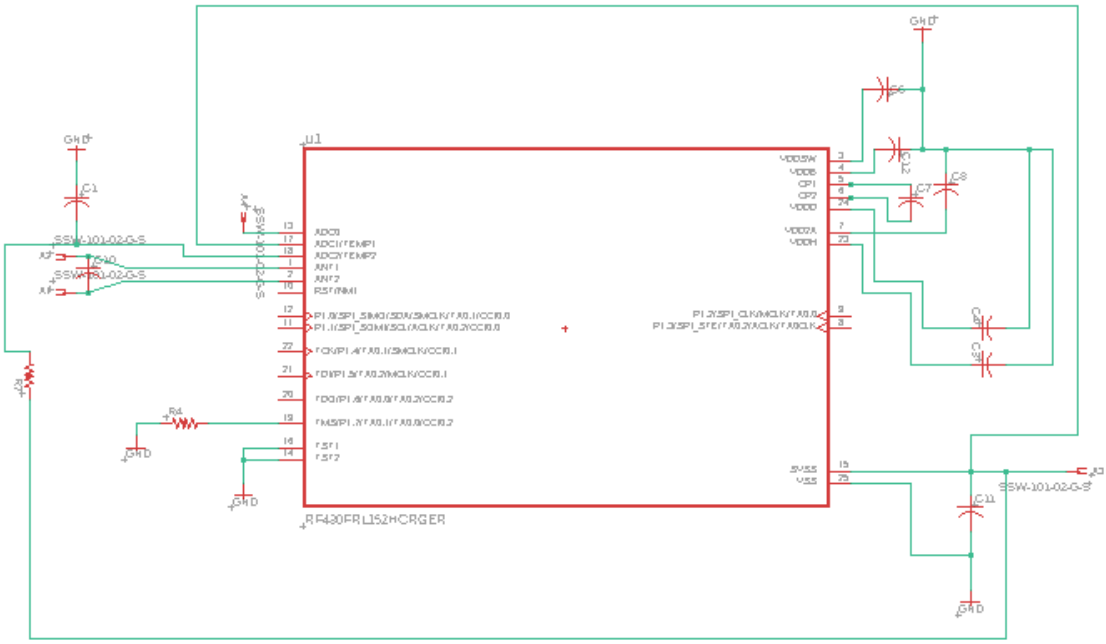

Figure 17. EAGLE Board schematic for RF430FRL152HCHRGER based sensor tag assembly.

The same procedure may be used with the Write Single Block command to verify that data is exclusively written to the RF430FRL152H. TI recommends using addressed

instructions for Write Single Block to ensure that data is exclusively written to the designated tag and not accidentally overwritten on other surrounding tags [132].

The Inventory command is the NFC command for initial tag detection, and it may be used for both single and multiple tag detection. When numerous tags are detected, the anticollision algorithm handles the tags and resolves all collisions. After identifying a tag or many tags, the Get System Information NFC command is used to detect whether a tag is a TI RF430FRL15xH transponder. If no tag is found, the procedure terminates. If an RF430FRL15xH transponder is discovered, the Write Single Block NFC command is used to set it up for sensor measurements. The sample firmware communicates ADC port settings, but these configurations can be adjusted to accommodate different specialized applications. The sensor data is read out after setup [149]. The NFC transmission is finished at this point. Using a custom-built android application and NFC library on the MSP430FR4133 and the raw data from the RF430FRL15xH transponder, the ADC values may be converted to glucose data. In this work, the fuel cell's glucose concentration is computed, and the resulting value is transferred to the smartphone to be displayed to the user. The procedure ends when the value is refreshed.

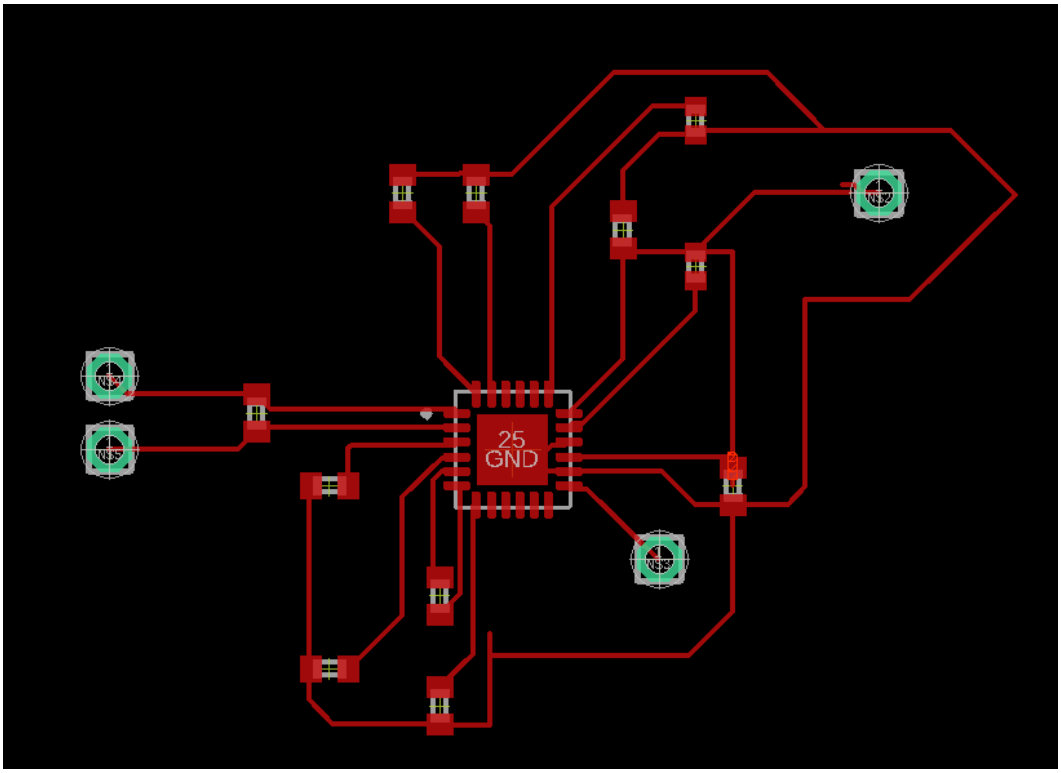

Figure 18. Board layout made on Eagle Autodesk for MSP 430 based assembly with external antenna of 13.56MHz.

The electrical voltage produced by this single biofuel cell was supplied as the input voltage for the RF430frl152H. The device is based on the NFC system technology. Figure 18 shows the board layout for a device made in the eagle software. The operating system is divided into two parts: the first is the wireless interface composed of the NFC chip and coil for wireless communication with smartphone. The second part is the biofuel cell interface with the NFC chip that reads the analog signal into 16-bit sigma delta ADC values. The circuit is designed following the guidelines established in the NFC chip datasheet, which includes an in-depth circuit diagram for operation of the NFC chip [133].

CHAPTER V

SMARTPHONE APPLICATION WITH DATA ANALYTICS

In this section the android application is configured with the near field communication module that allows the data to be received and recorded for further functionalities. An Android application framework is a software toolkit that allows app developers to assemble a final product that fits the needs of its owner. A framework serves as the structure for an application, which is then built out with visuals, animation, unique features, and functionality. The Android Application Framework, which includes NFC API [134], is the next layer. The Android NFC API supports NFC and enables developers to create applications that use NFC in all three communication modes (reader/writer, card emulation, and peer-to-peer mode).

This API's major classes are:

- NfcManager - used to obtain an instance of the NfcAdapter.
- NfcAdapter - represents the default adapter (NFC module), which is located inside the mobile device.
- NdefMessage - a class that provides support for reading and writing of NDEF messages.
- NdefRecords - represents NDEF records and provides methods for working with NDEF records.

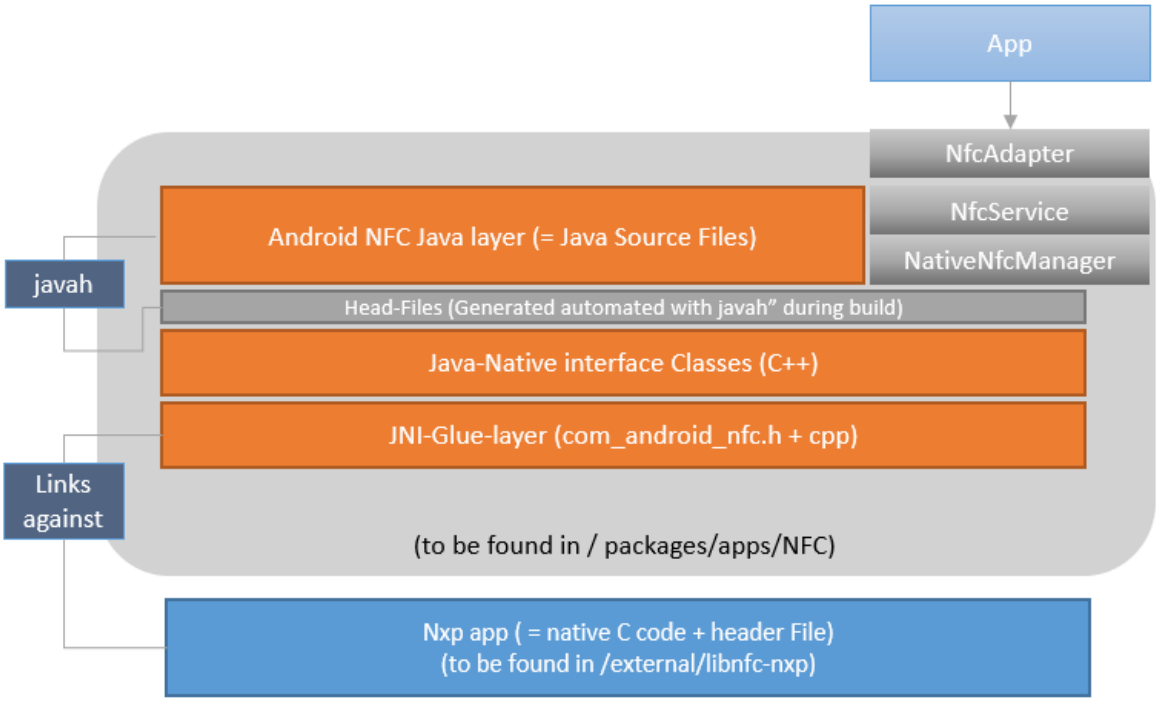

Figure 19. NFC software stack showing how the NFC modules are linked with the design process in the android application [134].

During the design process of an Android application, considerable attention is paid to core Android system components that are used in the application's implementation as shown in Figure 19. The following are the most essential features of the application's design that have been considered:

- definition of an Activity and possible states of Activity within the application
- definition of Intents
- structure of the Android manifest file

An Android application is made up of a main class that derives from the Android Activity class. An activity may be characterized as the main procedure in the program, and it is responsible for creating the application's window using the given user interface. Although an application may have one or more activities, only one may be designated as main [135]. The

Activity class implements methods that are responsible for transitions between distinct states of an Activity, and this is where the application begins.

For every Android application an Android manifest file must be specified. An Android manifest file contains information relevant for the Android system to successfully run an application [136]. This description, structured as an XML file, contains the following information:

- general information about the used Android version
- name of the application
- definition of permissions for accessing the individual smart phone’s hardware components
- definition of the application’s Intents
- main Application and User Interfaces

The main application's principal function is to provide capability for choosing between two or more user interfaces that demonstrate the target devices and executing the selected user interface. User interfaces graphically depict target devices and their appearances. Specific implementations are supplied for their functions and operations. User interfaces are meant to closely approximate the appearance and functionality of genuine target devices in order to improve the user experience of apps that represent target devices. As a consequence, graphical user interfaces that are simple, functional, and aesthetically appealing are built. Because each target device has its unique set of functionalities and actions, user interfaces are designed independently for each device [137]. The Android manifest file as shown in Figure 20 for the implemented application designates NFCAppActivity as the main class that implements the Activity and serves as the program's entry point. The Intent Filter is defined to inform the system of the application's intents, such as the intention to discover an NFC enhanced target device. Even when the application is not running and the NFC module identifies an NFC

upgraded target device, the system offers that the application be launched. Furthermore, the application's permissions are defined. In this situation, the application must be granted permission to utilize the NFC module.

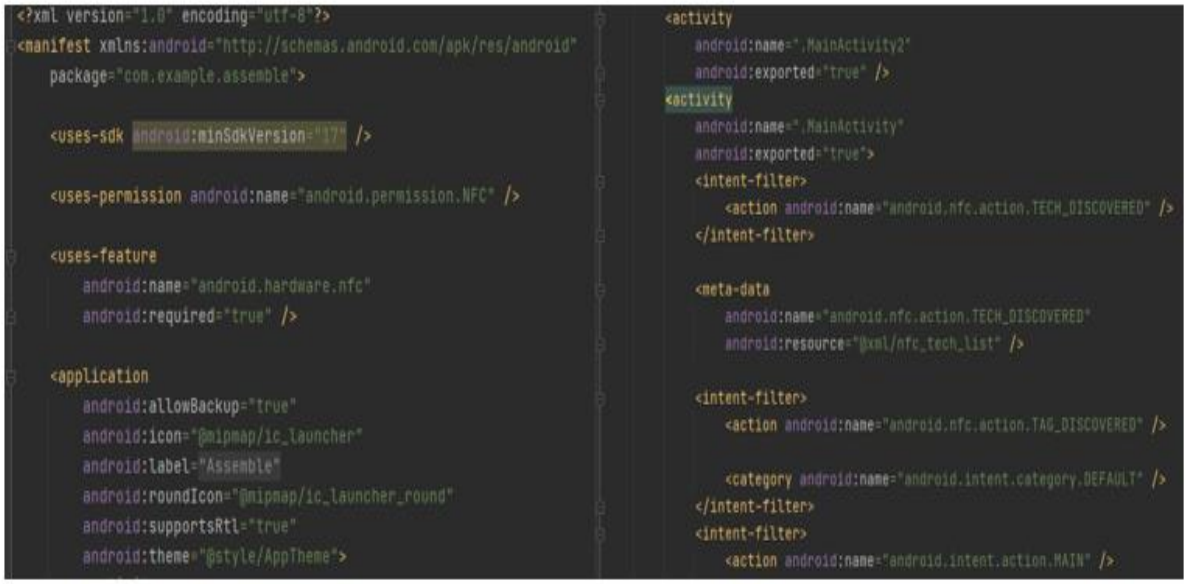

Figure 20. Code Snippet of an android manifest file displaying the structure.

Next one of the main task is the Basic Communication Library to provide functionalities for establishing connection and communication between the NFC module of the Android smart phone and the NFC [138]. The library consists of six classes and the following Android NFC API classes are used for the realization of this task:

- android.nfc.NfcAdapter
- android.nfc.Tag
- android.nfc.NdefMessage
- android.nfc.NdefRecord
- android.nfc.tech.IsoDep
- android.nfc.tech.Ndef

Figure 21 shows the relationship between the classes of the library. The core class of the library is NFCapp, and its instance is used by user programs and other libraries to establish connection with the NFC-app. At the top, library level, it serves as an interface and offers all essential communication activities. The NFC class controls the whole interaction with the NFC via the TagCommunicator and Node classes.

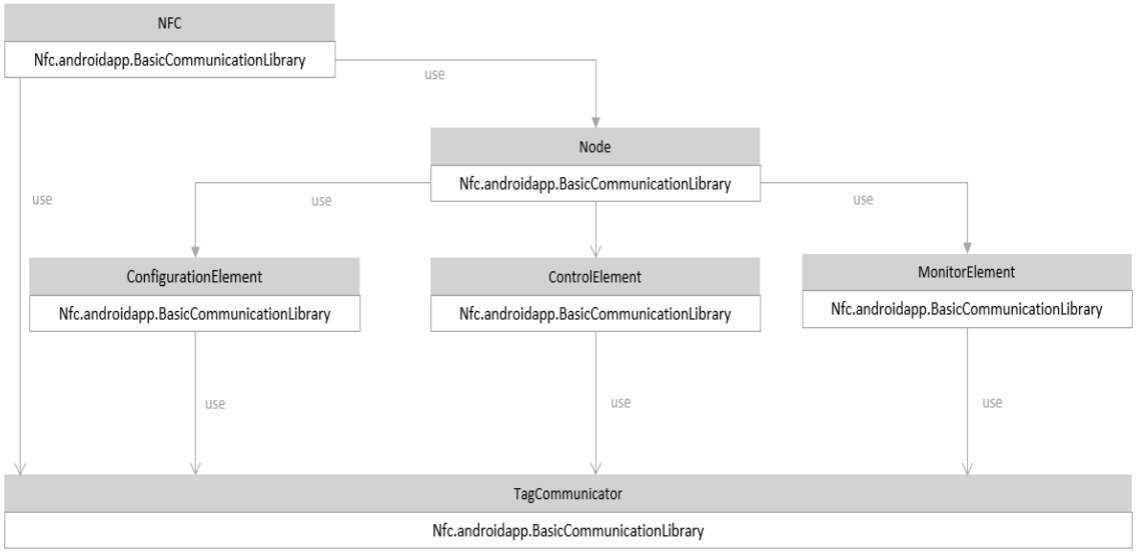

Figure 21. Android Smartphone – Basic Communication Library Class Diagram.

TagCommunicator is a low-level class which utilizes Android NFC API and other necessary packages to access and control the hardware NFC module [138]. This class provides methods for the following operations:

- detection of the NFC
- identification and activation of the NFC
- establishing the communication with the NFC
- accessing the NFC's NDEF tag application
- retrieving and writing the General Information Record

- native communication (sending C-APDUs and receiving R-APDUs)

When the user launches the Android program, the initialization procedure begins, and the application launches the primary user interface, which simply states that the application is ready and waiting for the Android NFC-enabled smart phone to discover the NFC upgraded target device. Furthermore, the application gains access to the NFC module and maps all NFC detections to itself. This is accomplished by specifying an Intent. Simply defined, the application expresses a desire to conduct specific activities with the detected tags or, in this example, the NFC upgraded target device. The program then waits for the NFC module to detect the target device and take control of it [139]. When the target device is discovered, the application uses an instance of the Basic Communication Library to connect to the target device and read the General Information Record. The program adjusts the user interface to one that matches the target device based on the information about the kind of NFC (target device). The procedure is repeated if the NFC module identifies another target device or if the current target device vanishes and reappears in the magnetic field of the NFC module. The reading of the General Information Record is completed before the program switches user interfaces, and the application now has access to information about nodes and their elements.

A distinct class with the name of the target device is defined as part of the application for each target device that is operated with the assistance of the Android application. User interfaces are created in such a manner that users can utilize them without difficulty to operate the target equipment. In other words, if the target device is a washing machine and the application is used to control the various washing programs for different clothing and temperatures, the application will provide an understandable user interface with graphics and explanations indicating the preferred washing program. This is performed via the usage of two

Android user interface packages android.view (block construction for user interface elements) and android.widget [140]. In addition, graphics and other resources are employed to develop the user interfaces as shown in Figure 22 with additional attributes declared. Event listeners are provided for each user interface element that conducts certain tasks. The native communication between the Android application and the NFC upgraded target device is executed when the user interacts with the user interface (e.g., by pressing a button). The instance of the NFC class is used by user application classes to communicate with the NFC upgraded target device.

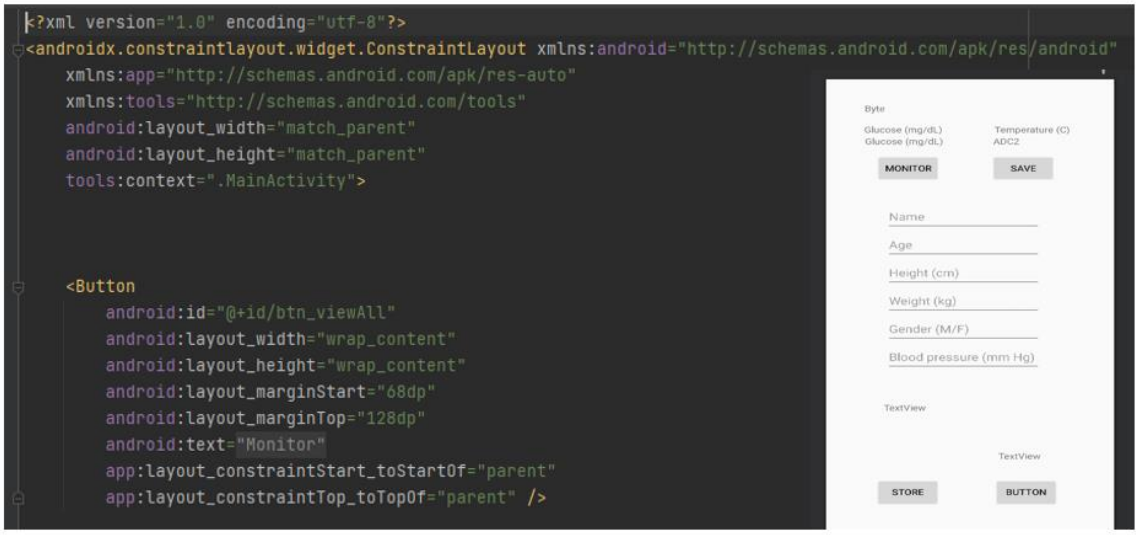

Figure 22. Code snippet for android view and widget application for initialing layout and applying parameters to a button.

The Android platform contains a system which is managing all the actions with regards to NFC and apps, called the NFC Dispatch System. The dispatcher mainly determines which app should receive the message when an NFC tag has been scanned [141]. There are three types of messages that can result from a scan: NDEF_DISCOVERED, TECH_DISCOVERED, and TAG_DISCOVERED. One of the scripts for tag discovery that, by using the intent filter, is displayed in Figure 23.

```
//communication and tag methods
private Tag currentTag;
private void resolveIntent(Intent intent) {
    String action = intent.getAction();
    //check if the tag is ISO15693 and display message
    if (NfcAdapter.ACTION_TAG_DISCOVERED.equals(action) || NfcAdapter.ACTION_TECH_DISCOVERED.equals(action)) {
        text_view.setText("Tag discovered!");
        text_val="Tag discovered!";
        //Log.i("life cycle", "NfcAdapter.ACTION_TECH_DISCOVERED");
        currentTag = (Tag) intent.getParcelableExtra(NfcAdapter.EXTRA_TAG);
        new NfcVReaderTask().execute(currentTag);// read ADC data in background
    }
}
```

Figure 23. Code snippet for tag discovery which uses NfcAdapter to check if the tag is ISO15693 and help in displaying the message of Tag discovered or not.

These three are prioritized in the presented order and which app they will go to depends on the following:

- content on Nfc tag (NDEF or not)
- any currently focused app requesting foreground dispatch
- nfc-filters in Manifest of installed apps

When an app expresses interest in receiving NFC events, it must always specify which events it is specifically interested in receiving. This registration can range from a particular registration, such as a specific URI pattern in an NDEF Record, to a wide wildcard registration of any NDEF Message and/or any NFC Tag technology. To guarantee that the app receives what it needs while not interfering with other Nfc applications on the device, developers must understand how the NFC dispatch mechanism on Android prioritizes and selects which apps (one or multiple) can receive the scanned Tag or NdefMessage [142]. This is done to avoid conflicts with other programs, if feasible. When there is a conflict, the user is provided with the application-picker, where they may select whether to send the NFC scan to an app once or by default. Figure 24 depicts a flowchart of the NFC dispatcher's decisions about Tag content and app filters.

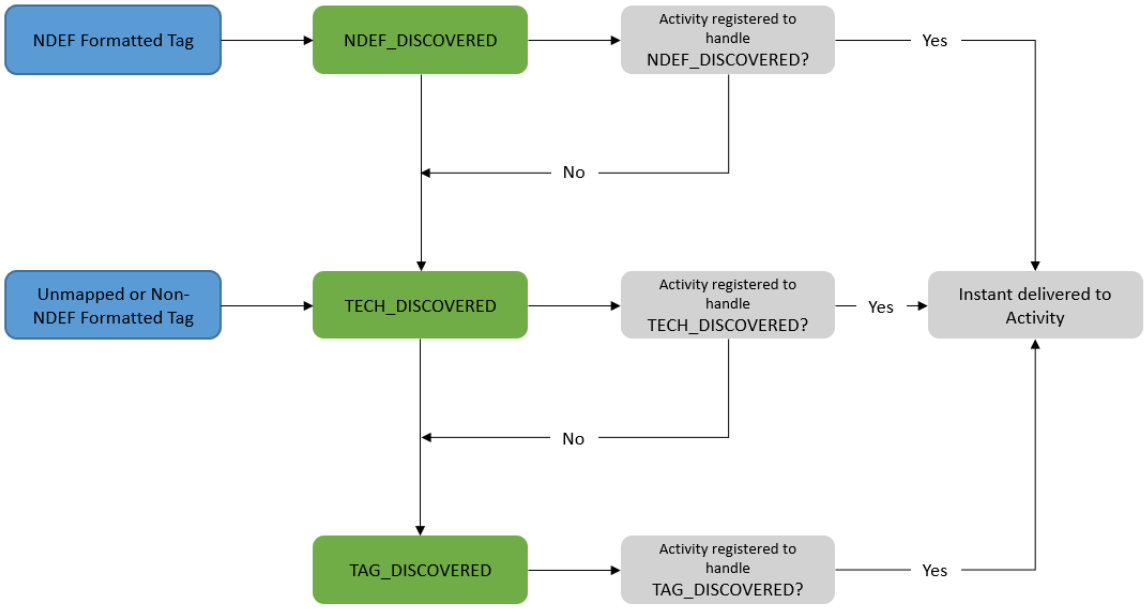

Figure 24. The priority of NDEF and tag dispatching by the android system [142].

An app registers interest in receiving NFC tags in two ways. The first involves the use of foreground listening, which can be engaged or stopped at any moment the program is running, is visible to the user and is active in the foreground on the device, and the other requires providing specific filters in the Manifest [143]. The foreground dispatch always takes precedence over other programs. The following filters are used for both foreground dispatching and manifest filtering:

- When filtering for TECH DISCOVERED was applied NfcV tag technology was used. When the tag did not contain an NDEF message or no app request matched it, these filters will not be iterated.

- Filtering for TAG DISCOVERED allowed to catch tags that did not match any TECH DISCOVERED requests. It was ineffective on its own since any higher priority event overrode it. Having only the TAG DISCOVERED filter in its Manifest allowed it to capture unknown tags while avoiding conflicts with other apps.

FIREBASE DATABASE

In this work, all acquired data will be kept on a cloud database (Firebase Realtime Database), forming temporal series that the patient/physician may view on the online platform. The patient will be able to input information such as blood pressure, heart rate, glycemia, and so on and events (other physical examinations).

Firebase is an online application and mobile development platform created in 2011 by Firebase, Inc. and acquired by Google in 2014 [144]. It provides several services that are extremely useful for creating online and mobile apps, including Firebase Authentication, the Realtime Database, and Firebase Storage. These services are simply linked into apps by utilizing an API key for the web and an SHA-1 key for Android. Firebase provides a service for managing user authentication across many paradigms. Aside from the Email-Password paradigm, Firebase authentication allows directly authentication of a user using his/her Google, Twitter, Facebook, or GitHub profiles, among others [145]. The Authentication service also includes several models for creating Email and SMS conversations. For example, there is a model to validate the email address used to establish an account or to reset the user's password if it is forgotten. Following the creation, each user is assigned a Uid, a unique identifier that is unrelated to the user's information or the authentication provider. That identity will be utilized in the database for two reasons: first, the database's rules can manage Uids to restrict access to a certain branch to the person who owns it, and second, this can make the database anonymous.

Firebase Realtime Database is a cloud database that is NoSQL ("non-SQL," which means it is not based on Structured Query Language). Data is synchronized in real time and remains accessible even if the program is shut off. Data is saved in the JSON (JavaScript Object Notation) format, which has a tree structure [146]. Because it is a real-time database, data

synchronization is used instead of traditional HTTP queries. This implies that if data changes, the linked devices receive an update within milliseconds. The onDataChange() function must be called when the program wants to read a database snapshot. Because the Firebase Realtime Database SDK (Software Development Kit) maintains data in local storage, Firebase apps stay responsive even while offline. When communication is restored, the client device receives any updates it missed, bringing it up to date with the current server state. Firebase also allows for the creation of programmer defined rules for accessing the database [147]. To access data, users must be logged in, but they may be redefined using the Firebase Realtime Database Security Rules, a versatile expression-based rules language with an example shown in Figure 25. This enables more precise control over who and how each database branch may be accessed.

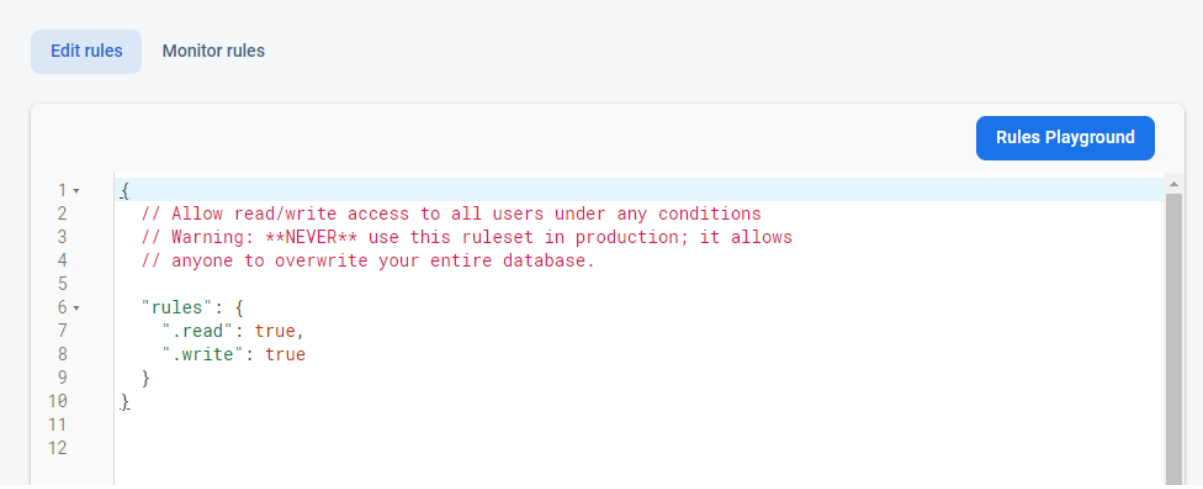

Figure 25. Basic rules in firebase database that allows any patient to edit the storage recordings.

The Firebase Realtime Database can handle up to 100,000 simultaneous connections, where a simultaneous connection is defined as one mobile device, browser, or server app connecting to the database [148]. It is critical to note that the maximum number of users is not the number of users that are connected at the same time. For example, apps with tens of millions of users often have fewer than a hundred thousand concurrent users. However, by creating numerous databases, it is feasible to go over this limit [149]. Each database can send roughly

100,000 replies per second, which is the maximum number of concurrent reading activities on the database as seen in one of the examples in Figure 26.

With UTF-8 encoding, the maximum size of a string is 10 MB. Each letter in UTF-8 is represented by 1 to 4 bytes; however, only 1 byte is required for each of the 128 characters in the ASCII alphabet [6]. Therefore, each string can be 5/10 million characters long. A single write request should be no larger than 256 MB through the REST API and no more than 16 MB from the SDKs [150]. The amount of RAM that the complete database can occupy in total varies depending on whether it is utilized for free or for a fee. The free version utilized for this thesis work has a memory limit of 1 GB [8].

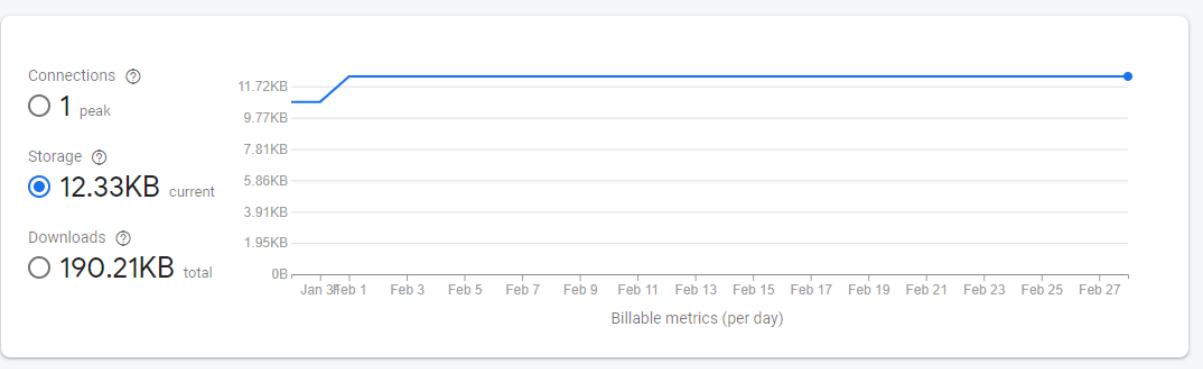

Figure 26. Storage metrics based on a month usage with connections and download speeds.

The application database rules specify who has access to each database branch and how they may access it. Using Uids as database keys allows the restriction of access to a certain branch to the user who owns it, via the $uid key of the Firebase Realtime Database Security Rules language. The patient branch is the one that is edited via the Web Application, so only physicians have writing access, but the information within must be viewable on the Android Application so that each patient may read their own record [151]. Data and events branches can be read and written by both physicians and patients, with each patient having their own;

however, the physicianUid branch can only be viewed by physicians. This is the one utilized in the web application

JSON (JavaScript Object Notation) is a simple data-transfer format. It is a language-independent text format that employs patterns known to the C-family of languages [152]. These characteristics make it a suitable data-transfer language. JSON is composed of two structures, a grouping of Key/Value pairs and a set of values in descending order.

These two data structures are well-known, and they are supported by all current programming languages in some form or another. As a result, JSON is a data format that is easily understood by multiple languages [152].

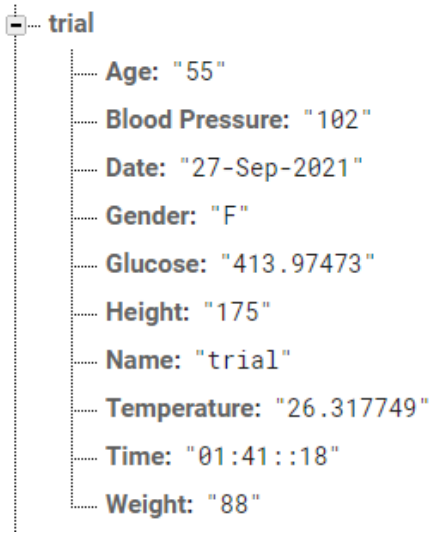

Figure 27. Storage format in J-SON for a test patient with other independent parameters.

Firebase Security Rules for Cloud Storage, like the Realtime Database, makes it simple to set storage access permissions. The fundamental rule is that users must be authorized in order to access files, but it is simple to specify certain paths that can be read and written only by specific users [153]. The patient's information is saved in the patient’s branch. The first

portion of the list of parameters is shown in Figure 27. The Data section comprises all the patient's health records. Data from the most recent examination are preserved in the History branch. This is the section of the database where patients save data using the Android App as shown in Figure 28. Each piece of information is saved in the appropriate branch with the date of the chosen day. It is natural for a person to not engage in all forms of physical activity on a daily basis, so the system automatically manages the missing fields [154].

Figure 28. Data communication using Firebase Realtime database.

MACHINE LEARNING

Glucose level monitoring is an essential part of diabetes self-management; diabetes patients and their families utilize it to make proper day-to-day treatment decisions about nutrition and physical activity, as well as insulin or other medication [155]. Zecchin et al. [159] have shown that by forecasting future glucose levels and informing patients when their blood sugar drops too low, patients can avoid hypoglycemic crises. Type 2 diabetes patients, on the other hand, are frequently less knowledgeable about their condition and do not always know what to do with their blood sugar monitoring data to keep their blood glucose within a reasonable range. That is why an application that advises these patients while precisely predicting and visualizing the impact of their actions on their future blood glucose results might

be useful. It can provide patients with a far better understanding of how their present behavior (mostly food consumption and physical activity) affects their future blood glucose levels and, as a result, how they should modify their behavior. It is critical that this application provides a relatively accurate forecast since an erroneous prediction may cause patients to take too much insulin (possibly resulting in hypoglycemia) or to inappropriately change their behavior (potentially causing hyperglycemia). It may also cause patients to lose faith in the application, making it less likely that they would change their behavior as a result.

This study aims to predict blood glucose levels 30 minutes to 120 minutes in the future (this is called the prediction horizon). This is believed to be the most helpful prediction horizon since a patient's blood glucose during this time is most impacted by behaviors (such as eating) at the time of the forecast. A secondary study aim is to establish how the prediction model should be used in a real-world application and whether it is preferable to train a different model for each patient or to utilize a patient-independent model. Finally, it is important to determine which input properties are critical for creating good predictions and how a prediction model acts. The blood glucose predictions in "Smartphone-based individualized blood glucose prediction" [157] is likewise based on manually submitted blood glucose measurements and physical activity, but they additionally incorporate diet and sleep. They have claimed to have developed a more accurate prediction of blood glucose using a mix of patient-based and population-based information. They are, however, employing a small and very contrived dataset [158], and it appears that they did not utilize a separate test and validation set, rendering purported speed benefits by clustering, for example, possibly inaccurate (could simply be overfitting to the dataset).

In Juang et al. [159] an algorithm is developed to predict the occurrence of hypoglycemia (too low blood glucose) using machine learning, but there was no attempt to

directly predict blood glucose levels. Because insulin management is so important for type 1 diabetes patients, more research is being conducted with the goal of precisely predicting blood glucose levels in type 1 diabetes patients. Because the dynamics of type 1 and type 2 diabetes are so similar, several studies believe that the performance of models employed for type 1 diabetes will generally transfer to type 2 diabetes [160]. Cunningham et al. [161] made no distinction between the two categories. However, in some models, type 2 diabetes is actually more difficult to simulate than type 1 diabetes since the model must also account for insulin that the body is still producing (which is not a factor in adult type 1 diabetes patients). It turns out that having more input characteristics improves prediction model accuracy, and it is believed that this is true for type 2 diabetes patients as well. As the prediction horizon (PH) is raised, performance suffers. Although the models are not directly comparable, hybrid models that combine Compartmental Models (CM) with a data-driven model such as Recurrent Neural Networks (RNNs) appear to have the lowest error [162].

An autoregressive model is a regression model that predicts the next value based on its own prior values. For example, we might use the last three blood glucose measurements to forecast the blood glucose in 60 minutes, using a weighted sum in the form of equation 1:

$$y_{60} = a*x_{-30} + b*x_{-15} + c*x_0 \quad (1)$$

where y_t is the predicted blood glucose at time t and x_t is a previous blood glucose value at time t . We can easily determine the optimal parameters for a, b and c by minimizing the error between the actual blood glucose value and the predicted value for all available data points. The number of previous values used as input to the model is a crucial consideration while training an autoregressive model [163]. In general, the most recent known value has the strongest connection with the value that must be predicted, and this correlation decreases when

values further in the past are considered. This means that when more past values are provided as extra input, the performance gains decrease.

Neural network regression

An artificial neural network (ANN) is a form of computing model that is loosely based on how neurons in biological brains work. When a neuron in the brain gets a signal from its dendrites, it fires a signal through its axon, which branches out to the dendrites of several additional neurons. Each neuron may learn by changing the weight it assigns to various inputs from other neurons.

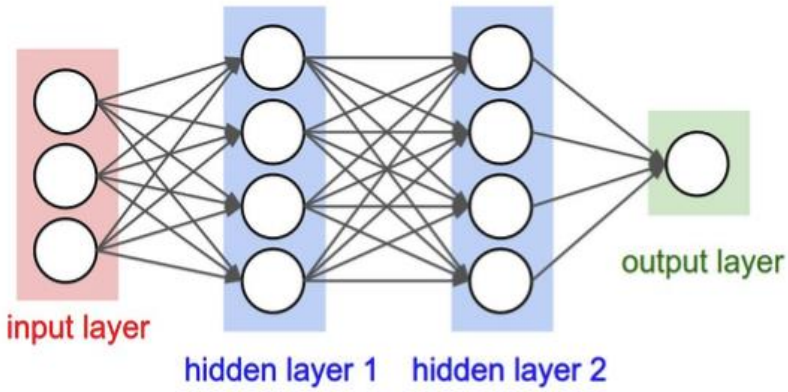

Figure 29. Graph visualization of a neural network [165].

In the computational model, each artificial neuron has one or more inputs that are weighted and summed with an additional bias, and then an activation function is applied to this value, which is comparable to a set threshold of when a neuron fires. Training an artificial neural network means optimizing these weights and biases for each neuron. The computational model based on a biological neuron was first presented in the 1940s [164], but it has only recently gained popularity due to other algorithmic breakthroughs (such as backpropagation [161]), higher computer power, and more accessible data.

A neural network is often represented graphically by a graph structure (see Figure 29) with each node representing a neuron and the connections between neurons representing weights. We receive a given output by putting input into the network from left to right, which we can compare to the predicted output using a cost function.

Using the Mean Squared Error (MSE) as an example with equation 2:

$$MSE = \frac{1}{N}\sum_{i=1}^{N}(y_i - \hat{y}_i)^2 \qquad (2)$$

where N is the number of cases, y represents the real value of the input and y_i represent the predicted value of input. We compute the derivative of this cost with respect to the model's weights and biases to determine in which direction to adjust these parameters in order to reduce the cost (this is called backpropagation). The model may then be improved repeatedly by continuously feeding a batch of data into the network and adjusting the weights and biases depending on the derived derivatives as shown in Figure 30.

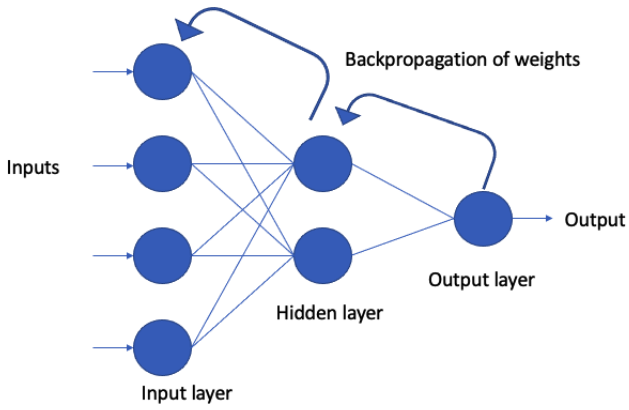

Figure 30. Backpropagation model visualization.

Overfitting is a typical issue with neural networks. This suggests that the network has become too acclimated to the noise of the training data and will therefore perform poorly on

new data (it does not generalize effectively). Weight regularization is one approach to attempting to overcome this problem. This entails assigning a cost to the weight parameters, providing the network an incentive to keep the weights as low as possible. Dropout is a relatively modern strategy for avoiding overfitting [165]. During each training cycle, a certain fraction of randomly chosen neurons is not taken into account. This avoids neuron co-dependence and makes it more difficult for the network to overfit on the training data.

Recurrent Neural Network

Another difficulty with traditional artificial neural networks is that they are unsuitable for use with sequential data. Assume we wish to use neural networks to anticipate the next word in a phrase. This would need knowledge of the previous words in the statement. We may opt to feed the past five words into the network and see whether the network can predict the next word with the architecture diagram shown in Figure 31. However, it is possible that information from a few lines before is needed to figure out which word follows next [166]. We may utilize a recurrent neural network (RNN) architecture to handle this problem. The neurons in the buried layer in this design can receive additional input from their prior state. This prior state is also linked by weights learned by backpropagation. It is feasible to preserve knowledge about previous inputs while just feeding the network data for one timestep in this manner.

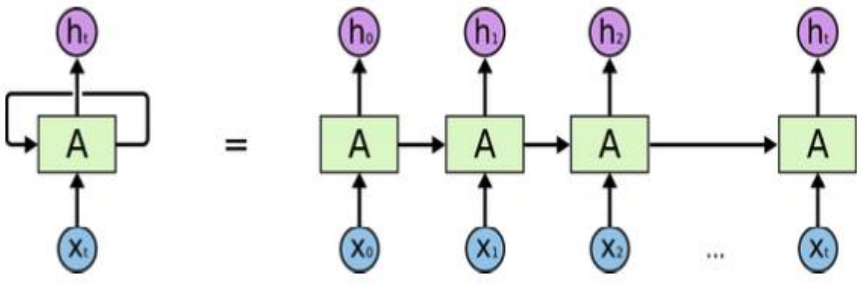

Figure 31. Graph visualization of a unrolled recurrent neural network [166].

The vanishing gradient problem is a common issue with this architecture. This is the phenomenon in which, as the network computes the gradient of the cost function based on an input many timesteps in the past, the gradient can vanish (become very small) due to a large number of computation steps between the output and an earlier input. In reality, this means that the network has a difficult time learning long-term dependencies.

Long-term memory networks

Hochreiter et al. [167] presented an adaption to the regular recurrent neural network (RNN) architecture to address the issue of vanishing gradients and make it simpler for a neural network to learn long-term as well as short-term dependencies.

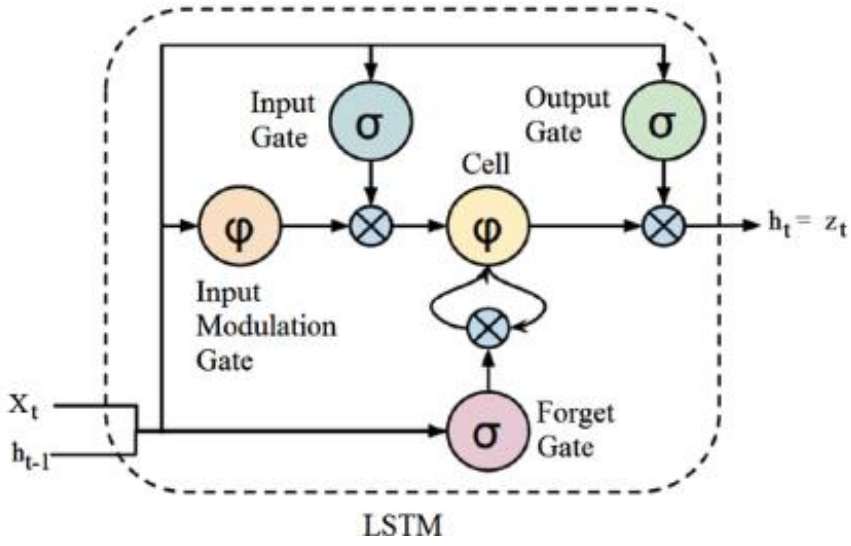

Figure 32. LSTM architecture using different gates [167].

This architecture as shown in Figure 32, known as the long short-term memory (LSTM) network, extends the standard RNN by adding gates to the hidden layer. These gates are essentially just extra weight parameters that the network uses to select which information from

the prior hidden state information from the current input to utilize, information to forget, and information to remember. Because these weights are all differentiable, they can also be optimized via backpropagation. RNNs have difficulty learning long-term dependencies with LSTM models essentially being the extension of RNNs' memory. Applying the LSTM twice as in bidirectional and stacked models leads to improvement in learning long-term dependencies which will consequently improve the accuracy of the model.

Bidirectional long-short term memory (bi-lstm) is the technique of allowing any neural network to store sequence information in both ways, either backwards (future to past) or forwards (past to future). Our input runs bidirectionally, distinguishing a bi-lstm from a conventional LSTM. We can make input flow in only one direction using a conventional LSTM, either backwards or forwards.

Stacked LSTMs or Deep LSTMs have been used in voice recognition, beating a benchmark on a difficult standard issue. Stacked LSTMs are already a well-established approach for solving difficult sequence prediction issues. A Stacked LSTM architecture is an LSTM model made up of many LSTM layers. An LSTM layer above sends a series of values to the LSTM layer below, rather than a single value. There is one output time step for each input time step rather than one output time step for all input time steps. The challenge is that most statistical measures summarize a large dataset to a single value, so it provides only projection of model error categorizing a certain aspect of error of the model performance. For time series forecasting, RMSE comes into consideration which measures the square deviations to keep the positive and negative deviations from canceling one another out.

The error metrics used to measure and compare the performance of the two baselines and the support vector regression S model are described. These measurements are Mean Absolute Error (MAE), Root Mean Square Error (RMSE). The mean absolute error represents

the average overall error between the actual and predicted values. The definition is given in equation 3.

$$MAE = \frac{\sum_{i=1}^{n} |y_i - \hat{y}_i|}{n} \quad (3)$$

where y is the actual value, $\hat{y}$ is the predicted value, and n is the number of test examples. The Root Mean Square Error is similar to the standard deviation of the error as seen in equation 4

$$RMSE = \sqrt{\frac{\sum_{i=1}^{n} (y_i - \hat{y}_i)^2}{n}} \quad (4)$$

where y is the actual value and $\hat{y}$ is the predicted value.

CHAPTER VI

ELECTROCHEMICAL CHARACTERIZATION

Electrochemical characterization is used to investigate the electrochemical behavior of materials under different electrochemical circumstances. There are three types of electrode systems in an electrochemical cell: two-electrode systems, three-electrode systems, and four-electrode systems. Any of these electrode systems can be used to perform electrochemical characterizations. A working electrode and a counter electrode make up an electrochemical cell. The potential of the working electrode is proportional to the concentration of the analyte. The circuit is closed by the counter electrode. The working electrode's potential is determined in relation to the counter electrode, which serves as a reference potential. As a result, the potential of the counter electrode is constant. If the potential of the counter electrode is not constant, two electrodes are used to complete the electrical circuit: a reference electrode with a constant potential and an auxiliary electrode. The area of the auxiliary electrode is large enough to handle the current flowing through the circuit.

In a two-electrode setup, the setup consists of only two electrodes, the working electrode and the counter electrode, which function as a two-electrode system to characterize the electrochemical cell. As a result, the voltage measured in the two-electrode system is the voltage between the counter and the working electrode, which is the cell voltage.

Cyclic voltammetry

Cyclic voltammetry (CV) is the most fundamental electrochemical test for materials. The current is measured by sweeping the potential back and forth (from positive to negative and negative to positive) within the predetermined limits. The information gained by CV may be utilized to describe the material's electrochemical behavior. A graphical study of a cyclic voltammogram yields the redox peaks (reduction and oxidation peaks), therefore enabling the

prediction of the capacitive behavior of the electrode. From this curve in Figure 33, the potential for oxidation and reduction of the material may be determined.

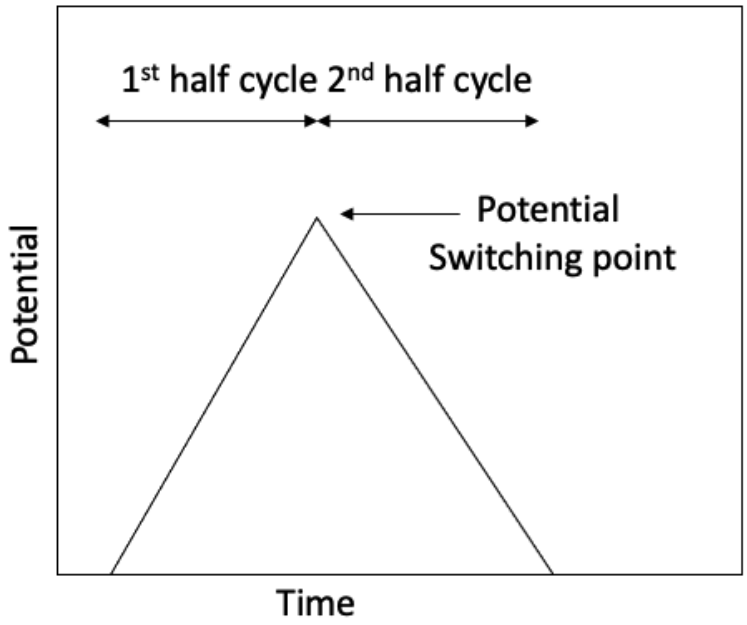

Figure 33. Schematic for Cyclic Voltammetry.

In a CV, a ramp signal is used as the input signal. The forward scan is given a positive ramp (with a positive slope), while the voltage is switched after the first half-cycle, which is followed by a negative ramp, essentially inverting the nature of the cyclic voltammogram for the next half-cycle. The system returns to the starting point as it attempts to achieve equilibrium through redox reactions. It follows a cyclic pattern, which provides information about the changes that the system has undergone. By carefully evaluating the CV curve, one may draw numerous key inferences about the material and its characteristics (such as capacitive nature, for example), as well as the system behavior. The CV experiment can be performed with a single cycle or with numerous cycles. The scan rate is defined as the slope of the ramp signal given in volts per unit time [168]. This scan rate can range from a few millivolts per second to several hundreds of volts per second. The system's scan rate may be changed to acquire a better

understanding of the cell's electrochemistry. As a result, the scan rate is critical in determining the voltammetric behavior of the material to be evaluated. The oxidation and reduction peak currents, as well as peak potentials, may shift depending on the scan rate. Due to the existence of electroactive species at the electrode's (working electrode) surface, a faster scan rate leads to a greater number of redox reactions. With a slower scan rate, however, there is a chance of missing the peak (either forward or reverse scan peak) because the products of the reduction or oxidation have enough time to engage in a chemical process whose products may not be electroactive. The Randles - Sevcik equation may be used to compute the peak current in the CV from equation 5:

$$i_p = 2.69 \times 10^5 n^{\frac{3}{2}} AC\sqrt{\nu D} \qquad (5)$$

where i_p is the peak current, n is the number of electrons in the redox reaction, A is the area of the working electrode, C is the concentration of the electroactive species at the electrode, D is the electroactive species diffusion coefficient and ν is the scan rate.

All of these characteristics are important in calculating the peak current in CV. From a CV, the electron transfer coefficient (number of electrons transferred), rate-limiting factor (factor limiting the pace of the reaction), and rate constant of the process can be determined. As shown in Figure 34, the difference between the two CV peak potentials indicates the influence of the analytes' diffusion rates. The ratio of currents peaks of cathode and anode may also be used to determine if the system is reversible, irreversible, or quasireversible. If the ratio is equal to one, it signifies that the anodic and cathodic peak currents are the same, and it indicates that the system is reversible. Because the CV is taken in a scenario where the solution is held undisturbed, the current peaks are essentially acquired; otherwise, the peak current may be substituted by the limiting current. The CV provides comprehensive capacitance behavior

by monitoring it at various sweep speeds. It also offers a sense of the material's specific capacitance, which may be computed using the formula 6:

$$C_s = \frac{\int IdV}{vm\Delta V} \qquad (6)$$

where ΔV is the potential window (V), m is the mass of electroactive material (g), and v is the scan rate (mV/s), and IdV is the area under the curve in the plot of I and V.

The pH of the medium also has a significant impact on the electrode response. In the case of polymers, CV can readily anticipate the electrochemical behavior of the polymer by utilizing the band gaps, electron affinities, and work functions of the materials [168]. As a result, CV is utilized to investigate the compound's chemical and electrochemical characteristics. In addition to the benefits listed above, CV can aid in the functionalization of materials by executing different redox reactions with numerous scans.

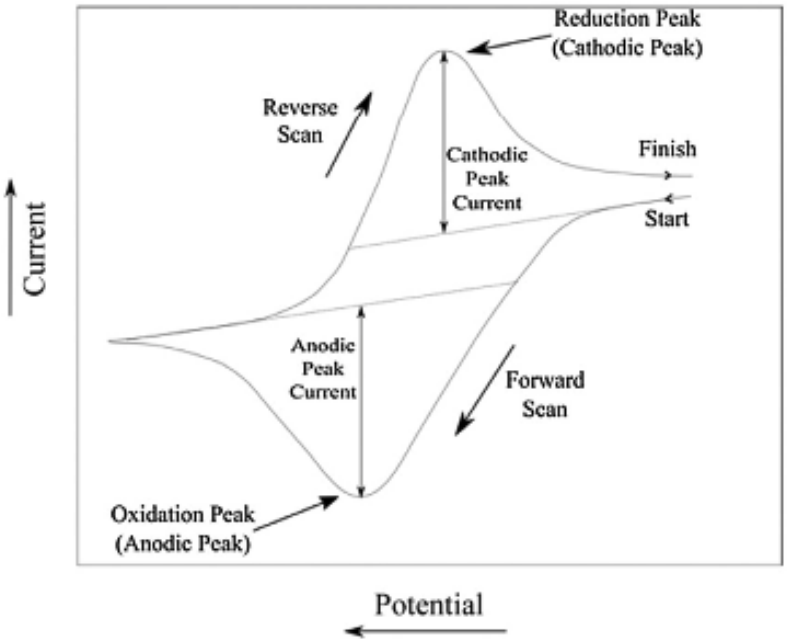

Figure 34. Cyclic Voltammetry waveform with description based on the process [168].

Chronoamperometry

A constant voltage is given to the working electrode in amperometry, and the current is measured as a function of time. Amperometry is utilized in flow systems to identify analytes. As a result, analytes from a patient's body can be identified even in vivo because the bulk of the human body is made up of liquid flows. Amperometry may also be utilized for sensor research, and portable amperometric sensors can be built. Chronoamperometry (CA)varies the input potential and records the resultant current fluctuation as a function of time. CA is based on Cottrell's equation 7:

$$i(t) = nFAC\sqrt{\left(\frac{D}{\pi t}\right)} = \frac{k}{\sqrt{t}} \qquad (7)$$

where *n, F, A, C, D, t,* and *i* are the number of electrons, Faraday constant, electrode surface area, analyte concentration (electrochemically active species), diffusion coefficient, time, and current, respectively.

Fick's second law of diffusion is used to generate Cottrell's equation. It aids in determining the diffusion coefficient D (cm^2/s) of the electroactive species present on the surface area of the working electrode. It predicts the variation in current over time (current time response or chronoamperometric response) when a potential step is applied in the presence of a significant overpotential. The Cottrell equation is only true in the situation of a diffusion current, which is essentially the diffusion of the analyte to the electrode surface.

CA provides the present time (I vs t curve) response since it follows the Cottrell equation as shown in Figure 35. The curve's behavior is Cottrellian, where the current is determined by the inverse square root of the time from equation 8:

$$I \propto \frac{1}{\sqrt{t}} \qquad (8)$$

where *I* is the current and *t* is the time.

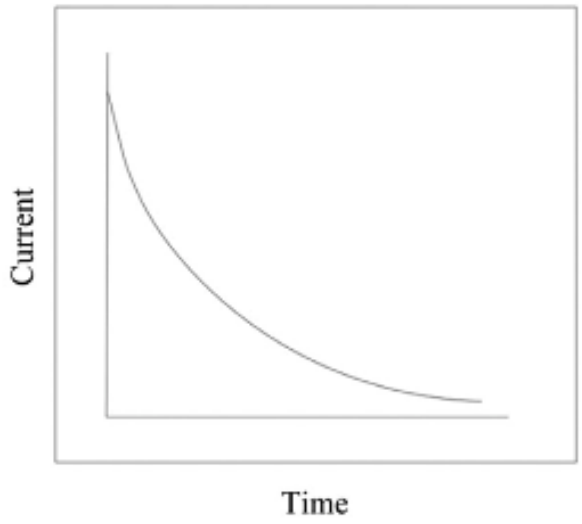

Figure 35. Graphical representation for current vs time in chronoamperometry process [168].

Initially, the working electrode is provided the step input potential, which raises its potential from the point where no faradaic reaction occurs to the point where the surface concentration of the electroactive species becomes zero, resulting in a fading current profile. The *I* vs *t* curve depicts the variance in the surface neighborhood's concentration gradient. A potential pulse is delivered to the working electrode at regular time intervals. CA may also be used to investigate the mechanisms of electrode processes [168].

Linear Sweep Voltammetry

Linear Sweep Voltammetry (LSV) is a fundamental potentiostatic sweep technique. It's the same as a one-segment cyclic voltammetry experiment. Working electrode potential is linearly swept between final and beginning values in LSV, and current is monitored as a function of time. The most frequent result of an LSV experiment is a voltammogram, which shows current vs. potential. LSV sweeps the potential vs. reference electrode in one direction, generally via the electroactive species to allow analysis of the ensuing electrochemical species formed at the electrode surface. Potential is swept linearly from a starting to a final potential in an LSV experiment, with current sampled at defined intervals. LSV delivers both qualitative and quantitative information about electrochemical systems and has proven itself a quick and dependable characterization technique. LSV is commonly used to study the kinetics of electron transfer reactions, including catalysis, and has since been extended for use in sensor and biological system evaluation, organic and inorganic synthesis, and in fundamental physical mechanics of electron transfer reactions, like reversibility, formal potentials, and diffusion coefficient determination.

Linear sweep voltammetry, like cyclic voltammetry, employs a three-electrode setup. A working electrode, a counter electrode, and a reference electrode are included. The three electrodes are linked by a potentiostat and put in an electrochemical cell containing the solution of interest. The potentiostat regulates the potential between the working and reference electrodes and monitors the current at the counter electrode to create a potential vs. current diagram. At the potential where oxidation or reduction begins, a peak or dip might be visible. Linear sweep voltammetry may be used to compute the peak current, peak current potential, and half-peak current potential. Several crucial factors can be measured using linear sweep voltammetry to identify a material's thermodynamic reversibility. These metrics include the

peak current (ip), the potential at the peak current (Ep), and the potential at half the peak current. These can be interpreted in this context for the system $O + e^- \rightleftharpoons R$, where R is absent initially (i.e. assuming no coupled reactions). At the reversible and quasireversible limits, these values can be used to calculate key electrochemical parameters. The LSV in a fuel cell permits the I-V characteristics to follow the same pattern as an ideal electrical circuit component (i.e. Ohm's law). More losses, such as kinetic loss (charge transfer), activation loss, mass transport loss (concentration), and ohmic loss (ion and electron transport) can be determined for any electrochemical system. Because the V/I ratio is not always constant, these losses influence the I-V characteristics curve.

CHAPTER VII

MATERIALS & METHODS

Materials

Silver nitrate, polyethylene glycol 3000 (PEG), sodium hydroxide, D (+) glucose, potassium phosphate monobasic, sodium azide, and Nafion were obtained from Sigma-Aldrich. The platinizing solution was purchased from YSI Inc., and NGP-J gold nanoparticle ink was acquired from Iwatani Corporation of America. The multiwalled carbon nanotube NINK-1000 was obtained from Nanolab, Inc. Gluconacetobacter xylinus (ATCC 10245) was purchased from ATCC. Hydrosulphite of sodium medium (HS medium) was purchased from Himedia Laboratories. All the solutions were prepared with 18.2 MΩ-cm Milli-Q water. Platinum counter electrode, Ag/AgCl reference electrode, and PalmSense4 potentiostat were purchased from BASI Inc. The S882Z charge pump integrated circuit (IC) was obtained from Seiko Electronics.

Bacterial nanocellulose synthesis

The Gluconacetobacter Xylinus culture was maintained in sterile HS medium as static cultures at 30 °C. Briefly, the cell pellet was rehydrated in HS medium and transfered to a 50 mL conical tube containing 5 mL broth at 30 °C to establish good growth for 72 h. To generate the inoculum, the pellicle was removed to disperse the cells by vortexing at maximum speed for 1 min. The suspended bacteria (1 mL each) solution was transferred to a fresh 50 mL HS medium in sterile 100 mm crystallization dishes. The inoculated crystallization dishes were incubated at 30 °C undisturbed for 1 week. The bacteria were fed at 1-week intervals by carefully adding 50 mL of HS medium to enable the formation of subsequent pellicles for a total of 6 weeks to form 6 uniform pellicles. To harvest the bacteria nanocellulose, the pellicles were incubated at 90 °C in 0.5 M NaOH for 1 h to denature the bacteria. The pellicles were

extensively washed in Milli-Q water for 48 h to remove the NaOH and achieve neutral pH. The washed pellicles were stored 0.02% sodium azide solution at 4 °C prior to use.

Electrode Fabrication

The bacterial nanocellulose pellicles were placed on 3-inch PET wafers, smoothed in Milli-Q water to remove all air bubbles, and allowed to dry at room temperature overnight prior to printing on the BNC substrate. Figure 36 provides an illustration of the electrode pattern with an overall dimension of 15 mm × 10 mm designed using CoralDRAW. A semicircle and a larger circle (r = 5 mm) shape design were implemented for the cathode and anode, respectively. The .bmp file was exported to the Fujifilm Dimatix 2850 Materials Printer to be converted to a .tf file for printing. The software then was configured with the thickness of the substrate (130 μm bacterial nanocellulose on PET), printing layers (2 layers), and jetting speed (50 Hz) for printing the electrodes. The NGP-J gold ink (650 μL) was injected into a DMC-11610 cartridge (10 pL drop-size) tank using a syringe followed by capping of the cartridge with the nozzle head. The platen and cartridge temperatures were set at 45 °C and 28 °C. A printing resolution of 1016 DPI was used, with the jetting voltage range between 22 and 25 V and all 16 jets were used. After printing, the substrate was dried in a conventional oven for 90 min at 85 °C to dry the ink, and then cooled to cool temperature overnight before the preparation of the fuel cell.

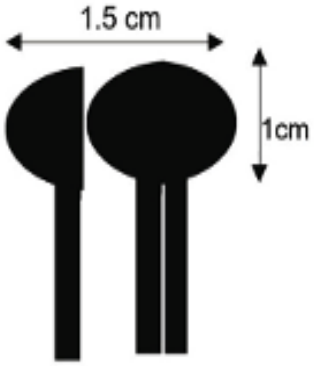

Figure 36. Coral draw design for electrode fabrication.

Preparation of Au-co-Pt

The dried printed electrodes were rinsed with isopropanol (IPA) for 5 min and dried with nitrogen gas to remove any impurities from the surface. Colloidal platinum (co-Pt) was electrodeposited on the anodic electrode using a three-electrode configuration consisting of the anodic working electrode, platinum counter electrode, and Ag/AgCl reference electrode immersed in platinizing solution. The co-Pt was electrodeposited onto the surface on the printed gold electrode at an applied potential of − 225 mV vs. Ag/AgCl for 1500 s. The electrode was then washed with Milli-Q water and dried at 80 °C for 30 min, followed by cooling in ambient air as shown in Figure 37.

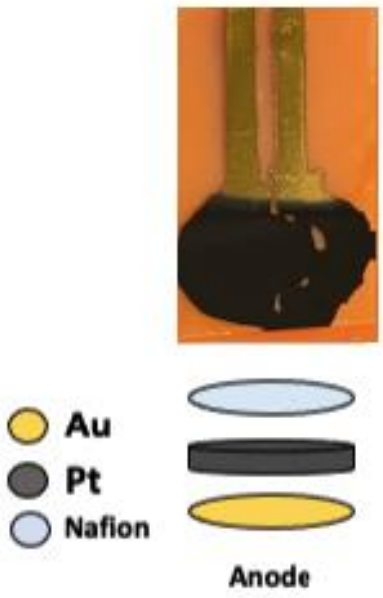

Figure 37. Au-co-Pt electrode after electrodeposition process.

Synthesis of silver oxide nanoparticles

The silver oxide nanoparticles (Ag_2O) solution was prepared by dissolving 20 g of PEG in 1 L of Milli-Q water, which was then heated to 75 °C under constant stirring for 1 h to ensure that

all the PEG was completely dissolved to form a homogeneous solution. The resulting PEG solution was filtered using Whatman ashless filter papers to remove any impurities. Under constant stirring, a silver nitrate solution was prepared from 0.5 g of silver nitrate and was added to the prepared PEG solution at 75 °C for 1 h. The pH was maintained at pH 9.8 to 10 throughout the reaction process using 0.1 M NaOH solution. Subsequently, the Ag_2O particles precipitated to the bottom of the solution, and the solution was centrifuged to extract the particles from the original solution. A 20 µL of MWCNTs solution was mixed in with the Ag_2O particles using ultra-sonication for 30 min to form the Ag_2O-MWCNTs solution.

The Ag_2O-MWCNTs solution was drop-casted onto the cathode surface, followed by soft baking at 60 °C for 30 min. Figure 38 provides a schematic illustration of the process involved in preparation of the cathodic functional components of the glucose abiotic fuel cell. For easy handling and device testing, a tungsten wire was attached to the electrodes using carbon wire glue.

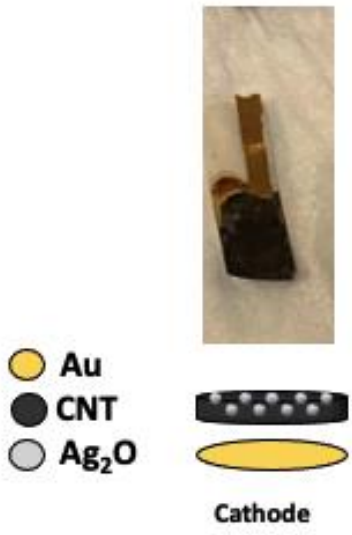

Figure 38. Cathode electrode after nanoparticle synthesis process.

RF430frl152h module

The RF430FRL15xH series of devices is well-suited for sensor-based applications that benefit from a wireless interface. The RF430FRL15xH employs NFC/RFID connectivity to wirelessly send data over short distances (typical range is 1 to 5 cm). The RF430FRL15xH can be powered by an RF field, enabling battery-free applications using one or more sensors. An NFC reader that supports ISO/IEC 15693 is required to receive sensor data from a tag employing the RF430FRL152H. Furthermore, depending on the sensor, computations may be necessary to turn raw results into usable data. The RF430FRL15xH line of devices can be used for a variety of sensor measurements.

The RF430FRL15xH has 2KB of FRAM, 4KB of SRAM, and 8KB of ROM. The Sensor App, the ISO/IEC 15693 RF Stack, and the device's Boot Code are all stored in the ROM, which cannot be modified. The 4KB of SRAM, which is made up of eight 512-byte sectors, is utilized to store sensor data. Individual sections of SRAM can be switched off to save power, but any data held in a turned off section of SRAM is lost. The 2KB of FRAM is used to store data and create custom applications. FRAM is a nonvolatile memory that retains data even when the device is switched off. The FRAM may be partitioned to serve as additional RAM memory to store extra sensor data, and it is divided into four 512-byte blocks. The Battery-less NFC/RFID Temperature Sensing Patch TI Design was created using the RF430FRL152H. This patch is constructed on a flexible PCB and features a single thermistor that is interfaced with the RF430FRL152H to provide temperature measurements. The tag gets its energy from the RF field provided by NFC/RFID scanners. The conversion of the analog signal was carried out in an on-air Android application to remove additional firmware coding that allowed in creating a custom algorithm to calculate the incoming bits to glucose concentrations as shown in Figure 39.

```
mTimer = new Runnable() {
    @Override
    public void run() {
        //Glucose conversion from substring to integer
        text_view.setText(text_val);

        int tmp = (Integer.parseInt(f_val.substring(3,4), 16)<<4)+
(Integer.parseInt(f_val.substring(4,5), 16))+
(Integer.parseInt(f_val.substring(6,7), 16) << 12) +
(Integer.parseInt(f_val.substring(7,8), 16) << 8);
        ADC2 = (float)(45*tmp)/(float)16384;
        tmp = (Integer.parseInt(f_val.substring(9,10), 16)<<4)+
(Integer.parseInt(f_val.substring(10,11), 16))+
(Integer.parseInt(f_val.substring(12,13), 16) << 12) +
(Integer.parseInt(f_val.substring(13,14), 16) << 8);
        ADC1 = (float)(0.45*tmp)/(float)16384;
        tmp = (Integer.parseInt(f_val.substring(15,16), 16)<<4)+
(Integer.parseInt(f_val.substring(16,17), 16))+
(Integer.parseInt(f_val.substring(18,19), 16) << 12) +
(Integer.parseInt(f_val.substring(19,20), 16) << 8);
        ADC0 = (float)(9*50*tmp)/(float)16384;
        init_display(f_val,b_val,ADC0,ADC1,ADC2);
        //if(b_val>0)
        //{   graphLastXValue += 1d;
        //    mSeries.appendData(new DataPoint(graphLastXValue, ADC0), true,
40);}
        mHandler.postDelayed(this, 100);
    }
};
```

Figure 39. Code snippet for glucose conversion based on the input string transferred from the wireless module.

Android Application

Android is a mobile operating system built especially for touchscreen mobile devices such as smartphones and tablets. It is based on a modified version of the Linux kernel and other open-source applications. Android is created by a group of developers known as the Open Handset Alliance, with Google serving as the primary contributor and commercial marketer [127]. The Android Open Source Project (AOSP) is the name given to the core Android source code, which is predominantly released under the Apache License. This has enabled Android variations to be built for a variety of different technologies, including gaming consoles, digital cameras, and personal computers (PCs) and others, each with its own user interface. Google's Android TV for televisions and Wear OS for wearable devices are two well-known adaptations.

The source code of Android has been utilized as the foundation of other ecosystems – most notably Google's, which is coupled with a suite of proprietary software known as Google Mobile Services (GMS) [127] that commonly comes pre-installed on those devices. This comprises essential programs like Gmail, the Google Play digital distribution network, the accompanying Google Play Services development platform, and apps like the Google Chrome web browser. These apps are licensed by Android device makers who have met Google's criteria. Amazon.com's Fire OS and LineageOS are two more Android ecosystems to consider. In most cases, software distribution is done over the internet. Applications ("apps") that increase device capabilities are created with the Android software development kit (SDK) and, in many cases, the Java programming language.

Java may be integrated with C/C++, as well as a variety of non-default runtimes that provide improved C++ compatibility. A debugger, software libraries, a handset emulator based on QEMU, documentation, sample code, and tutorials are all included with the SDK. Initially, Eclipse with the Android Development Tools (ADT) plugin was Google's supported integrated development environment (IDE). Google announced Android Studio in December 2014 as their primary IDE for Android application development, based on IntelliJ IDEA. Because of the open nature of Android, a number of third-party application marketplaces for Android exist, either to serve as a replacement for devices that are not permitted to ship with the Google Play Store, to provide applications that cannot be offered on the Google Play Store due to policy violations, or for other reasons. The Amazon Appstore, GetJar, and SlideMe are a few examples of third-party storefronts. Another alternative marketplace, F-Droid, aims to only deliver programs licensed under free and open-source licenses. This enables anybody with access to the source code to modify it and use it as needed.

CHAPTER VIII

RESULTS & DISCUSSION

The abiotic fuel cell was constructed from Au-co-Pt anode and silver oxide nanoparticles and carbon nanotubes composite cathode, as illustrated in Figure 40.

Figure 40. Fabricated Au-co-Pt anode on left and silver oxide nanoparticles and carbon nanotubes composite cathode on the right.

The gold surface on the BNC was characterized by scanning electron microscopy (SEM). Figure 41A shows the printed gold electrode surface. The gold electrode surface exhibited a plain surface with nanostructures ($\phi = 22.4 \pm 6.2$ nm), thereby making it ideal for use as electrode substrate material. As noted in Figure 41B, the electrodeposition was performed to deposit co-Pt on the printed gold electrode. The electrodeposited co-Pt presented a fractal-like distribution of microstructures, measuring on average 3.8 ± 1.1 μm in diameter. The co-Pt structures were found to be uniformly deposited on the printed gold surface. They also exhibited a porous morphology with a high surface area to volume ratio and appear to be composed of nanostructures. The co-Pt structures act as an inorganic catalyst at the electrode–electrolyte interface to improve the catalysis of glucose at the anode when compared to the bare printed gold electrode. Figure 41C shows the Ag_2OMWCNTs nanocomposite drop casted on the printed gold electrode. A network of MWCNTs ($\phi = 53 \pm 0.8$ nm) intertwined with the

Ag_2O nanostructures with diameters ranging from 12 nm to 389 nm was observed. Smaller Ag_2O nanostructures were observed to be directly attached to the MWCNT's surface. This interconnected network of Ag_2O-MWCNTs nanocomposite is essential in creating a porous environment to enable Ag_2O reduction at the cathode [170].

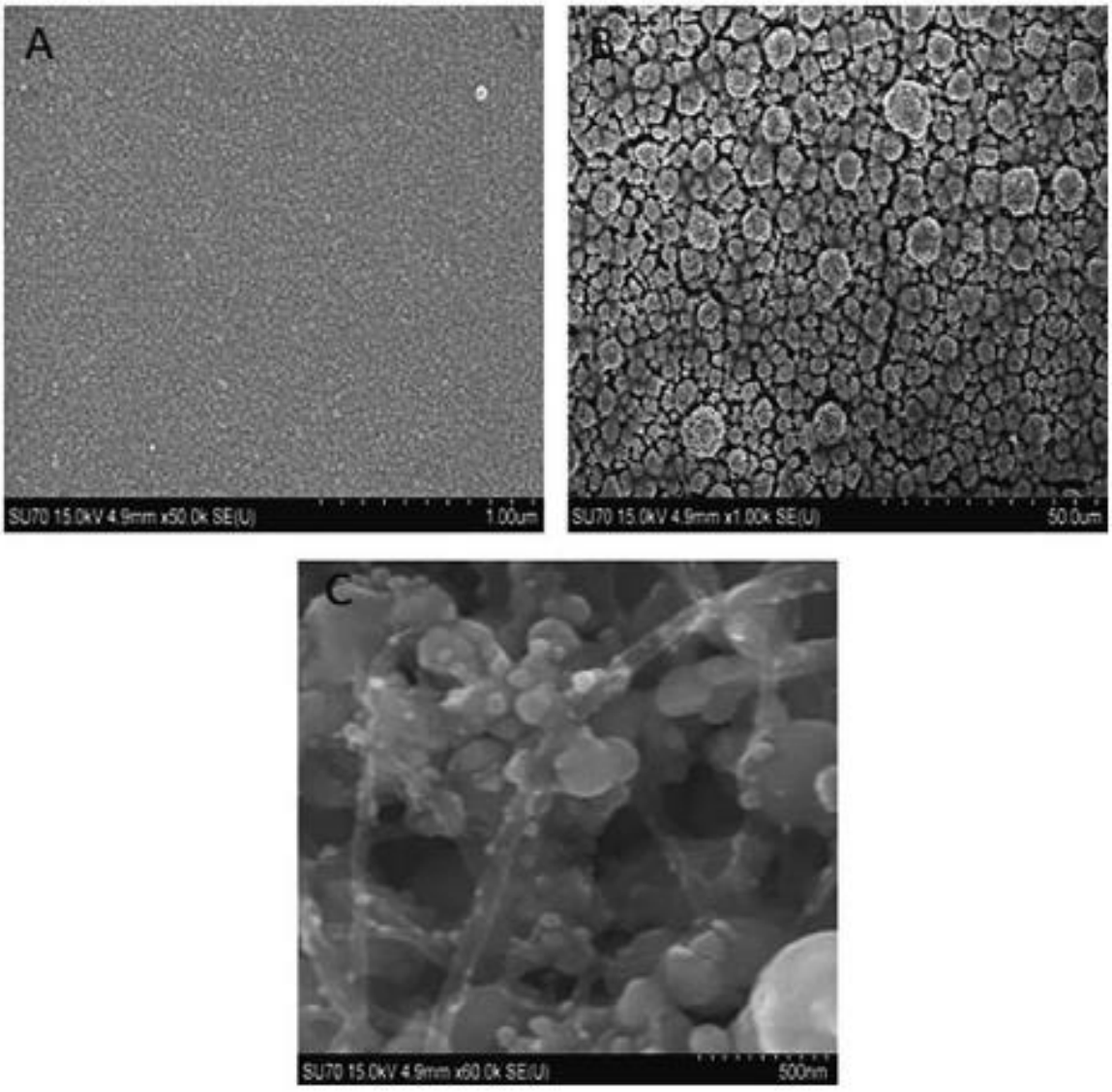

Figure 41. Scanning electron micrographs of (A) bare printed gold nanoparticles (AuNPs) on bacterial nanocellulose sheet, (B) colloidal platinum (co-Pt) electrodeposited on printed gold nanostructures, (C) sliver oxide-multiwalled carbon nanotubes (Ag2O-MWCNTs) nanocomposite drop cast on printed Au electrode.

The cyclic voltammogram in Figure 42A shows the electrooxidation of glucose in the

presence of co-Pt electrodeposited on printed gold nanostructures to produce gluconic acid and electrons according to equation (9).

$$Glucose + Au - co - Pt \ = Gluconic\ Acid + 2H^{+} + 2e^{-} \qquad (9)$$

At the anodic electrode, hydrogen adsorbed to the co-Pt electrode surface and the co-Pt acts as the dehydrogenation site wherein the gold nanostructure surface facilitates the regeneration of co-Pt from poisoning due to adsorbed intermediates from the oxidation of glucose. At the onset potential of −0.428 V, surface Pt-OH particles are formed which oxidizes the intermediates produced by the absorption of glucose, and thus frees up active Pt sites for direct oxidation of glucose [271]. During the electrooxidation of the glucose, a well-defined peak was observed around a potential of −0.052 V with higher current density of 1.435 mA/cm2 in comparison to the current density of 0.85 mA/cm^2 in the absence of glucose. The presence of an oxidation peak is attributed to the electron transfer occurring at the gold co-Pt surface in the presence of glucose. This shows that co-Pt exhibits a catalytic effect in the direct oxidation of glucose. Therefore, the electrodeposition of co-Pt on the gold printed BNC provides a large surface area decorated with nanostructures to enhance the electrocatalytic performance of the anode. The offset panel in Figure 42B shows the linearity of the peaks from 1 mM to 30 mM glucose (r^2 = 0.9887) with a sensitivity of 35.01 μA/mM-cm^2 and a limit of detection of 0.88 mM (3 S/N).

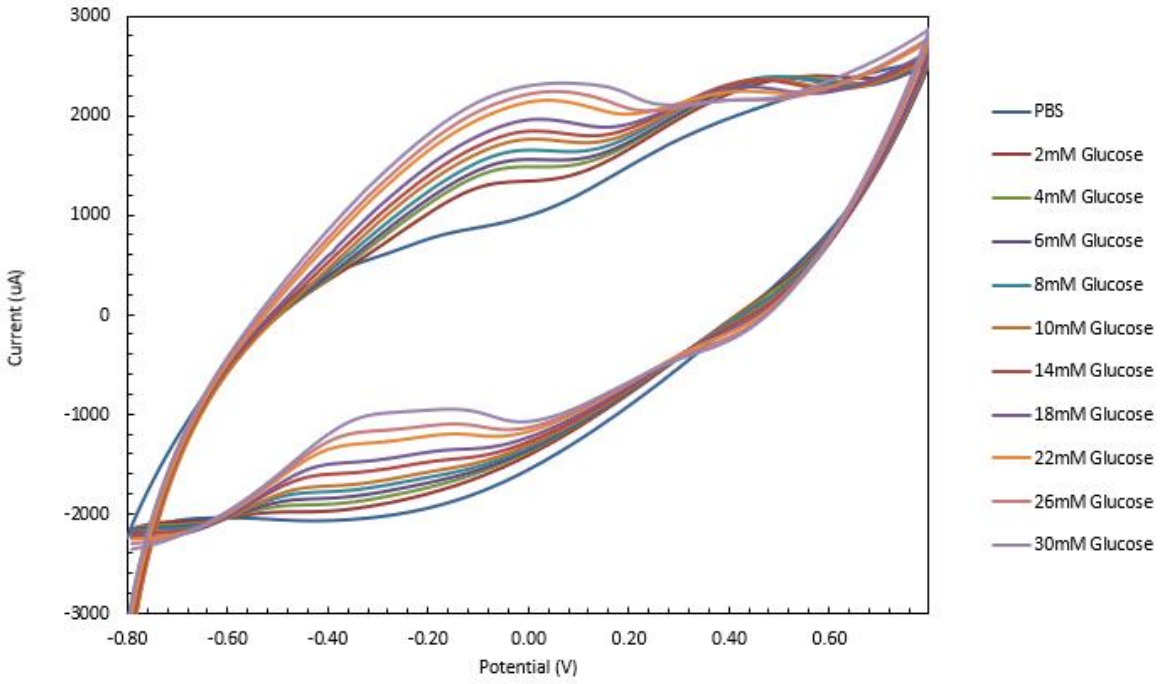

Figure 42. A Cyclic voltammetry performed on the Au-co-Pt showing linear increase in current with increase in glucose concentration.

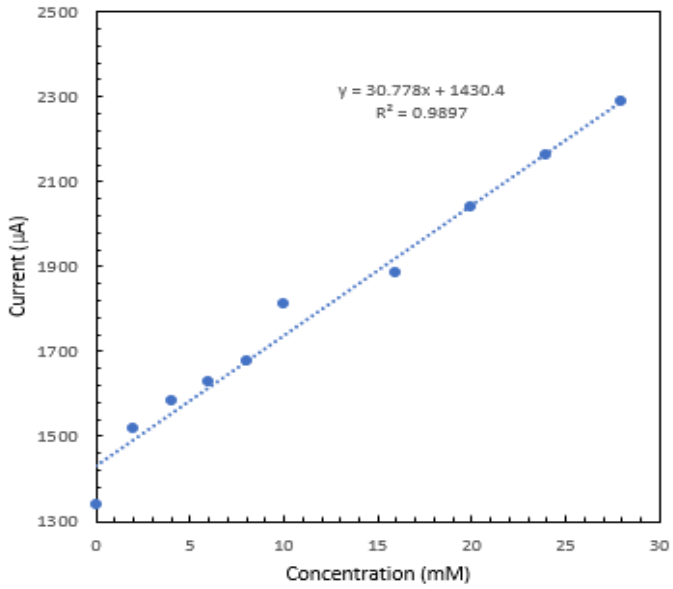

Figure 42B. Calibration curve for the cyclic voltammetry performed.

Figure 43 shows the electrocatalytic behavior of the Ag_2O-MWCNT cathode in a non-stirring air-saturated PBS. The shape of the voltammogram is consistent with those previously

reported [172]. The electrode was then placed under oxygen purging for 5 and 10 min to achieve oxygen saturation conditions. From the voltammogram, the reduction current density of the Ag_2O-MWCNT cathode increases in the presence of oxygen with an onset potential of 0.231 V in a similar manner to oxygen reduction at noble metal or enzyme-based cathodes [173]. The Ag_2O-MWCNT composite is used here as an alternative cathode material and thus serves as the cathodic electron acceptor in the biofuel cell. Ag_2O accepts the electrons generated at the anode and is reduced to Ag. As Ag_2O is reduced to Ag, hydroxyl (OH–) is generated as depicted in Equation 10.

$$Ag_2O + H_2O + 2e^- = 2Ag + 2OH^- \qquad (10)$$

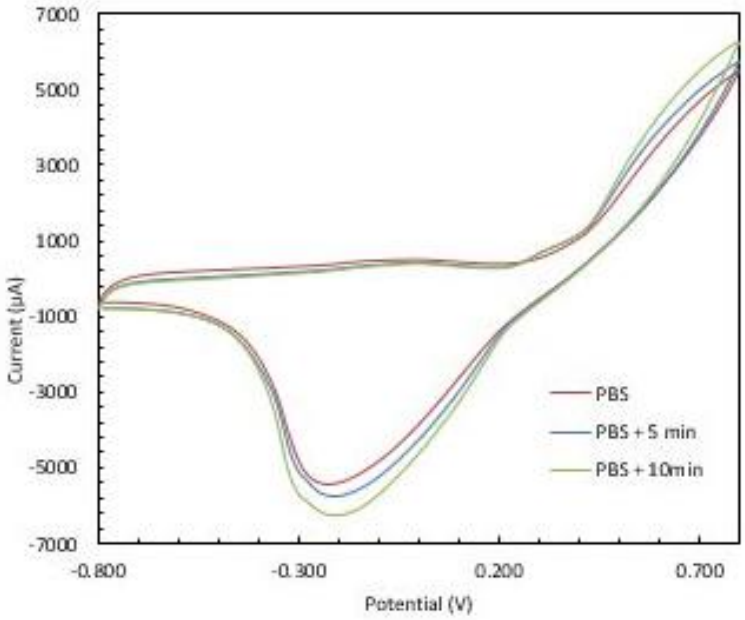

Figure 43. Cyclic voltammetry performed on the sliver oxide-multiwalled carbon nanotubes (Ag2O - MWCNTs) nanocomposite showing linear increase in current with increase in current with increase in purged oxygen.

The abiotic fuel cell was constructed with the co-Pt anode and Ag_2O-MWCNT composite cathode arranged side by side on a PET substrate to provide structural support for characterization. The fuel cell was placed in a beaker containing various concentrations of

glucose. Glucose electrolyte solutions ranging from 1 mM to 20 mM were prepared within PBS. The polarization performance of the fuel cell is shown in Figure 44. The co-Pt anode was used as the negative electrode, and the Ag_2O-MWCNTs cathode was used as the positive electrode. The polarization curves were measured using linear sweep voltammetry (LSV), and power density curves were acquired to determine the peak power of the abiotic fuel cell. The open-circuit voltage (Voc) of the fuel cell was 0.43 V and the short current density was 0.405 mA/cm^2 when operating on 5 mM glucose, although the Voc was smaller than the expected maximum theoretical thermodynamic redox potential for glucose oxidation and Ag_2O reduction [174]. However, the high current observed is attributed to the increased surface area caused by the incorporation of nanostructures on the printed gold substrate.

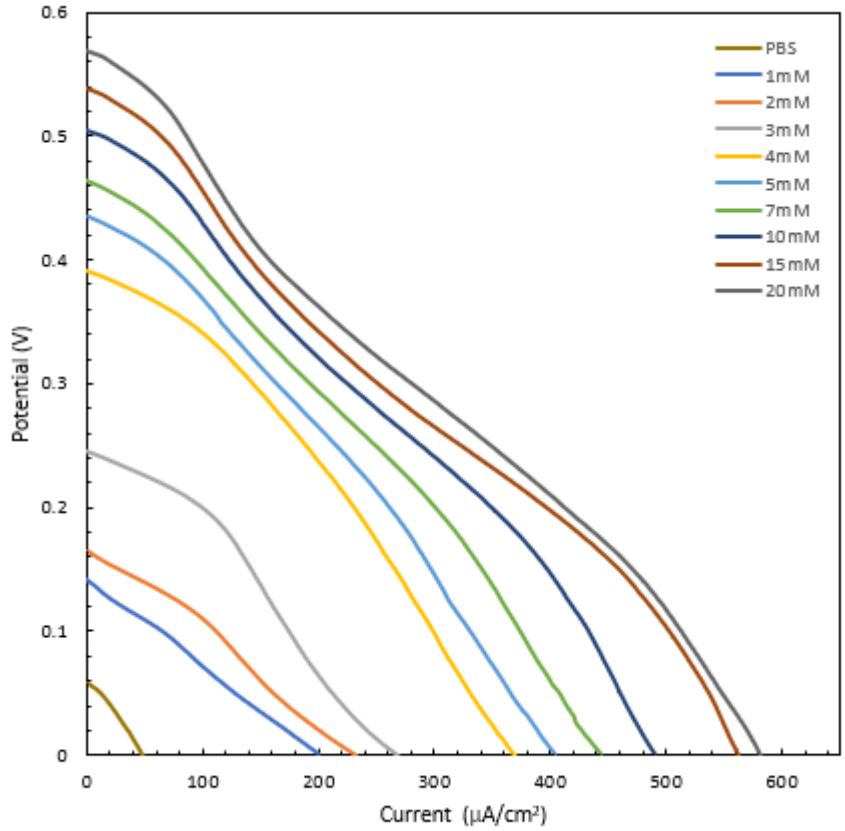

Figure 44. Power curve obtained from the abiotic fuel cell from glucose concentration of 0mM to 20M using Linear sweep voltammetry technique.

Figure 45 presents the power density profiles. The peak power densities achieved in 5 mM and 20 mM glucose were 0.055 mW/cm^2 at a cell voltage of 0.23 V and 0.087 mW/cm^2 at 0.35 V, respectively. The obtained power densities were the result of the decoration of the highly conductive printed AuNPs with electrodeposited co-Pt or Ag_2O-MWCNTs on the surface of the electrodes, which further improve the overall conductivity of the electrodes and provide a porous structure to enable the catalysis of glucose and Ag_2O. The glucose fuel cell output power response was collected in triplicates and the calibration curve is shown in Figure 46A. The abiotic fuel cell exhibited a curve that has a linear response over a range of glucose concentrations from 1 mM to 10 mM (r^2=0.9458) with a detection sensitivity of 7.84 µW/ mM-cm^2.

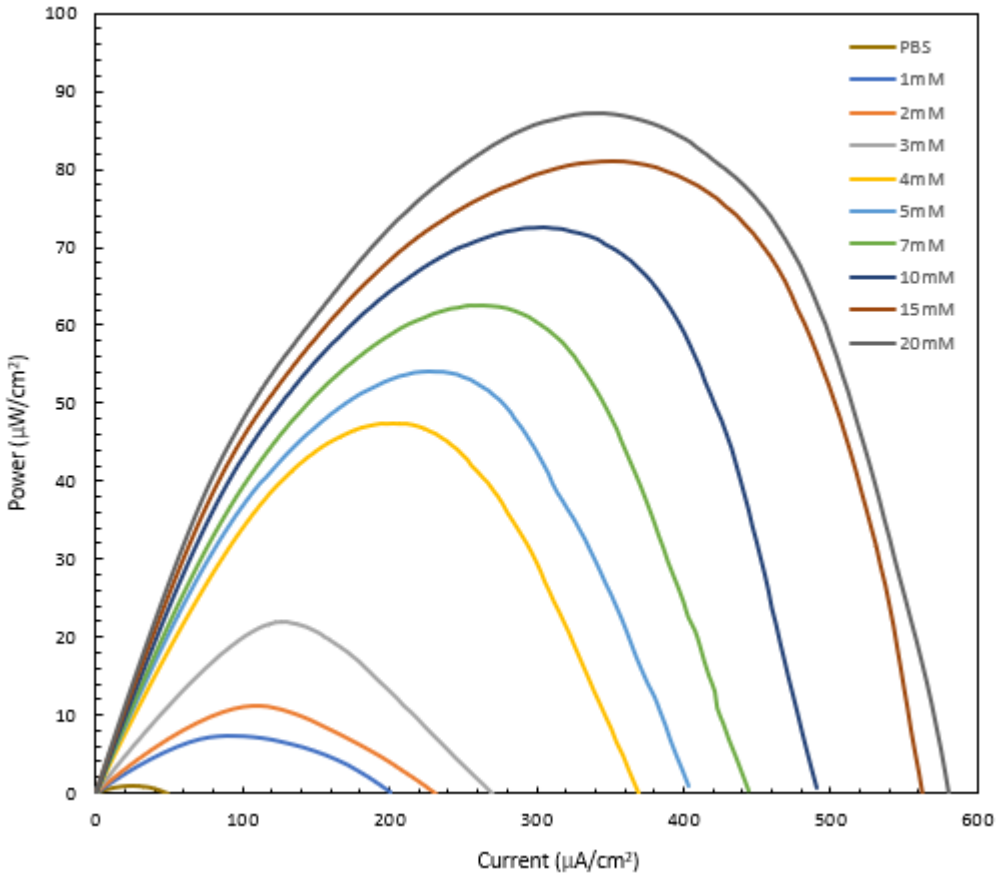

Figure 45. Polarization curve obtained from the abiotic fuel cell from glucose concentration of 0mM to 20M.

Furthermore, the glucose abiotic fuel cell was set up using serum solution as an electrolyte and the polarization curve and power output were recorded (Figure 46B). The glucose concentrations of serum were 1 mM and 5 mM. The peak power output was observed to be 0.045 mW/cm^2 at 0.21 V in serum as shown in Figure 46B. This value was obviously smaller as compared with the oxidation of 5 mM glucose solution. The fall in power from the 0.055 mW/cm^2 at 0.23 V observed for 5 mM glucose could be due to the interaction of protein molecules present in the serum electrolyte solution with the electrode surfaces, thereby inhibiting the catalytic reaction [175]. The porosity of the nanocellulose enables the vertical wicking of glucose fluid from the source to the active area of the electrodes to enable the redox reaction to take place in the presence of glucose.

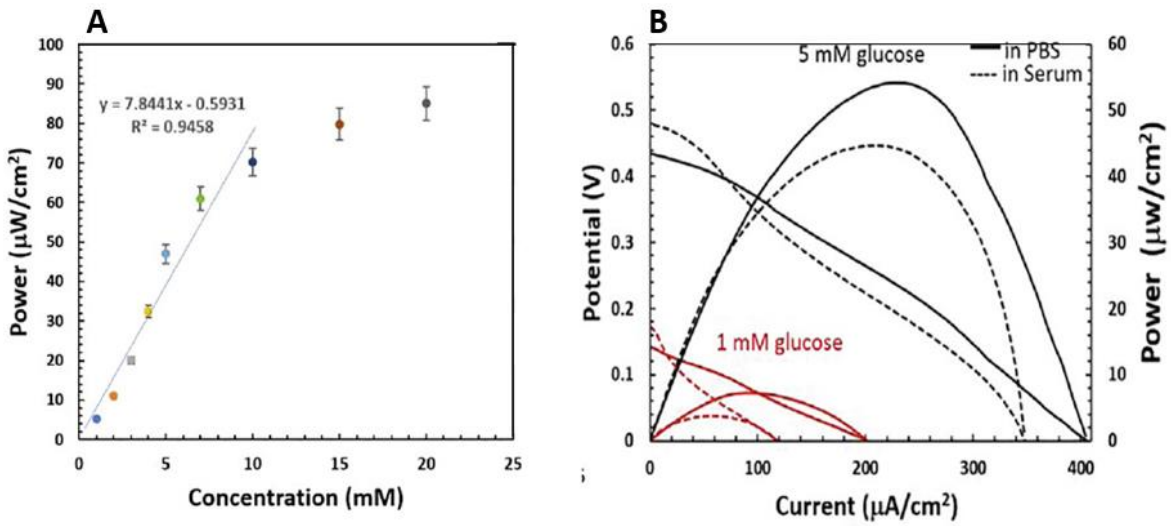

Figure 46. (A) Calibration curve for abiotic fuel cell with error bars (triplicates). (B) Polarization and power curves in serum and glucose solutions.

Glucose sensing application

For the amperometry sensing application, the Au-co-Pt electrode was evaluated by measuring current response at a fixed potential with sequential addition of the glucose analyte.

Figure 47 displays the amperometry response of the Au-co-Pt electrode to successive addition of four times 1 mM glucose and then increment by 1mM glucose in a 0.1 M PBS solution after every 100 seconds at a fixed potential of 0.5 V.

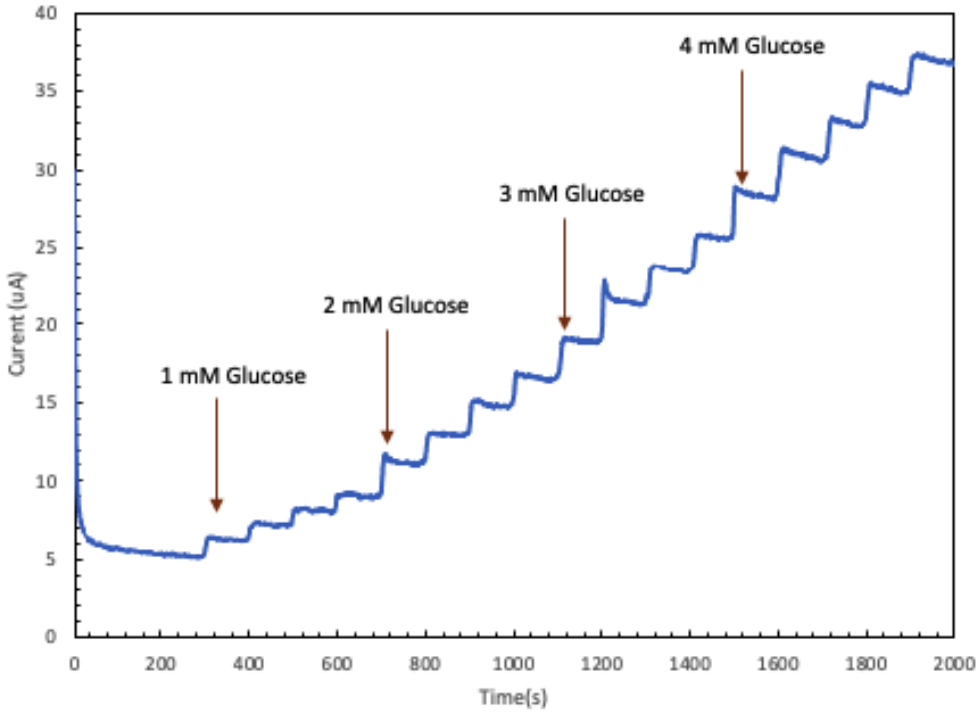

Figure 47. Amperometry response of the Au-co-Pt electrode to successive addition of glucose in 0.1 M PBS solution after every 100 seconds interval for four times each.

The Au-co-Pt electrode showed an enhanced linear response to the changes of glucose concentration, producing steady-state oxidation current signals as illustrated in Figure 48. The Au-co-Pt electrode gives a linear dependence with a correlation coefficient of 0.9893 in the glucose concentration range of 1 mM to 45 mM with a sensitivity of 1.87 μA mM^{-1}.

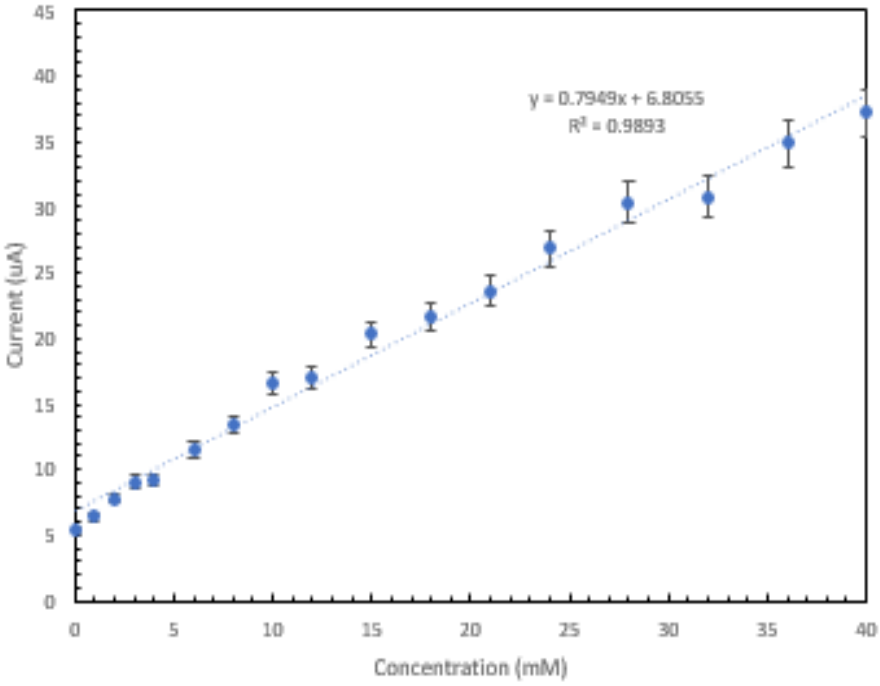

Figure 48. Calibration curve from the linear response of the sensor to change in glucose concentration.

Sensing changes in glucose concentration is only one part of the process of developing a sensing system; another critical task is the accurate measurement of glucose concentration values, as well as continuous monitoring of the glucose concentration level via communication of sensed glucose readings to the user, treating specialists, etc. Throughout the literature, wearable healthcare devices have mostly focused on device miniaturization and wireless operation (e.g., Bluetooth and near-field communication (NFC)) [122–123]. Although the wearable device has mostly used Bluetooth technology, its large size and weight may affect wearability [124].

A solution presented in this work is a miniaturized glucose monitoring system comprising a glucose abiotic fuel cell and battery-less wireless module using NFC technology. The voltage generated from the abiotic fuel cell serves as the analog signal for the data transfer from the NFC module to a handheld smartphone application. The data transfer module uses a low power microcontroller that is enabled using a smartphone with NFC antenna receiving the

respective instantaneous glucose value from the abiotic fuel cell. A smartphone application is developed and deployed to communicate the data between the NFC device and the smartphone for end-user visualization.

The Au-co-Pt anode and the silver oxide with carbon nanotube composite cathode were assembled to make an abiotic fuel cell. The electrical voltage produced by this single fuel cell was supplied as the input signal for the NFC based RF430FRL152H circuit as interface in Figure 49. The fabricated abiotic fuel cell generated voltage in the range of 100 – 700 mV which was detectable by the low power microcontroller on the wireless system. The electrical voltage produced by this single abiotic fuel cell was supplied as the input voltage for the RF430frl152H. The device is based on the NFC system technology. As shown in the block diagram for device operation, the operating system is divided into two parts: the first is the wireless interface composed of NFC chip and coil for wireless communication with smartphone. The second part is the abiotic fuel cell interface with the NFC chip that reads the analog signal into 16-bit sigma delta ADC values. The last part is the NFC reader (i.e., smartphone) that provides sufficient power to the device and obtains data transferred from the wireless device. Figure 49 explains the circuit diagram of the device. R1 (100 kΩ) is the reference resistor for the abiotic fuel cell, C1 (9 pF) is resonance capacitor for resonance frequency tuning of NFC system and C2 (0.1 μF) is the decoupling capacitor used to remove noise. The circuit is designed by relating to the NFC chip datasheet, which includes an in-depth circuit diagram for operation of the NFC chip.

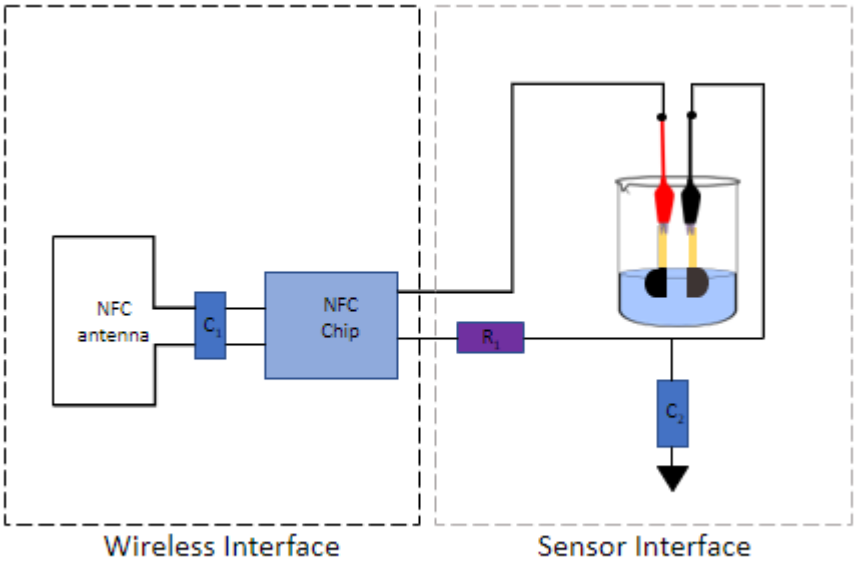

Figure 49. Lower power microcontroller-based NFC wireless interface and fuel cell as input signal.

The circuit consists of a low power microcontroller of the MSP430 family and three ADC analog to digital conversion inputs on it. The module was obtained from Texas instruments. This microcontroller can work at a nominal input range of 0 – 0.9 V and transmit the data through the RF antenna communication. It is a completely battery-less module as the necessary voltage to start up the device drawing through RF field of any reader device (smartphone). Also, a cell battery of 1.5 V can also switch the device ON. The programmable MSP430 core is interfaced with an analog front end to make it as a single chip solution. This allows the abiotic fuel cell, which acts as an analog sensor, to interface and support transmission of sensor data over the short-range wireless NFC technology as seen in Figure 50.

The RF430FRL15xH uses NFC / RFID communication to transmit data wirelessly over short distances typically ranging from 1 to 5 cm. The RF430FRL152H is a passive 13.56 MHz RFID transponder chip that contains an ISO 15693 and ISO 180003 compliant RFID interface as well as a programmable 24-bit microcontroller MSP430 with 2 KB integrated FRAM, Sigma-Delta-ADC Interfaces. A built-in 14-bit sigma-delta analog-digital converter (ADC) in this case enables the sensor readings with high resolution analog to digital conversion with

sampling frequency of up to 2kHz. For our experiment Google based Pixel 3a with an ISO / IEC 15693 capable phone was configured for the device to run. When the device completes the configured number of sensor scans, it turns itself off. The device can be restarted by applying an RF field again. The ADC on the device has an analog front end that includes a programmable gain amplifier so that the input signal does not reach the upper limits of input power.

The Sigma Delta modulator is the heart of the Sigma delta-ADC, it is responsible for scanning the analog input signal and reducing noise at lower frequencies. The resulting samples are always saved in 14-bit format, whether for an analog result or not. The data received is stored in raw format which comes through the modulator outputs, namely high frequency and 1-bit output speed [134]. A low pass digital filter function is used to attenuate high frequency noise causing the signal with high resolution from the abiotic fuel cell.

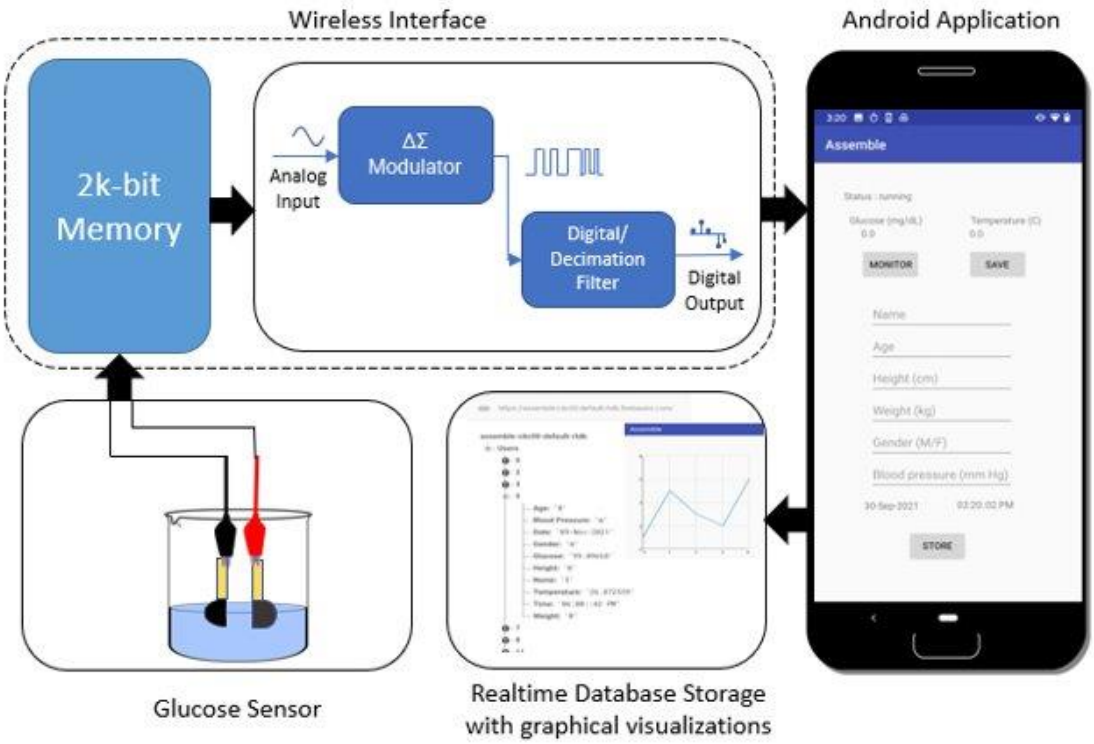

Figure 50. Calibration curve derived from the linear response of the sensor to change in glucose concentration.

The analog signals from the abiotic fuel cell are directly correlated to the changes in glucose concentration. By monitoring the change in analog signal, the exact concentration of the analyte can be deduced. After the NFC enabled wireless system communicates with a smartphone, the data received in 14 bit format is recognized by the android environment. Android studio is used to build a custom algorithm that correlates the analog signals from the abiotic fuel cell to the respective glucose concentrations. For the application development, Nfc based libraries allow the discovery, communication and read/write operations. In the main activity class of the application the 14 bits are stored as strings, and when the phone is placed on the tag it delivers a message that the tag has been discovered or not. This action is executed using an intent function that checks whether the tag is ISO15693 meaning that it is detected as shown in Figure 51.

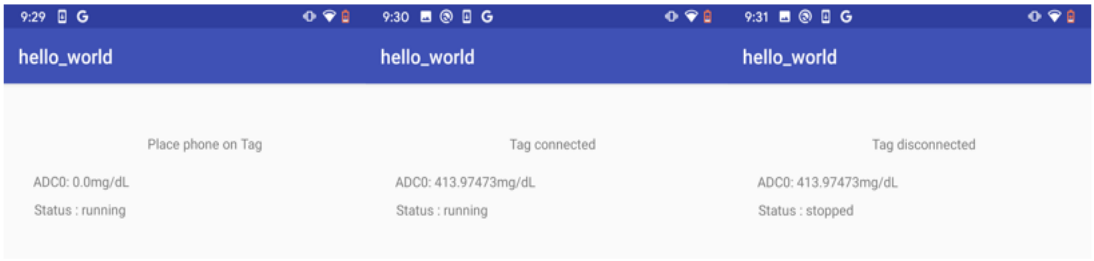

Figure 51. Sequential image from left to right displaying the tag discovery from idle state to disconnection on an android app.

After over the air reading of the tag is executed, the main function starts to convert the incoming 14-bit string value to an integer value by parsing the string into substrings. Using the correlation coefficient from the glucose sensing characterization, an algorithm was developed that allows the exact conversion of the analyte concentration in the beaker to the respective glucose value on the android application. Creating independent features for a user profile included features that would allow for the user to keep track of the glucose reading and other

vital signs. More in depth information has been included in the code implementation in Appendix A. The features added to the android application as shown in Figure 52A are age, height, weight, gender, and blood pressure as displayed. These parameters could be beneficial when it comes to diabetes management. Keeping track of the body mass index is essential for the user to validate glucose readings over a certain period. The features also play a vital role in data collection especially when a physician is involved in analyzing the situation better and prescribing an appropriate solution.

Remote access with data recording is also added to the smartphone application using the Firebase Realtime database. This No-SQL cloud-based database allows recording of the data which is linked to the store button on the interface. It stores the data in a key value format as a JSON object as shown in Figure 52B. The parent branch is usually assigned by the user and the child branch enables storing the independent features, glucose values and the time and date stamps that allow us to create a proper database for further analytics. One of the features involves the database working offline, capturing the data in the device memory and synchronizing it after reconnecting to the internet. The data acquired are some of the important parameters that will eventually lead to better diabetes management for an individual.

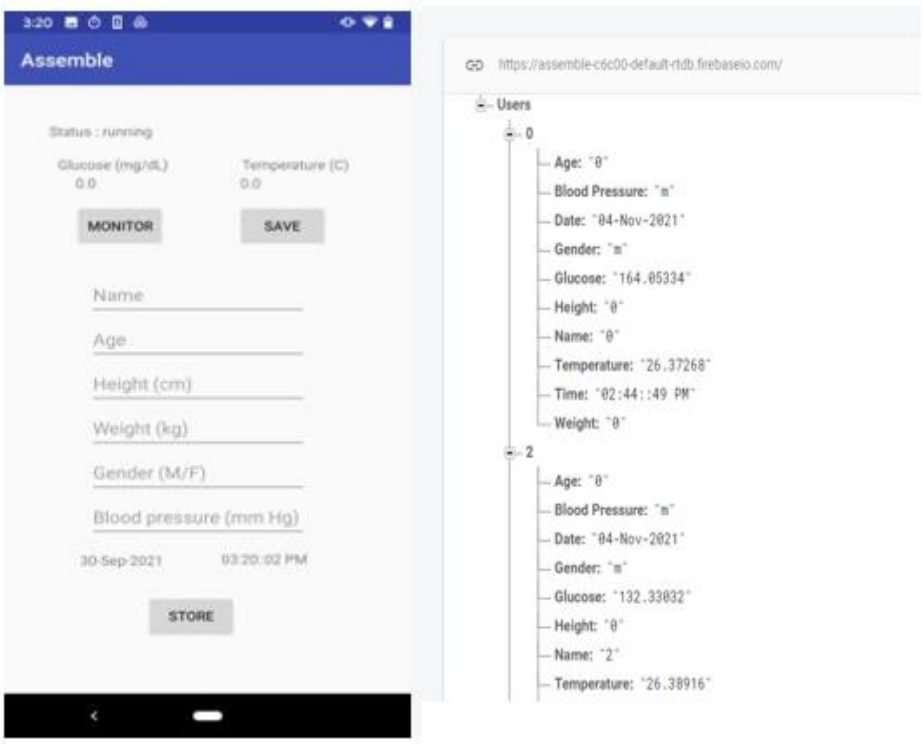

Figure 52. (A) User Interface with features for glucose recording and independent features like height, weight, age with a store button that transfers to database. (B) Firebase Realtime database format for data recording with dependent and independent features.

A representation of the entire sensing system consisting of the abiotic fuel cell and the NFC based wireless system with mobile glucose sensing is shown in Figure 53. The entire system was simplified by adding a wireless based data transfer module with a smartphone application that can act as a remote access and data storage unit. This holds the user accountable for monitoring and making necessary life changes to improve their state with diabetes. This approach makes the framework affordable and less bulky for users and healthcare providers.

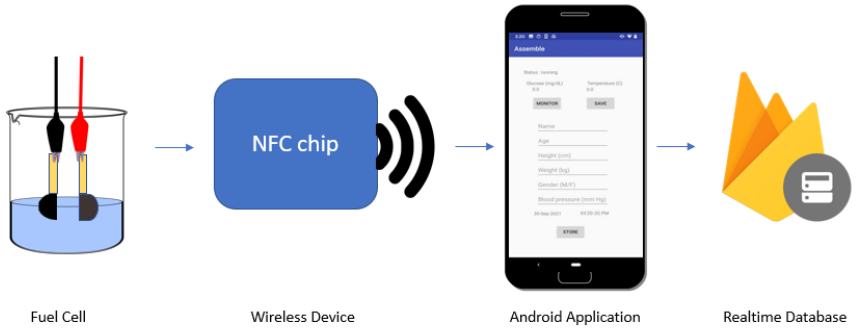

Figure 53. A model of a novel abiotic glucose monitoring system with wireless data acquisition and data storage using android application.

An experimental setup involving three components involving a fuel cell, NFC module and smartphone were used to study the performance as seen in Figure 54. The database recording was done with a local PC with a login through the Firebase webpage. To verify the fuel cell performance, multimeter was used to verify the output with the respective glucose concentration. In addition, the biofuel cell assembly was connected to a charge pump integrated circuit (S-882Z) through resistor, capacitor, and light emitting diode (LED). The voltage generated by the single biofuel cell was fed into the charge pump circuit, which then charges and discharges the charge pump through an output capacitor (0.1 μF) to increase the nominal input voltage to 1.8 V and illuminate the LED.

Figure 54. Assembled fuel cell setup with NFC/smartphone data recording and with voltage measurement using multimeter.

The convenient smartphone-based wireless system enabled an experiment to understand the stabilization time for the abiotic fuel cell at a particular lower concentration. It was observed that after approximately 2 min the signal started to get consistent and noise free for the respective concentrations. The experiment was performed with a 100 mM phosphate buffer solution with glucose concentration of 1, 3, 5, 7 mM aliquots over time and data recording using a smartphone. From Figure 55, it can be deduced that the surge in the glucose level after addition of glucose concentration within 30 sec the signal starts to get consistent and level out. This gave a clear picture of the performance of the fabricated sensor with the wireless module for the stabilization of the startup value for a respective concentration of glucose.

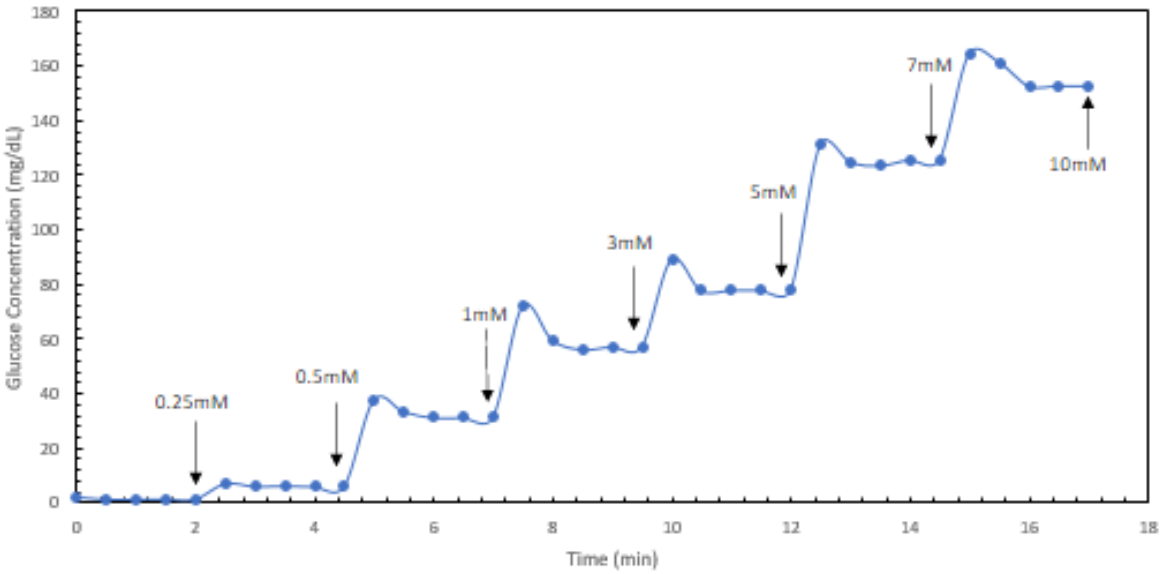

Figure 55. Stabilization Plot for glucose concentration from 0mM – 10mM.

The objective moving forward was to create a database of glucose values from the abiotic fuel cell to further analyze the performance of the system. Random glucose concentrations were given to the abiotic fuel cell at three-minute intervals to check the accuracy of the glucose value received from the application. Overall, 50 recordings were carried out over a day with each random value generated from a random Python script generator. The margin of error was found to be 1.09 during three trials. The experiment was repeated for the next two days to provide triplicate data to monitor the repeatability for the glucose reading from the smartphone application as shown in Figure 56.

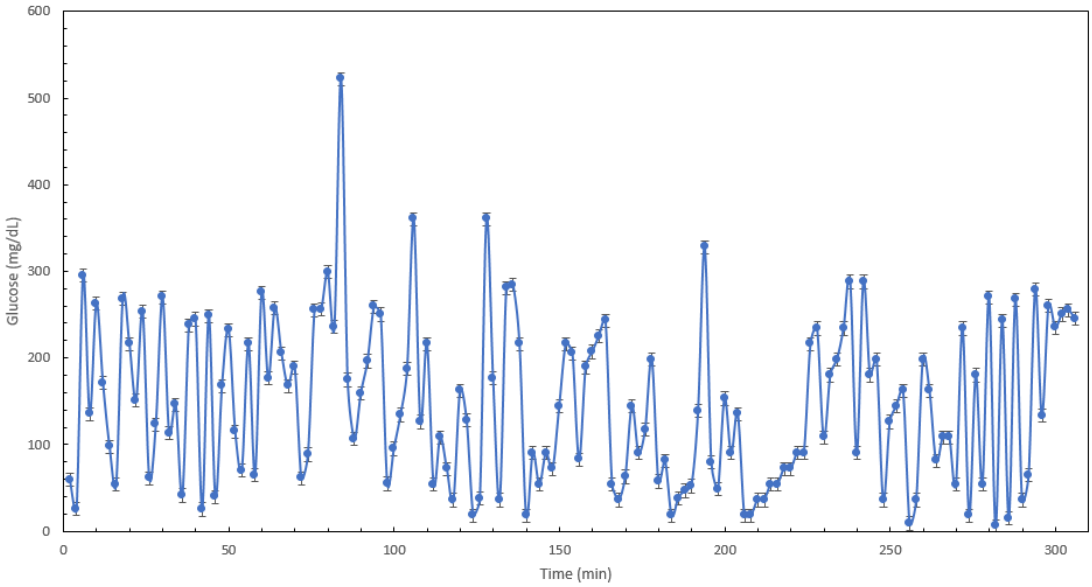

Figure 56. Random triplet plot for glucose concentration to understand the repeatability of the fuel cell.

Tensorflow Lite is a package in the android development environment that allows the addition of machine learning (ML) based analytics onto the smartphone application. Also, a local server is used to collect data points from the database to perform analytics. For this purpose, Python scripts were prepared for a time series prediction for the glucose reading. Experiments were conducted over the period of a week with 286 datapoints collected for a day. Within the in vitro setting, a dataset for 2000 data points were collected by mimicking a data from a patient with Type 2 diabetes. For future glucose prediction, time series-based forecasting models were explored, namely Recurrent Neural Networks (RNN) and Long short term memory (LSTM) with its types with every model performance described in Appendix B. To validate the performance the predicted horizon was set to 15, 30 and 60 min. Usually 60min was observed to have the worst performance for the prediction models. Performance metrics that were used to understand the best model for future glucose prediction are the root mean square error and mean absolute error. The Python-based script was developed by data preprocessing of the data set. Libraries like matplotlib, numpy and sklearn were used to import

cleanly and plot the data. Below is the data visualization plot on the recordings for glucose reading for 7 days as seen in Figure 57.

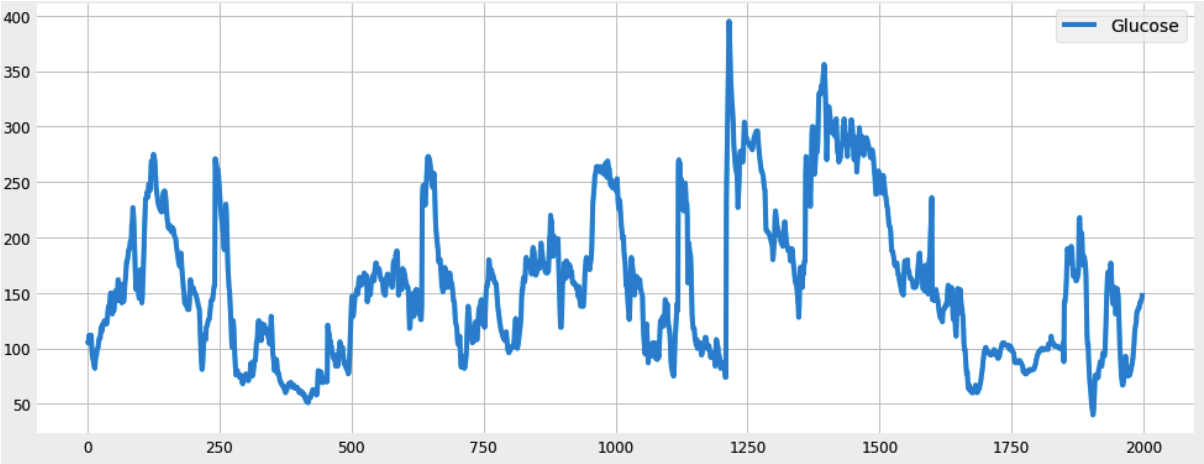

Figure 57. 2000 datapoints across 7 days run after 5 mins.

Threshold values for hyperglycemic (185mg/dL) and hypoglycemic (75mg/dL) levels were created to visualize the data points as illustrated in Figure 58.

Figure 58. 2000 datapoints with label for glycemic levels.

Training and validation set were divided into 1399 and 599 data points. At each prediction horizon, the average RMSE over the datapoints are reported. There are four models

that are used to evaluate the performance of the prediction models. The models namely are RNN, LSTM, Stacked LSTM and Bidirectional LSTM. With glucose concentration as a feature in the model and other features being BMI, life events etc., the RMSE and MAE were used to evaluate the performance of the model. The difference in layers results in better prediction of the future glucose value.

Figure 59 presents results for predictions made at 15 minutes. An interesting result is that for a 15-minute prediction horizon, the RNN which does not use life event data, scored a better RMSE and MAE -- more than LSTM and its types. The RMSE and the MAE best values amongst the models were 14.74 and 9.63. There is room for improvement in the model development for better time series forecasting by increasing the layers for prediction. While comparing the models for 15 minute predicted horizon the peaks were well established in comparison with the predicted value in RNN model. This provides a good basis for the model development in Bidirectional and stacked LSTM to improve deviation from the actual value for future glucose monitoring.

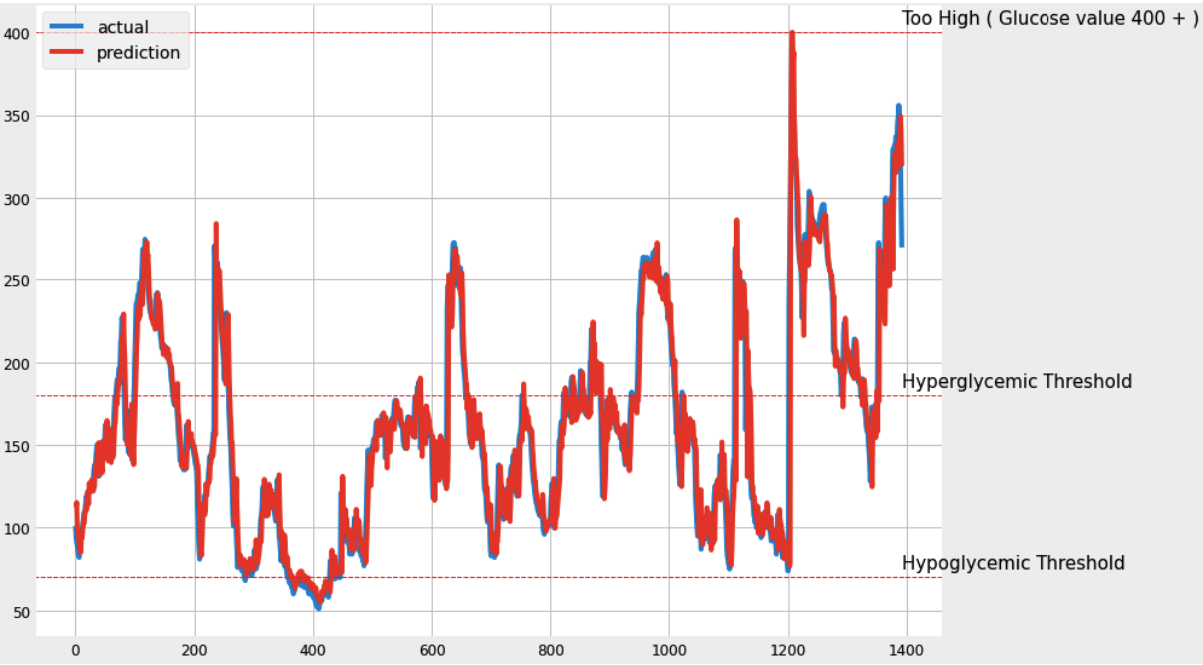

Figure 59. 15 minute prediction for RNN along with actual targets.

For the 30 min best scenario, Figure 60 represents results for predictions made at 30 minutes. In this comparison of models, LSTM performed better according to the error metrics. The RMSE and MAE that resulted in the best scenario of the LSTM based model are 29.53 and 18.66 respectively. It solves the huge issue that RNN struggles with -- short-term memory. With each peak in the LSTM prediction as compared to the RNN model, it helps in solving vanishing gradient descent by repeated weight adjustments that allows the values to be predicted more accurately. The only concern with the LSTM models are that they computationally expensive depending on the window and data size for which the scenario to build a better model that iterates bidirectionally in the LSTM model.

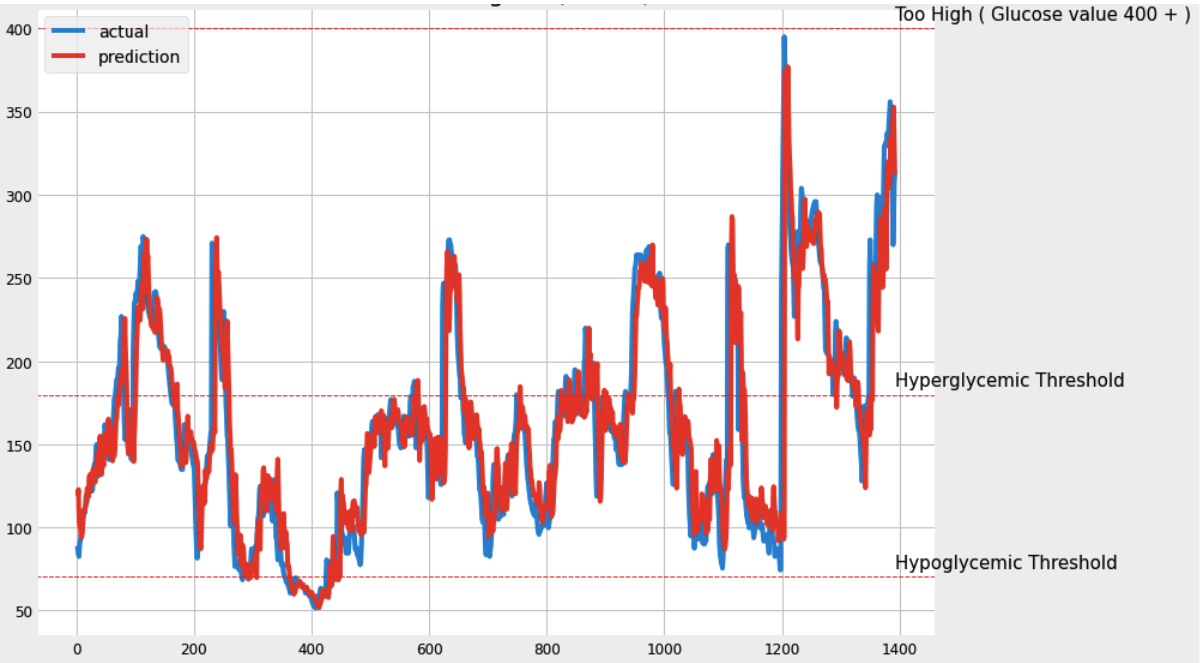

Figure 60. 30 minute prediction for LSTM along with actual targets.

With the increase in prediction horizon the 60 min best scenario was seen in the bidirectional LSTM model as seen in Figure 61. The increase in complexity of the model and the bidirectional LSTM provided a better prediction peak as compared to other models. The

target was the long-term preservation of the information and two direction input sequence scanning which was available by bidirectional LSTM models that enabled better error metrics than others. Usually, as the prediction horizon increases the prediction gets worse which leads to more error-based prediction. The RMSE and MAE were seen to be 35.80 and 26.25 respectively. With bidirectional LSTM, the model was much deeper and more accurate compared to the other models with bidirectional sequence layers.

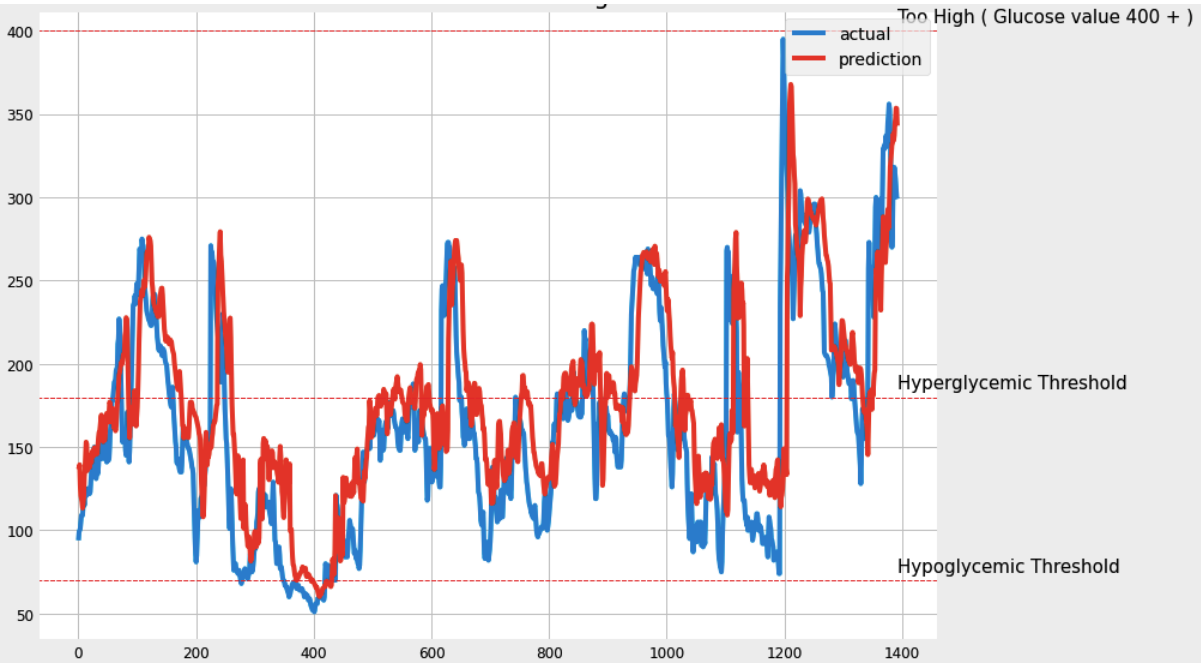

Figure 61. 60 minute prediction for Bidirectional LSTM along with actual targets.

Table 3 provides all the performance metrics based on RMSE and MAE values. Observation was made during the outcomes of each model that according to the prediction horizon each model performance varies, i.e as model complexity increase so does the requirement for a larger set of data and the prediction horizon varies. Performances based on 1 day and 4 days were also performed which showed results that were based on the lower number of data points. For 7 day testing interesting results were seen when it came down to the error metrics that concluded the performance of the model was improving as with the dataset. The

RNN model performance was better for the 15 min prediction horizon as compared to others whereas for 30 minute the LSTM performed much better due to short term memory allowing more accurate prediction. For 60 minutes with increase in complexity the bidirectional LSTM performed much better to allow peaks that were predicted better as compared to other models but not totally accurately. This might be enhanced by improving features like BMI, food intake, insulin intake, life events etc. based on the validation data. This optimization may be approached in two ways: by optimizing the parameters of each feature template and by optimizing feature combinations. Evaluation of the accuracy of predictions during meals and exercise should also be noted. Although they cannot be directly compared since they would be assessed using distinct methods, patient dependent models appear to outperform patient independent models. The inclusion of more independent features would provide greater information about the link between input data (such as food intake) and anticipated blood glucose levels. Patient-independent models have the potential to improve as more data is collected in the future. The ultimate goal of this categorization is to create a viable clinical tool that would automatically screen for high glycemic fluctuation in diabetic patients. A systematic clinical screening for high glycemic fluctuation would allow for the early identification of individuals at risk of avoidable diabetes complications. Preventing diabetes complications increases patients' quality of life while lowering the financial burden of healthcare expenses. As a result, future plans include the creation of a commercial software package for clinical usage.

Table 3. RMSE and MAE values for different models with prediction horizons

Model / Prediction Horizon	15 min (RMSE), (MAE)	30 min (RMSE), (MAE)	60 min (RMSE), (MAE)
Vanilla RNN	14.74, 9.63	22.57, 16.66	32.00, 23.86
LSTM	14.80, 10.3	21.74, 16.35	33.38, 26.37
Stacked LSTM	16.08, 11.71	22.49, 16.69	35.33, 30.76
Bidirectional LSTM	14.93, 9.86	22.51, 17.53	31.80, 23.25

CHAPTER IX

CONCLUSION

In conclusion, we demonstrated an abiotic glucose fuel cell with glucose sensing and battery-less NFC based data acquisition using a mobile android application. The wearable sensing system consists of a novel abiotic cell with co-Pt as anode and silver oxide with carbon nanotubes composite as cathode, NFC wireless module, smartphone android application with analytical capabilities. The non-enzymatic glucose fuel cell comprises a glucose oxidizing co-Pt anode and Ag_2O reducing Ag_2O-MWCNTs cathode fabricated on the surface of gold inkjet-printed on a thin-film of nanocellulose synthesized via bacteria G. xlyinus. A linear dynamic range of 1 mM – 45 mM glucose with a sensitivity of 1.87 μA mM cm^{-2} was observed. The Android application took a diabetes management approach by creating dependent and independent features in glucose measurements, age, body mass index, etc. to enable proper tracking over a period.

The analog signals from the abiotic fuel cell act as the input received on the android application. The custom-built algorithm then converts the signal into the corresponding glucose level which is then stored onto a cloud based Realtime database. The data stored has the time and date stamp that allows the patient / physician to validate the levels in glucose. Electrochemical characterizations showed that the performance of the abiotic fuel cell was ideal for the proposed glucose sensing. Further analytics involving machine learning based future glucose level prediction showed the characteristics of continuous glucose monitoring and how it has the potential to help in diabetes management.

For future work, the system can be tested in real environments through animal testing to real patient testing. More work to develop the stability of these biosensors is needed. Introducing highly porous nanofibers using electrospinning and combining them with a

bioreceptor is an example for enhancing sensor sensitivity, sensing range. Likewise, conductive metal nanoparticles can be used to enhance the performance of non-conductive but highly selective materials. In conclusion, this framework allowed an abiotic glucose fuel cell and battery-less sensing system to be realized. The cost-effectiveness and less bulky tattoo-like characteristics enable easy management for the end-user to track and modify their lifestyle accordingly.

REFERENCES

[1] "What Is Diabetes?" *National Institute of Diabetes and Digestive and Kidney Diseases*, U.S. Department of Health and Human Services, 1 Dec. 2016, www.niddk.nih.gov/health-information/diabetes/overview/what-is-diabetes.

[2] Rachel Nall, RN. "Diabetes: Symptoms, Treatment, and Early Diagnosis." *Medical News Today*, MediLexicon International, 9 Jan. 2020, www.medicalnewstoday.com/articles/323627.

[3] "Diabetes Overview." *Diabetes Overview - Symptoms, Causes, Treatment*, www.diabetes.org/diabetes.

[4] "Diabetes." *Mayo Clinic*, Mayo Foundation for Medical Education and Research, 8 Aug. 2018, www.mayoclinic.org/diseases-conditions/diabetes/symptoms-causes/syc-20371444.

[5] Watson, Stephanie. "Everything You Need to Know About Diabetes." *Https://Www.healthline.com/Health/Diabetes*, 4 Oct. 2018, www.healthline.com/health/diabetes.

[6] Centers for Disease Control and Prevention. "National diabetes statistics report: estimates of diabetes and its burden in the United States, 2014."*Atlanta, GA: US Department of Health and Human Services* (2014).

[7] Dansinger, Michael. "Glucometer Types, Features, Guidelines, Results." *WebMD*, WebMD, 18 Apr. 2018, www.webmd.com/diabetes/glucometers-features-guidelines.

[8] "Glucose Meter, Blood Glucose Meters - IHealth." *IHealth® Official Site for Personal Health Management*, 25 Jan. 2019, ihealthlabs.com/glucometer/wireless-smart-gluco-monitoring-system/.

[9] Manzella, Debra. "10 Steps for Using a Glucometer." *Verywell Health*, Verywell Health, 12 Oct. 2019, www.verywellhealth.com/how-to-use-a-glucometer-1087304.

[10] "Continuous Glucose Monitoring System." *Continuous Glucose Monitoring System*, www.freestylelibre.us/.

[11] "Continuous Glucose Monitoring." *National Institute of Diabetes and Digestive and Kidney Diseases*, U.S. Department of Health and Human Services, 1 June 2017, www.niddk.nih.gov/health-information/diabetes/overview/managing-diabetes/continuous-glucose-monitoring.

[12] Dansinger, Michael. "Continuous Glucose Monitoring for Diabetes." *WebMD*, WebMD, 1 Dec. 2019, www.webmd.com/diabetes/guide/continuous-glucose-monitoring.

[13] Zak.huber. "Continuous Glucose Monitoring (CGM): 24 Hour Glucose Monitor." *Dexcom*, 1 Aug. 2019, www.dexcom.com/continuous-glucose-monitoring.

[14] "Rechargeable Battery Market: Global Industry Trends, Share, Size, Growth, Opportunity and Forecast 2019-2024", *Researchandmarkets.com*, 2019. [Online]. Available:

https://www.researchandmarkets.com/reports/4775741/rechargeable-battery-market-global-industry.

[15] B. Schweber, "Lithium Batteries: The Pros and Cons", Electronics360, 2015. [Online]. Available: https://electronics360.globalspec.com/article/5555/lithium-batteries-the-pros-and-cons.

[16] Andújar JM, F Segura (2009) Fuel cells: History and updating, a walk along two centuries. Renewable and sustainable energy reviews 13: 2309-2322.

[17] G. Slaughter and T. Kulkarni, " Enzymatic glucose biofuel cell and it's application", Biochip and Tissue chip, 2015.

[18] Hoff AJ, Deisenhofer J (1997) Photophysics of photosynthesis, Structure and spectroscopy of reaction centers of purple bacteria. Physics reports 287: 1-247.

[19] S.S. Mahshid, S. Camire, F. Ricci, A. Vallee-Belisle, "A highly selective electrochemical DNA-based sensor that employs steric hindrance effects to detect proteins directly in whole blood", J. Am. Chem. Soc., 137, pp. 15596-15599, 2015.

[20] S. Jeong, J. Park, D. Pathania, C.M. Castro, R. Weissleder, H. Lee, "Integrated magneto−electrochemical sensor for exosome analysis", ACS Nano, 10, pp. 1802-1809, 2016.

[21] G. Slaughter, "Current Advances in biosensor design and fabrication", R.A. Meyers (Ed.), Encyclopedia of Analytical Chemistry, John Wiley, Chichester (June 14 2018),

[22] J.S. Narayanan, G. Slaughter, "The preparation of AuNPs-HRP needle-type biosensor for ultrasensitive detection of hydrogen peroxide Med. Devices Sens., 1 (2018), pp. 1-9 .

[23] E. Bakker, "Electrochemical sensors", Anal. Chem., 76 (2004), pp. 3285-3298 .

[24] D. Chen, H.B. Feng, J.H. Li, "Graphene oxide: preparation, functionalization, and electrochemical applications Chem. Rev., 112 (2012), pp. 6027-6053 .

[25] H.B. Wang, H.D. Zhang, Y. Chen, Y. Li, T. Gan, "H2O2-mediated fluorescence quenching of double stranded DNA templated copper nanoparticles for label-free and sensitive detection of glucose, RSC Adv., 5 (2015), pp. 77906-77912 .

[26] L. Wang, J. Zheng, Y. Li, S. Yang, C. Liu, Y. Xiao, J. Li, Z. Cao, R. Yang, "AgNP-DNA@GQDs hybrid: new approach for sensitive detection of H2O2 and glucose via simultaneous AgNP etching and DNA cleavage", Anal. Chem., 86 (2014), pp. 12348-12354.

[27] G. Slaughter, "Fabrication of Nano-indented-electrodes for glucose detection", J. Diab. Sci. Technol., 4 (2) (2010), pp. 320-327.

[28] D. Ivnitski, K. Artyushkova, P. Atanassov, “Surface characterization and direct electrochemistry of redox copper centers of bilirubin oxidase from fungi Myrothecium verrucaria”, Bioelectrochemistry, 74 (2008), pp. 101-110.

[29] B. Haghighi, B. Karimi, M. Tavahodi, H. Behzadneia, “Electrochemical behavior of glucose oxidase immobilized on Pd-nanoparticles decorated ionic liquid derived fibrillated mesoporous carbon”, Electroanal., 26 (2014), pp. 2010-2016.

[30] G. Slaughter, J. Sunday, “Fabrication of enzymatic glucose hydrogel biosensor based on hydrothermally grown ZnO nanoclusters”, IEEE Sensors J., 14 (2014), pp. 1573-1576.

[31] Z. Wang, S. Liu, P. Wu, C. Cai, “Detection of glucose based on direct electron transfer reaction of glucose oxidase immobilized on highly ordered polyaniline nanotubes”, Anal. Chem., 81 (2009), pp. 1638-1645.

[32] C.X. Guo, C.M. Li, “Direct electron transfer of glucose oxidase and biosensing of glucose on hollow sphere-nanostructured conducting polymer/metal oxide composite”, Physical. Chem. Chem. Phy., 12 (2010), pp. 12153-12159.

[33] S.I. Brahim, G. Slaughter, A. Guiseppi-Elie, “Electrical and electrochemical characterization of electroconductive PPy-p(HEMA) composite hydrogels”, Smart Struct. Mat., 5053 (2003), pp. 1-12.

[34] B. Liang, L. Fang, G. Yang, Y. Hu, X. Guo, X. Ye, “Direct electron transfer glucose biosensor based on glucose oxidase self-assembled on electrochemically reduced carboxyl graphene”, Biosens. Bioelectron., 43 (2013), pp. 131-136.

[35] P. Yang, L. Wang, Q. Wu, Z. Chen, X. Lin, “A method for determination of glucose by an amperometric bienzyme biosensor based on silver nanocubes modified Au electrode”, Sensors Actuators B Chem., 194 (2014), pp. 71-78 .

[36] X. Che, R. Yuan, Y. Chai, J. Li, Z. Song, W. Li, X. Zhong, “A glucose biosensor based on chitosan-Prussian blue-multiwall carbon nanotubes-hollow PtCo nanochains formed by one-step electrodeposition”, Colloids Surf. B: Biointerfaces, 84 (2011), pp. 454-461.

[37] Md.Q. Hasan, R. Kuis, J. Shankara Narayanan, G. Slaughter, “Fabrication of highly effective hybrid biofuel cell based on integral colloidal platinum and bilirubin oxidase on gold support”, Nat. Sci. Rep., 8 (2018), Article 16351

[38] J. Russell and R. Cohn, “Gas diffusion electrode”, JBookvika publications., 638 (2012), pp. 196

[39] G. Slaughter, T. Kulkarni, “Fabrication of palladium nanowire array electrode for biofuel cell application”, Microelectron. Eng., 149 (2016), pp. 92-96

[40] N. Furuya, "A technique is described for production of a gas diffusion electrode by electrophoresis". *Journal of Solid State Electrochemistry*. **8**: 48–50, 2003.

[41] S. Ernst, "The electrooxidation of glucose in phosphate buffer solutions Part I. Reactivity and kinetics below 350 mV/RHE", *Journal of Electroanalytical Chemistry*, vol. 100, no. 1, pp. 173-183, 1979. Available: 10.1016/0368-1874(79)85110-2.

[42] F. Kubannek, T. Turek and U. Krewer, "Modeling Oxygen Gas Diffusion Electrodes for Various Technical Applications", *Chemie Ingenieur Technik*, vol. 91, no. 6, pp. 720-733, 2019. Available: 10.1002/cite.201800181

[43] "Fuel Cells." *SpringerLink*, Springer, London, 1 Jan. 1970, link.springer.com/chapter/10.1007%2F978-1-84882-511-6_7.

[44] Spiridigliozzi, Luca. "Fuel Cells." *SpringerLink*, Springer, Cham, 1 Jan. 1970, link.springer.com/chapter/10.1007/978-3-319-99395-9_2.

[45] "Types of Fuel Cells." *Energy.gov*, Department of Energy, www.energy.gov/eere/fuelcells/types-fuel-cells.

[46] Davis, Frank. "Biofuel Cells–Recent Advances and Applications." *Researchgate*, Biosensor and Bioelectronics, Mar. 2007, www.researchgate.net/publication/7001687_Biofuel_Cells-Recent_Advances_and_Applications.

[47] Service, Robert F. "Biofuel Cells." *Science*, American Association for the Advancement of Science, 17 May 2002, science.sciencemag.org/content/296/5571/1223.

[48] Yadav, Mukesh, and Ram Singh. "Biofuel Cells: Concepts and Perspectives for Implantable Devices." *ResearchGate*, CRC Press, Jan. 2017, www.researchgate.net/publication/311576436_Biofuel_Cells_Concepts_and_Perspectives_for_Implantable_Devices.

[49] Moehlenbrock, M. J.; Minteer, S. D. Chem. Soc. Rev. 2008, 37, 1188-1196.

[50] Aulenta, F.; Tocca, L.; Verdini, R.; Reale, P.; Majone, M. Envir. Sci. Tech. 2011, 45, 8444-8451.

[51] Zhang, F.; Ge, Z.; Grimaud, J.; Hurst, J.; He, Z. Envir. Sci. Tech. 2013, 47, 4941-4948.

[52] Arechederra, R.; Minteer, S. D. Electrochim. Acta 2008, 53, 6698-6703.

[53] Atanassov, Palamev, and Scott Bantta. "Enzymatic Biofuel Cells." *Researchgate*, Electrochemical Society Interface, June 2007, www.researchgate.net/publication/260192029_Enzymatic_Biofuel_Cells.

[54] Barton, Scott, and Josh Gallaway. "Enzymatic Biofuel Cells for Implantable and Microscale Devices." *Enzymatic Biofuel Cells for Implantable and Microscale Devices | Chemical Reviews*, Chem. Rev, Sept. 2004, pubs.acs.org/doi/10.1021/cr020719k.

[55] Bullen, R.A, and F.C Walsh. “Biofuel Cells and Their Development.” *Biosensors and Bioelectronics*, Elsevier, Jan. 2006, blogs.epfl.ch/biofuelcells/documents/Biofuel%20cells%20and%20their%20development.pdf.

[56] Yu, Ellen, and Scoot Keith. “Enzymatic Biofuel Cells—Fabrication of Enzyme Electrodes.” *Research Gate*, Energies, Mar. 2010,

[57] Chen, Yun, et al. “Design of an Enzymatic Biofuel Cell with Large Power Output.” *Journal of Materials Chemistry A*, The Royal Society of Chemistry, 20 Apr. 2015, pubs.rsc.org/en/content/articlelanding/2015/ta/c5ta01432h#!divAbstract.

[58] Sidney, Aquino, and De Andrade. “New Energy Sources: the Enzymatic Biofuel Cell.” *Journal of the Brazilian Chemical Society*, Brazilian Chemical Society, Dec. 2013, www.scielo.br/scielo.php?script=sci_arttext&pid=S0103-50532013001200002.

[59] Kerzenmacher, Sven, and Arne Kloke. “Biofuel Cells for Energy Supply of Distributed System: State of the Art and Application.” *Researchgate*, Sensoren and Messsysteme, May 2010.

[60] Yadav, Mukesh, et al. “Biofuel Cells: Concepts and Perspectives for Implantable Revices.” *Researchgate*, CRC Press, Jan. 2017.

[61] Potter, M. C.; *Proceedings of the Royal Society of London. Series B, Containing Papers of a Biological Character* **1911**, *84*, 260. Available in http://m.rspb.royalsocietypublishing.org/content/84/571/260.full.pdf, accessed in November, 2013.

[62] Yahiro, A. T.; Lee, S. M.; Kimble, D. O.; *Biochim. Biophys. Acta (Specialized Section on Biophysical Subjects)* **1964**, *88*, 375.

[63] Bhalla, Nikhil, et al. “Introduction to Biosensors.” *Essays in Biochemistry*, Portland Press Limited, 30 June 2016, www.ncbi.nlm.nih.gov/pmc/articles/PMC4986445/.

[64] Kawamura, Akifumi, and Takashi Miyata. “Biosensors.” *Biosensors - an Overview | ScienceDirect Topics*, 2016, www.sciencedirect.com/topics/engineering/biosensors.

[65] Mehrotra, Parikha. “Biosensors and Their Applications - A Review.” *Journal of Oral Biology and Craniofacial Research*, Elsevier, 2016, www.ncbi.nlm.nih.gov/pmc/articles/PMC4862100/.

[66] Makaram, P.; Owens, D.; Aceros, J. Trends in Nanomaterial-Based Non-Invasive Diabetes Sensing Technologies. Diagnostics 2014, 4, 27–46, doi:10.3390/diagnostics4020027.

[67] Do Amaral, C.E.F.; Wolf, B. Current development in non-invasive glucose monitoring. Med. Eng. Phys. 2008, 30, 541–549, doi:10.1016/j.medengphy.2007.06.003.

[68] Yoo, E.H.; Lee, S.Y. Glucose biosensors: An overview of use in clinical practice. Sensors 2010, 10, 4558–4576, doi:10.3390/s100504558.

[69] Coyle, S.; Curto, V.F.; Benito-Lopez, F.; Florea, L.; Diamond, D. Wearable bio and chemical sensors. In Wearable Sensors; Elsevier Inc.: Amsterdam, The Netherlands, 2014; pp. 65–83.

[70] American Diabetes Association. Diagnosis and classification of diabetes mellitus. Diabetes Care 2004, 27, 5–10

[71] Badugu, R.; Lakowicz, J.R.; Geddes, C.R. Ophthalmic glucose monitoring using disposable contact lenses— A review. J. Fluoresc. 2004, 14, 617–633, doi:10.1023/B:JOFL.0000039349.89929.da

[72] Badugu, R.; Lakowicz, J.R.; Geddes, C.R. Fluorescence sensors for monosaccharides based on the 6- methylquinolinium nucleus and boronic acid moiety: Potential application to ophthalmic diagnostics. Talanta 2005, 65, 762–768, doi:10.1016/j.talanta.2004.08.003.

[73] Clark Jr., L.C.; Lyons, C. Electrode systems for continuous monitoring in cardiovascular surgery. Ann. N. Y. Acad. Sci. 1962, 102, 29–45, doi:10.1111/j.1749-6632.1962.tb13623.x.

[74] Price, C.P. Point-of-care testing in diabetes mellitus. Clin. Chem. Lab. Med. 2003, 41, 1213–1219, doi:10.1515/ CCLM.2003.185.

[75] D'Costa, E.J.; Higgins, I.J.; Turner, A.P. Quinoprotein glucose dehydrogenase and its application in an amperometric glucose sensor. Biosensors 1986, 2, 71–87, doi:10.1016/0265-928X(86)80011-6.

[76] Heller, A.; Feldman, B. Electrochemical glucose sensors and their applications in diabetes management. Chem. Rev. 2008, 108, 2482–2505, doi: 10.1021/cr068069y.

[77] Bankar, S.B.; Bule, M.V.; Singhal, R.S.; Ananthanarayan, L. Glucose oxidase - an overview. Biotechnol. Adv. 2009, 27, 489–501, doi:10.1016/j.biotechadv.2009.04.003.

[78] Guilbault, G.G.; Lubrano, G.J. An enzyme electrode for the amperometric determination of glucose. Anal. Chim. Acta 1973, 64, 439–455, doi:10.1016/S0003-2670(01)82476-4.

[79] Wang, J. Glucose biosensors: 40 Years of advances and challenges. Electroanalysis 2001, 13, 983–988.

[80] Clark, L.C., Jr. Monitor and control of blood and tissue oxygen tensions. Trans. Am. Soc. Artif. Intern. Organs 1956, 2, 41–48.

[81] Hilditch, P.; Green, M. Disposable electrochemical biosensors. Analyst 1991, 116, 1217–1220.

[82] Matthews, D.; Holman, R.; Brown, E.; Streemson, J.; Watson, A.; Hughes, S. Pen-sized digital 30-s blood glucose meter. Lancet 1987, 1, 778–779.

[83] Fang, H.; Kaur, G.; Wang, B. Progress in boronic acid-based fluorescent glucose sensors, J. Fluoresc. 2004, 14, 481–489, doi:10.1023/B:JOFL.0000039336.51399.3b.

[84] Pickup, J.C.; Hussain, F.; Evans, N.D.; Rolinski, O.J.; Birch, D.J.S. Fluorescence-based glucose sensors. Biosens. Bioelectron. 2005, 20, 2555–2565, doi:10.1016/j.bios.2004.10.002.

[85] Wang, J. Electrochemical glucose biosensors. Chem. Rev. 2008, 108, 814–825, doi:10.1021/cr068123a.

[86] Badugu, R.; Lakowicz, J.R.; Geddes, C.R. Boronic acid fluorescent sensors for monosaccharide signalling based on the 6-methoxyquinolinium heterocyclic nucleus: Progress toward noninvasive and continuous glucose monitoring. Bioorgan. Med. Chem. 2005, 13, 113–119, doi:10.1016/j.bmc.2004.09.058.

[87] Badugu, R.; Lakowicz, J.R.; Geddes, C.R. Ophthalmic glucose sensing: A novel monosaccharide sensing disposable and colourless contact lens. Analyst 2004, 129, 516–521, doi:10.1039/b314463c.

[88] Badugu, R.; Lakowicz, J.R.; Geddes, C.R. Noninvasive continuous monitoring of physiological glucose using a monosaccharide-sensing contact lens. Anal. Chem. 2004, 76, 610–618, doi:10.1021/ac0303721.

[89] Badugu, R.; Lakowicz, J.R.; Geddes, C.R. A glucose sensing contact lens: A non-invasive technique for continuous physiological glucose monitoring. J. Fluoresc. 2003, 13, 371–374.

[90] Moreno-Bondi, M.C.; Wolfbeis, O.S. Oxygen optrode for use in a fiber-optic glucose biosensor. Anal. Chem. 1990, 62, 2377–2380, doi:10.1021/ac00220a021.

[91] Larin, K.V.; Motamedi, M.; Ashitkov, T.V.; Esenaliev, R.O. Specificity of noninvasive blood glucose sensing using optical coherence tomography technique: A pilot study, Phys. Med. Biol. 2003, 48, 1371–1390.

[92] Nathan, D.M. The Diabetes Control and Complications Trial/Epidemiology of Diabetes Interventions and Complications Study at 30 years: Overview. Diabetes Care 2014, 37, 9–16, doi:10.2337/dc13-2112.

[93] Clarke, A.; O'Kelly, S. Glucose Monitoring Systems. Available online: http://www.diabetes.ie/living-withdiabetes/educational-articles/diabetes-and-research-articles/continuous-glucose-monitoring-cgmsystems/ (accessed on 8 October 2014). 4

[94] Badugu, R.; Lakowicz J, R.; Geddes C, D. Wavelength-ratiometric and colorimetric robes for glucose determination. Dyes and Pigments. 2006, 68, 159-163, doi: 10.1016/j.dyepig.2004.12.020.

[95] Badugu, R.; Lakowicz, J.R.; Geddes, C.R. A glucose-sensing contact lens: From bench top to patient. Curr. Op. Biotechnol. 2005, 16, 100–107, doi:10.1016/j.copbio.2004.12.007.

[96] Newman, J.; Turner, A.P.F. Home blood glucose biosensors: A commerical perspective. Biosens. Bioelectron. 2005, 20, 2435–2453, doi:10.1016/j.bios.2004.11.012. 4

[97] Boiroux, D.; Batora, V.; Hagdrup, M.; Tarnik, M.; Murgas, J.; Schmidt, S.; Norgaard, K.; Poulsen, N.K.; Madsen, H.; Jorgensen, J.B. Comparison of prediction models for a dual-hormone artifical pancreas. IFACPapersOnLine 2015, 48, 7–12, doi:10.1016/j.ifacol.2015.10.106.

[98] Nishida, K.; Shimoda, S.; Ichinose, K.; Araki, E.; Shichiri, M. What is the artificial endocrine pancreas? Mechanism and history. World J. Gastroenterol. 2009, 15, 4105–4110, doi:10.3748/wjg.15.4105.

[99] Albisser, A.M.; Leibel, B.S.; Ewart, T.G.; Davidovac, Z.; Botz, C.K.; Zingg, W.; Schipper, H.; Gander, R. Clinical control of diabetes by the artificial pancreas. Diabetes 1974, 23, 397–404, doi:10.2337/diab.23.5.397.

[100] Bindra, D.S.; Zhang, Y.; Wilson, G.S.; Sternberg, R; Thévenot, D.R.; Moatti, D.; Reach, G. Design and in vitro studies of a needle-type glucose sensor for subcutaneous monitoring. Anal. Chem. 1991, 63, 1692–1696.

[101] McGreevy, R. Flash glucose monitoring latest concept in testing. The Irish Times, 22 October 2013. Available online: www.irishtimes.com (22 October 2013).

[102] Worsley, G.J.; Tourniaire, G.A.; Medlock, K.E.S.; Sartain, F.K.; Harmer, H.E.; Thatcher, M.; Horgan, A.M.; Pritchard, J. Continuous blood glucose monitoring with a thin-film optical sensor. Clin. Chem. 2007, 53, 1820–1826, doi:10.1373/clinchem.2007.091629.

[103] Hong, Y.J.; Lee, H.; Kim, J.; Lee, M.; Choi, H.J.; Hyeon, T.; Kim, D.H. "Multifunctional wearable system that integrates sweat-based sensing and vital-sign monitoring to estimate pre-/post-exercise glucose levels." Advanced Functional Materials *(*2018), pp. *1805754*.doi.org:10.1002/adfm.201805754

[104] Lee, H.; Song, C.; Hong, Y.S.; Kim, M.S.; Cho, H.R.; Kang, T.; Shin, K.; Choi, S.H.; Hyeon, T.; Kim, D.H. "Wearable/disposable sweat-based glucose monitoring device with multistage transdermal drug delivery module." *Sci. Adv.(*2017), *3*, pp. 1601314. doi: 10.1126/sciadv.1601314

[105]Emaminejad, S.; Gao, W.; Wu, E.; Davies, Z.A.; Nyein, H.Y.Y.; Challa, S.; Ryan, S.P.; Fahad, H.M.; Chen, K.; Shahpar, Z.; et al. "Autonomous sweat extraction and analysis applied to cystic fibrosis and glucose monitoring using a fully integrated wearable platform." *Proc. Natl. Acad. Sci. USA (*2017**)**, *114*, pp.4625–4630. doi:10.1073/pnas.1701740114

[106]Lan, T.; Zhang, J.J.; Lu, Y. “Transforming the blood glucose meter into a general healthcare meter for in vitro diagnostics in mobile health.” *Biotechnol. Adv. (*2016), *34*, pp. 331–341. doi:10.1016/j.biotechadv.2016.03.002

[107]Toghill, K.E.; Compton, R.G.” Electrochemical non-enzymatic glucose sensors: A perspective and an evaluation.” *Int. J. Electrochem. Sci. (*2010), *5*, pp. 1246–1301.

[108]Kim, J.; Campbell, A.S.; Wang, J. “Wearable non-invasive epidermal glucose sensors: A review. “*Talanta (*2018), *177*, pp. 163–170. doi:10.1016/j.talanta.2017.08.077

[109]Hwang, D.W.; Lee, S.; Seo, M.; Chung, T.D. “Recent advances in electrochemical non-enzymatic glucose sensors—A review.” *Anal. Chim. Acta (*2018), pp. *1033*, 1–34. doi:10.1016/j.aca.2018.05.051

[110]Gao, W.; Emaminejad, S.; Nyein, H.Y.Y.; Challa, S.; Chen, K.V.; Peck, A.; Fahad, H.M.; Ota, H.; Shiraki, H.; Kiriya, D.; et al. “Fully integrated wearable sensor arrays for multiplexed in situ perspiration analysis.” *Nature (*2016), *529*, pp. 509–514.

[111]Zhao, J.Q.; Lin, Y.J.; Wu, J.B.; Nyein, H.Y.Y.; Bariya, M.; Tai, L.C.; Chao, M.H.; Ji, W.B.; Zhang, G.; Fan, Z.Y.; et al. “A fully integrated and self-powered smartwatch for continuous sweat glucose monitoring.” *ACS Sens. (*2019), *4*, pp. 1925–1933. doi:0.1021/acssensors.9b00891

[112]Kim, J.; Sempionatto, J.R.; Imani, S.; Hartel, M.C.; Barfidokht, A.; Tang, G.D.; Campbell, A.S.; Mercier, P.P.; Wang, J. “Simultaneous monitoring of sweat and interstitial fluid using a single wearable biosensor platform.” *Advanced Science. (*2018), *5*, pp. 1800880. doi:10.1002/advs.201800880

[113]Hong, S.; Lee, H.; Lee, J.; Kwon, J.; Han, S.; Suh, Y.D.; Cho, H.; Shin, J.; Yeo, J.; Ko, S.H.” Highly stretchable and transparent metal nanowire heater for wearable electronics applications.” *Advanced Materials (*2015), *27*, pp. 4744–4751. doi:10.1002/adma.201500917

[114]Corrie, S.J.; Coffey, J.W.; Islam, J.; Markey, K.A.; Kendall, M.A.F. Blood, sweat, and tears: Developing clinically relevant protein biosensors for integrated body fluid analysis. Analyst 2015, 140, 4350–4364, doi:10.1039/c5an00464k.

[115]Bandodkar, A.J.; Wang, J. Non-invasive wearable electrochemical sensors: A review. Trends Biotechnol. 2014, 32, 363–371, doi:10.1016/j.tibiotech.2014.04.005.

[116]Hanashi, T.; Yamazaki, T.; Tsugawa, W.; Ikebukuro, K.; Sode, K. BioRadioTransmitter: A self-powered wireless glucose-sensing system. J. Diabetes Sci. Technol. 2011, 5, 1030–1035

[117]Jina, A.; Tierney, M.J.; Tamada, J.A.; McGill, S.; Desai, S.; Chua, B.; Chang, A.; Christiansen, M. Design, development, and evaluation of a novel microneedle array-based

continuous glucose monitor. J. Diabetes Sci. Technol. 2014, 8, 483–487, doi:10.1177/1932296814526191.

[118]Zhang, W.; Du, Y; Wang, M.L. On-chip highly sensitive saliva glucose sensing using multilayer films composed of single-walled carbon nanotubes, gold nanoparticles, and glucose oxidase. Sens. Bio-Sens. Res. 2015, 4, 96–102, doi:10.1016/j.sbsr.2015.04.006.

[119]Corrie, S.J.; Coffey, J.W.; Islam, J.; Markey, K.A.; Kendall, M.A.F. Blood, sweat, and tears: Developing clinically relevant protein biosensors for integrated body fluid analysis. Analyst 2015, 140, 4350–4364, doi:10.1039/c5an00464k.

[120]Lee, H.; Song, C.; Hong, Y.S.; Kim, M.S.; Cho, H.R.; Kang, T.; Shin, K.; Choi, S.H.; Hyeon, T.; Kim, D. Wearable/disposable sweat-based glucose monitoring device with multistage transdermal drug delivery module. Sci. Adv. 2017, 3, e1601314, doi:10.1126/sciadv.1601314.

[121]Heikenfeld, J. Non-invasive analyte access and sensing through eccrine sweat: Challenges and outlook circa 2016. Electroanalysis 2016, 28, 1242–1249, doi:10.1002/elan.201600018.

[122]Morris, D.; Coyle, S.; Wu, Y.; Lau, K.T.; Wallace, G.; Diamond, D. Bio-sensing textile based patch with integrated optical detection system for sweat monitoring. Sens. Actuators B Chem. 2009, 139, 231–236, doi:10.1016/j.snb.2009.02.032.

[123]Mitsubayashi, K.; Suzuki, M.; Tamiya, E.; Karube, I. Analysis of metabolites in sweat as a measure of physical condition. Anal. Chim. Acta 1994, 289, 27–34, doi:10.1016/0003-2670(94)80004-9.

[124]Gao, W.; Emaminejad, S.; Nyein, H.Y.Y.; Challa, S.; Chen, K.; Peck, A.; Fahad, H.M.; Ota, H.; Shiraki, H.; Kiriya, D.; et al. Fully integrated wearable sensor arrays for multiplexed in situ perspiration analysis. Nature 2016, 529, 509–514, doi:10.1038/nature16521.

[125]Moser, T.; Celma, C.; Lebert, A.; Charrault, E.; Brooke, R.; Murphy, P.J.; Browne, G.; Young, R.; Higgs, T.; Evans, D. Hydrophilic organic electrode on flexible hydrogels. ACS Appl. Mater. Interfaces 2016, 8, 974–982, doi:10.1021/acsami.5b10831.

[126]CA Naval Air Warfare Center Weapons Div Point Mugu, “Electronic Warfare and Radar Systems Engineering Handbook.” Storming Media, 1997.

[127]K. Finkenzeller, *RFID handbook: “*Fundamentals and applications in contactless smart cards, radio frequency identification and near-field communication.” Wiley, 3 ed., 2010.

[128]ISO/IEC, “ISO-15693 Contactless integrated circuit (s) cards - Part 2 : Radio frequency power and signal interface,” 1999.

[129]Nfc Forum, “NFC Forum : Members.” Available: http://www.nfc-forum.org/member_companies/.

[130]Google, “NFC Basics | Android Developers.” Available: http://developer.android.com/guide/topics/connectivity/nfc/nfc.html.

[131]https://www.omicron-lab.com/bode-100/product-description.html, Bode 100 Vector Network Analyzer. Omicron Lab.

[132]Eddie LaCost, Battery-Less NFC/RFID Temperature Sensing Patch. Texas Instruments, Application Report, SLOA212-December 2014.

[133]http://www.ti.com/lit/ds/slas834c.pdf, RF430FRL15xH NFC ISO 15693 Sensor Transponder. Texas Instruments, SLAS834CNovember 2012-Revised December 2014.

[134]Nfc Forum, “Technical Specifications.” Available: http://www.nfc-forum.org/specs/spec_list/.

[135]Nfc Forum, *Type 1 Tag Operation Specification*. 2011. https://members.nfc-forum.org/apps/group_public/download.php/17506/NFCForum-TS-Type-1-Tag_1.2_For_Feedback_Only.pdf

[136]Nfc Forum, *Type 2 Tag Operation Specification*. 2011. https://members.nfc-forum.org/apps/group_public/download.php/17506/NFCForum-TS-Type-2-Tag_1.2_For_Feedback_Only.pdf

[137]Nfc Forum, *Type 3 Tag Operation Specification*. 2011.

[138]Nfc Forum, *Type 4 Tag Operation Specification*. 2011.

[139]Google, “Advanced NFC | Android Developers.” Available: http://developer.android.com/guide/topics/connectivity/nfc/advanced-nfc.html.

[140]SkyRFID Inc., “RFID Active and Passive Tag Frequencies | RFID Transmission Power.” Available: http://www.skyrfid.com/RFID_Frequencies.php.

[141]Nfc Forum, “Frequently Asked Questions.” Available: http://www.nfc forum.org/resources/faqs#operating.

[142]Nokia, “Introduction to NFC,” no. July, pp. 1–34, 2011.

[143]Nfc Forum, “NFC Data Exchange Format (NDEF) Technical Specification,” 2006.

[144]Google, “Android 2.3.3 Platform | Android Developers.” Available: http://developer.android.com/about/versions/android-2.3.3.html.

[145]Google, “Features Galaxy Nexus S.” Available: http://www.google.com/nexus/s/features.html.

[146]http://www.statista.com/statistics/347315/nfc-enabled-phoneinstalled-base/, “The forecasted global installed base of NFC-enabled phones from 2013 to 2018.” Statista: 2016.

[147]J. Fischer, “Near-field communications: NFC in cell phones: The new paradigm for an interactive world.” IEEE Commun. Mag, Jun. 2009, vol. 47, no. 6, pp. 22–28.

[148]H. Eun, H. Lee, and H. Oh, “Conditional privacy preserving security protocol for NFC applications.” IEEE Trans. Consum. Electron., Feb. 2013 vol. 59, no. 1, pp. 153–160.

[149]H. M. GreenHouse, “Design of Planar Rectangular Microelectronic Inductors.” IEEE Transactions on parts, hybrids, and packaging, Vol. PHP-10, No. 2, June 1974.

[150]M.Gebhart,R.Neubauer,M.Stark,andD.Warnez,”Design of 13.56MHz smartcard stickers with ferrite for payment and authentication.” in Proc. 3nd Int. Workshop Near Field Commun. (NFC), Feb. 2011, pp. 59–64.

[151]Firebase.google.com, *Read and Write Data on Android*, https://firebase. google.com/docs/database/android/read-and-write

[152]Wikipedia.org, *UTF-8*, https://it.wikipedia.org/wiki/UTF-8

[153]Firebase.google.com, *Realtime Database Limits*, https://firebase.google. com/docs/database/usage/limits

[154]*Introducing JSON*, https://www.json.org/index.html

[155]Firebase.google.com, *Cloud Storage*, https://firebase.google.com/docs/storage/

[156]Firebase.google.com *Get Started with Storage Security Rules*, https:// irebase.google.com/docs/storage/security/start

[157]Diabetic Hypoglycemia, https://www.mayoclinic.org/diseases-conditions/diabetic-hypoglycemia/symptoms-causes/syc-203 71525, retrieved at 24-8-2018.

[158]Vahidi O, Kwok KE, Gopaluni RB, Knop FK. “A comprehensive compartmental model of blood glucose regulation for healthy and type 2 diabetic subjects,” Med Biol Eng Comput. (2015); pp. 1–16.

[159]L. R. Rabiner and B. H. Juang. (1986) “An introduction to hidden Markov models,” IEEE Acoust., Speech, Signal Processing Mag., Jan. 1986, pp. 4–16.

[160]Hyperglycemia in Diabetes, https://www.mayoclinic.org/diseases-conditions/hyperglycemia/symptoms-causes/syc-20373631, retrieved at 16-9-2018

[161]Cunningham, K., & Read, N.. “The effect of incorporating fat into different components of a meal on gastric emptying and postprandial blood glucose and insulin responses.” British Journal of Nutrition, 61(2), (1989) pp.285-290. doi:10.1079/BJN19890116

[162]W. S. McCulloch and W. Pitts*.” A logical calculus of ideas immanent in nervous activity”*, Bulletin of Mathematical Biophysics, (1943) vol. 5, pp. 115–133, 1943.

[163]D. E. Rumelhart, G. E. Hinton, and R. J. Williams. “Learning internal representations by error propagation, Parallel Distributed Processing: Explorations in the Microstructure of Cognition,” Eds., vol. 1, ch. 8,. Cambridge, MA: MIT Press, (1986). pp. 318-362

[164]LeCun, Y.. “A theoretical framework for back-propagation,” Proceedings of the 1988 Connectionist Models Summer School, (1988) pp. 21–28.

[165]Xu, K., Ba, J., Kiros, R., Cho, K., Courville, A. C., Salakhutdinov, R., Zemel, R. S., and Bengio, Y.” Show, attend and tell: Neural image caption generation with visual attention,” CoRR,(2015) doi:abs/1502.03044.

[166]N.Srivastava , G. Hinton, A. Krizhevsky, I. Sutskever, and R. Salakhutdinov “Dropout: A simple way to prevent neural networks from overfitting,” Journal of Machine Learning Research, (2014) 15: pp.1929–1958.

[167]Sud harsan B, Peeples M, Shom ali M (2015). “Hypoglycemia prediction using machine learning models for patients with type 2 diabetes,” J Diabetes Sci Technol (2015) pp. 86–90. Doi:10.1177/1932296814554260

[168]Fisher, R. A. “Frequency distribution of the values of the correlation coefficient in samples of an indefinitely large population,” Biometrika. Biometrika Trust. (1915)10 (4): pp.507–521. doi:10.2307/2331838

[169]Gani, A.; Gribok, A. V.; Lu, Y.; Ward, W. K.; Vigersky, R. A. & Reifman, J. “Universal Glucose Models for Predicting Subcutaneous Glucose Concentration in Humans,” IEEE Transactions on Information Technology in Biomedicine, Vol. 14, No. 1, (2010) pp.157-165.

[170]A. Abbadi, H. van Bekkum, “Effect of pH in the Pt-catalyzed oxidation of D-glucose to D-gluconic acid,” J. Mol. Catal. A: Chem. 97 (2) (1995) 111–118.

[171]X. Yan, X. Ge, S. Cui, “Pt-decorated nanoporous gold for glucose electrooxidation in neutral and alkaline solutions,” Nanoscale Res. Lett. 6 (2011) 1–6.

[172]T. Ikeda, “Bioelectrochemical studies based on enzyme-electrocatalysis,” E Electrochimica acta 82 (2012) 158–164.

[173]Y. Wang, T. Hosono, Y. Hasebe, “Hemin-adsorbed carbon felt for sensitive and rapid flow-amperometric detection of dissolved oxygen,” Microchim. Acta 180 (13-14) (2013) 1295–1302.

[174]X. Xie, M. Ye, P.C. Hsu, N. Liu, Criddle, C.S., Cui, Y. “Microbial battery for efficient energy recovery.” Proc. Natl. Acad. Sci. 110 (2013) 15925-15930.

[175]A.J. Bandodkar, J.M. You, N.H. Kim, Y. Gu, R. Kumar, A.V. Mohan, J. Kurniawan, S. Imani, T. Nakagawa, B. Parish, M. Parthasarathy, “Soft, stretchable, high power density electronic skin-based biofuel cells for scavenging energy from human sweat,” Energy Environ. Sci. 10 (7) (2017) 1581–1589.

[176]T. Kulkarni, N. Mburu, G. Slaughter, “Characterization of a self-powered glucose monitor, “Sens. Transducers 203 (8) (2016) 1.

[177]K. Sharma, Carbohydrate-to-hydrogen production technologies: a mini-review, Renew. Sustain. Energy Rev. 105 (2019) 138–143.

[178]G. Pandey, Biomass based bio-electro fuel cells based on carbon electrodes: an alternative source of renewable energy, Sn Appl. Sci. 1 (5) (2019) 408.

[179]A. Nasar, R. Perveen, Applications of enzymatic biofuel cells in bioelectronic devices–A review, Int. J. Hydrogen Energy 44 (29) (2019) 15287–15312.

[180]L. Fu, J. Liu, Z. Hu, M. Zhou, Recent advances in the construction of biofuel cells based self-powered electrochemical biosensors: a review, Electroanalysis 30 (11) (2018) 2535–2550.

[181]G. Slaughter, T. Kulkarni, Enzymatic glucose biofuel cell and its application, J. Biochips Tissue Chips 5 (1) (2015) 1.

[182]A. Arsalis, A comprehensive review of fuel cell-based micro-combined-heat-and- power systems, Renew. Sustain. Energy Rev. 105 (2019) 391–414.

[183]A. Arshad, H.M. Ali, A. Habib, M.A. Bashir, M. Jabbal, Y. Yan, Energy and exergy analysis of fuel cells: a review, Therm. Sci. Eng. Progr. 9 (2019) 308–321.

[184]C. Abreu, Y. Nedellec, O. Ondel, F. Buret, S. Cosnier, A.L. Goff, M. Holzinger, Towards eco-friendly power sources: in series connected glucose biofuel cells power a disposable ovulation test, Sens. Actuat. B Chem. 277 (2018) 360–364. G. Slaughter, Current Advances in biosensor design and fabrication, Encyclopedia of Analytical Chemistry: Applications Theory and Instrumentation (2006) 1–25.

[185]M. Gamella, A. Koushanpour, E. Katz, Biofuel cells–activation of micro-and macro-electronic devices, Bioelectrochemistry 119 (2018) 33–42.

[186]Q. Xu, F. Zhang, L.i. Xu, P. Leung, C. Yang, H. Li, The applications and prospect of fuel cells in medical field: a review, Renew. Sustain. Energy Rev. 67 (2017) 574–580.

[187]D. Ivnitski, K. Artyushkova, P. Atanassov, Surface characterization and direct electrochemistry of redox copper centers of bilirubin oxidase from fungi myrothecium verrucaria, Bioelectrochemistry 74 (1) (2008) 101–110.

[188]B. Haghighi, B. Karimi, M. Tavahodi, H. Behzadneia, Electrochemical behavior of glucose oxidase immobilized on Pd-nanoparticles decorated ionic liquid derived fibrillated mesoporous carbon, Electroanalysis 26 (9) (2014) 2010–2016.

[189]G. Slaughter, J. Sunday, Fabrication of enzymatic glucose hydrogel biosensor based on hydrothermally grown ZnO nanoclusters, IEEE Sens. J. 14 (5) (2014) 1573–1576.

[190]C.X. Guo, C.M. Li, Direct electron transfer of glucose oxidase and biosensing of glucose on hollow sphere-nanostructured conducting polymer/metal oxide composite, PCCP 12 (38) (2010) 12153–12159.

[191]H.B. Wang, H.D. Zhang, Y. Chen, Y. Li, T. Gan, H2O2-mediated fluorescence quenching of double-stranded DNA templated copper nanoparticles for label-free and sensitive detection of glucose, RSC Adv., 2015.

[192]L. Wang, J. Zheng, Y. Li, S. Yang, C. Liu, Y. Xiao, J. Li, Z. Cao, R. Yang, AgNP- DNA@ GQDs hybrid: new approach for sensitive detection of H2O2 and glucose via simultaneous AgNP etching and DNA cleavage, Anal. Chem. 86 (24) (2014) 12348–12354.

[193]B.o. Liang, L.u. Fang, G. Yang, Y. Hu, X. Guo, X. Ye, Direct electron transfer glucose biosensor based on glucose oxidase self-assembled on electrochemically reduced carboxyl graphene, Biosens. Bioelectron. 43 (2013) 131–136.

[194]P. Yang, L. Wang, Q. Wu, Z. Chen, X. Lin, A method for determination of glucose by an amperometric bienzyme biosensor based on silver nanocubes modified Au electrode, Sens. Actuators, B 194 (2014) 71–78.

[195]Y. Zhu, X. Zhang, J. Sun, M. Li, Y. Lin, K. Kang, Y. Meng, Z. Feng, J. Wang, Y. Zhu, A non-enzymatic amperometric glucose sensor based on the use of graphene frameworks-promoted ultrafine platinum nanoparticles, Microchim. Acta 186 (8) (2019) 1–10.

[196]M.Q. Hasan, R. Kuis, J.S. Narayanan, G. Slaughter, Fabrication of highly effective hybrid biofuel cell based on integral colloidal platinum and bilirubin oxidase on gold support, Sci. Rep. 8 (1) (2018) 1–10.

[197]A. Baingane, G. Slaughter, Enzyme-free self-powered glucose sensing system, In Proc. IEEE SENSORS, Oct. (2018) 1–4.

[198]N. Shah, M. Ul-Islam, W.A. Khattak, J.K. Park, Overview of bacterial cellulose composites: a multipurpose advanced material, Carbohydr. Polym. 98 (2) (2013) 1585–1598.

[199]W. Hu, S. Chen, J. Yang, Z. Li, H. Wang, Functionalized bacterial cellulose derivatives and nanocomposites, Carbohydr. Polym. 101 (2014) 1043–1060.

APPENDIX A

ANDROID APPLICATION DEVELOPMENT

For application-based development the android studio used as the native environment enabled a lot of features for NFC tag detection and incoming signal modification. The application was initiated by the development of the latest build using a Java version that basically allows new features to be compatible. We started with gradle build which is a build automation tool based on groovy and kotlin. It is an open source and flexible tool which supports many dependencies that allow addition of multiple features for the application. The gradle build used in this application is as shown in the code snippet comprised of the software development kit (sdk) version with default configuration having minimum and maximum requirements for the app to run on multiple generations of Android devices.

```
android {
    compileSdk 30

    defaultConfig {
        applicationId "com.example.assemble"
        minSdk 17
        targetSdk 30
        versionCode 1
        versionName "1.0"

        testInstrumentationRunner "androidx.test.runner.AndroidJUnitRunner"
    }

    buildTypes {
        release {
            minifyEnabled false
            proguardFiles getDefaultProguardFile('proguard-android-
optimize.txt'), 'proguard-rules.pro'
        }
    }
    compileOptions {
        sourceCompatibility JavaVersion.VERSION_1_8
        targetCompatibility JavaVersion.VERSION_1_8
    }
}
```

Dependencies involved in this project are mentioned in the code snippet where latest contrait layout and android material were implemented. Also, an external dependency was used for graphical purposes using a graph based library to enable that plot. And a firebase database dependency was added to call upon when data was stored in the database.

```
dependencies {

    implementation 'androidx.appcompat:appcompat:1.3.1'
    implementation 'com.google.android.material:material:1.4.0'
    implementation 'androidx.constraintlayout:constraintlayout:2.1.0'
    implementation 'com.google.firebase:firebase-database:20.0.2'
    testImplementation 'junit:junit:4.+'
    androidTestImplementation 'androidx.test.ext:junit:1.1.3'
    androidTestImplementation 'androidx.test.espresso:espresso-core:3.4.0'
    implementation 'com.jjoe64:graphview:4.2.1'
}
```

In the main activity section where the actual functions are initiated, variables associated with the NFC tag detection are written with the ADC input parameters set to 0 so that the RF430FRL152H is able to communicate and transmit the bits into the right location. As shown in the code snippet, the values are assigned to the variable to perform the read function for the NFC based tag.

```
public class MainActivity extends AppCompatActivity {

    TextView Value,Byte_text,text_view,adc0,adc1,adc2, date_value,
time_value;
    Button increase, decrease,dig_out;
    private NfcAdapter nfc;
    float ADC0=0,ADC1=0,ADC2=0;
    private PendingIntent mpendingIntent;
    private final Handler mHandler = new Handler();
    private Runnable mTimer;
    private Button button3;
    //private Runnable mTimer;
    //display variables
    String f_val="00 00 00 00 00 00 00 00 00",text_val="Place phone on
Tag";
    byte b_val=0x01,dig_op=0x00;
    public final static String EXTRA_MESSAGE =
"com.example.assemble.MESSAGE";
```

Among the variables assigned, functions were created to create a tag discover intent filter such that the respective tag from the emitter is read by the application. Detection involves

whether the NFC is disabled or the tag is not readable as shown in the code snippet. Features involving Calendar and time format were also inscribed among the function so that the recording can be tracked for the application.

```
nfc = NfcAdapter.getDefaultAdapter(this);
if (nfc == null) {
    text_view.setText("No NFC!!");
    text_val="No NFC!!";}
if (!nfc.isEnabled()) {
    text_view.setText("NFC is disabled.");
    text_val="NFC is disabled.";
}
mpendingIntent = PendingIntent.getActivity(
        this, 0, new Intent(this,
getClass()).addFlags(Intent.FLAG_ACTIVITY_SINGLE_TOP), 0);

//Date and time functionality
date_value = findViewById(R.id.textView4);
time_value = findViewById(R.id.textView5);

Calendar calendar = Calendar.getInstance();
SimpleDateFormat simpleDateFormat = new SimpleDateFormat("dd-MMM-yyyy");
SimpleDateFormat simpleDateFormat1 = new SimpleDateFormat("hh:mm::ss a");
String Timedate = simpleDateFormat.format(calendar.getTime());
String Timedate1 = simpleDateFormat1.format(calendar.getTime());
date_value.setText(Timedate);
time_value.setText(Timedate1);
```

The database used here, firebase Realtime, is initiated using the child and parent command which enables communication to the cloud with the respective features. Referencing the names of the features that are stored in the user profile as a parent is shown in the code snippet. This allows values to be input by the user and converted to a string to be communicated to the cloud and stored as a JSON object.

```
String child = editTextName.getText().toString();
reference = database.getReference("Users").child(child);

reference.child("Name").setValue(editTextName.getText().toString());
reference.child("Glucose").setValue(adc0.getText().toString());
reference.child("Temperature").setValue(adc2.getText().toString());
reference.child("Age").setValue(editTextGlucose.getText().toString());
reference.child("Height").setValue(editTextheight.getText().toString());
reference.child("Weight").setValue(editTextWeight.getText().toString());
reference.child("Gender").setValue(editTextgender.getText().toString());
reference.child("Blood
Pressure").setValue(editTextBP.getText().toString());
reference.child("Date").setValue(date_value.getText().toString());
reference.child("Time").setValue(time_value.getText().toString());
```

Another important snippet that allows the user to parse the data in one field in the source file and write the parts of the data to a field (in this scenario, the input string that is recognized by the application) is converted to a hex array in which all the characters are converted to return a string value that could be passed on to be recognized as ADC0, ADC1 and ADC2 values using the custom built algorithm.

```
//parsing function
final protected static char[] hexArray = "0123456789ABCDEF".toCharArray();
public static String bytesToHex(byte[] bytes) {
    char[] hexChars = new char[bytes.length * 3];
    for ( int j = 0; j < bytes.length; j++ ) {
        int v = bytes[j] & 0xFF;
        hexChars[j * 3] = hexArray[v >>> 4];
        hexChars[j * 3 + 1] = hexArray[v & 0x0F];
        hexChars[j * 3 + 2] = ' ';
    }
    return new String(hexChars);
}
```

To read the data from the tag, a class in NfcV is created which acquires an object using get tag value as shown in snippet 68. This tech allows us to read the incoming data from the tag by creating an instance for the tag. Reading the register bits in which the components of the flags, block number, ADC0, ADC2, sensor configuration registers, delay periods are programmed as pe the datasheet of RF430FRL152H. This enables us to create a format for the input signals that is recognizable by the tag and the NFC based module datasheet. This works in the background for reading the data, which is an important function to distinguish the input data read.

```
//read data
private void readTagData(Tag tag) {

    byte[] id = tag.getId();
    boolean techFound = false;
    for (String tech : tag.getTechList()) {

        // checking for NfcV
        if (tech.equals(NfcV.class.getName())) {
            techFound = true;


            // Get an instance of NfcV for the given tag:
            NfcV nfcv_senseTag = NfcV.get(tag);
```

```
            try {
                nfcv_senseTag.connect();
                text_val="Tag connected";
            }catch (IOException e) {
                text_val="Tag connection lost";
                return;
            }



            //read register test
            byte[] cmd = new byte[] {
                    //    (byte)0x18, // Always needed, everything after
this 18 is sent over the air, response is given in the text box below
                    (byte)0x02, // Flags (always use same)
                    (byte)0x20, // ISO15693 command code, in this case it
is Read Single Block
                    (byte)b_val, // Block number
            };

            byte[] systeminfo;
            try {
                systeminfo = nfcv_senseTag.transceive(cmd);
            }catch (IOException e) {
                text_val="Tag transfer failed";
                //Log.i("Tag data", "transceive failed");
                return;
            }


            //Log.i("Tag data", "result= " + bytesToHex(systeminfo));

            //write  to block 2
            cmd = new byte[] {
                    //    (byte)0x18, // Always needed, everything after
this 18 is sent over the air, response is given in the text box below
                    (byte)0x02, // Flags (always use same)
                    (byte)0x21, // ISO15693 command code, in this case it
is Write Single Block
                    (byte)0x02, //block number
                    (byte)0x11, //reg1 Reference-ADC1 Configuration
Register DECIMATION 12 BIT
                    (byte)0x11, //reg2 ADC2 Sensor Configuration Register
                    (byte)0x10, //reg3 ADC0 Sensor Configuration Register
                    (byte)0x00, //reg4 Internal Sensor Configuration
Register
                    (byte)0x00, //reg5 Initial Delay Period Setup Register
                    (byte)0x00, //reg6  JTAG Enable Password Register
                    (byte)0x00, //reg7 Initial Delay Period Register
                    (byte)0x00, //reg8 Initial Delay Period Register
            };
            byte[] ack;
            try {
                ack = nfcv_senseTag.transceive(cmd);
            }catch (IOException e) {
                text_val="Tag transfer failed";
                Log.i("Tag data", "transceive failed");
                return;
            }
            //Log.i("Tag data", "ack= " + bytesToHex(ack));
            while(b_val>0) {
```

```
                //write 01 00 04 00 01 01 00 40 to block 0
                cmd = new byte[]{
                        //    (byte)0x18, // Always needed, everything after
this 18 is sent over the air, response is given in the text box below
                        (byte) 0x02, // Flags (always use same)
                        (byte) 0x21, // ISO15693 command code, in this case
it is Write Single Block
                        (byte) 0x00, //block number
                        (byte) 0x21, //Start bit is set, after this is
written this starts the sampling process, interrupt enabled for On/Off
                        (byte) 0x00, //Status byte
                        (byte) 0x07, //Reference resisitor, thermistor,
ADC0 sensor selected selected
                        (byte) 0x00, //Frequency register, this is do not
care since only one sample or pass is done
                        (byte) 0x01, //only one pass is needed
                        (byte) 0x01, //No averaging selected
                        (byte) 0x0E, //Interrupt enabled, push pull active
high options selected
                        (byte) 0x40, //Selected using thermistor
                };
                if(dig_op==1)
                    cmd[3]|=0x40;
                ack = new byte[]{0x01};

                try {
                    ack = nfcv_senseTag.transceive(cmd);
                } catch (IOException e) {
                    text_val="Tag transfer failed";
                    //Log.i("Tag data", "transceive failed");
                    return;
                }
```

APPENDIX B

PREDICTION RESULTS

Machine learning models were prepared after data preprocessing for time series forecasting. Forecast errors on time series regression problems are called residuals or residual errors. Careful exploration of residual errors on your time series prediction problem can describe a lot about the designed forecast model and even suggest improvements. For all the models, after the validation dataset prediction residual errors were visualized using a Q-Q plot. This is the prequel before the actual models were optimized to perform results as explained in the results and discussion section. A Q-Q plot, also known as a quantile plot, compares two distributions and may be used to determine how similar or dissimilar they are. Using the statsmodels library's qqplot() method, we can make a Q-Q plot. The Q-Q plot is used to rapidly verify the normality of the residual error distribution. The comparison is depicted as a scatter plot (theoretical on the x-axis and observed on the y-axis), with a match between the two distributions depicted as a diagonal line running from the bottom left to the top right of the plot. The graphic is useful for identifying obvious deviations from this assumption.

A. 15 minutes

In Figures 62 – 69, predictions based on validation set are displayed with residual error plots that help in understanding the deviations from the prediction made by the algorithm, with outliers being presently detectable in the Q-Q plot. Also, the table provides an additional comparison between the models based on the error metrics. RNN performed much better than other error metrics of models.

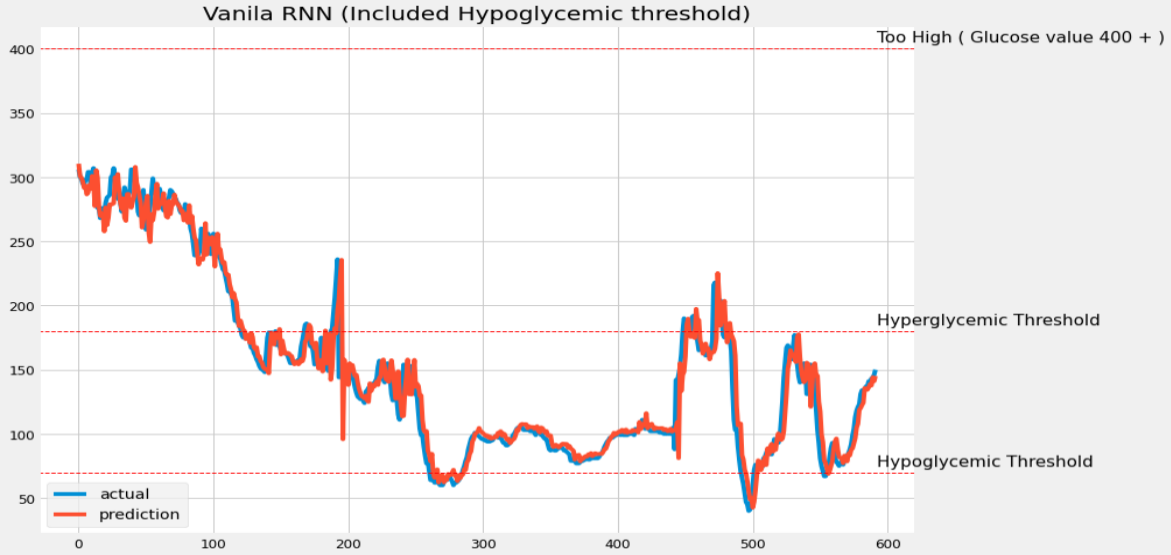

Figure 62. A Vanilla RNN implementation with validation set for 15min.

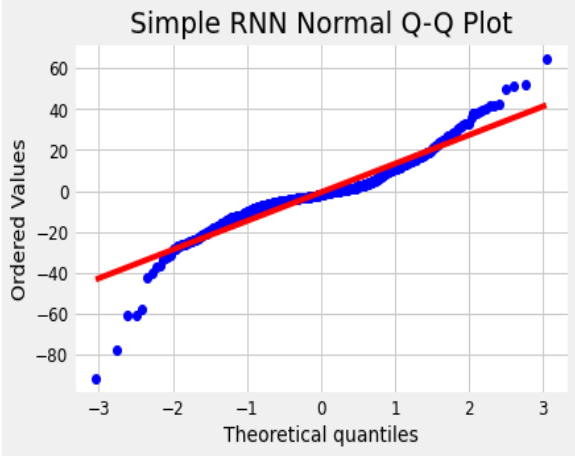

Figure 63. Q-Q plots for Vanilla RNN representation in 15 min.

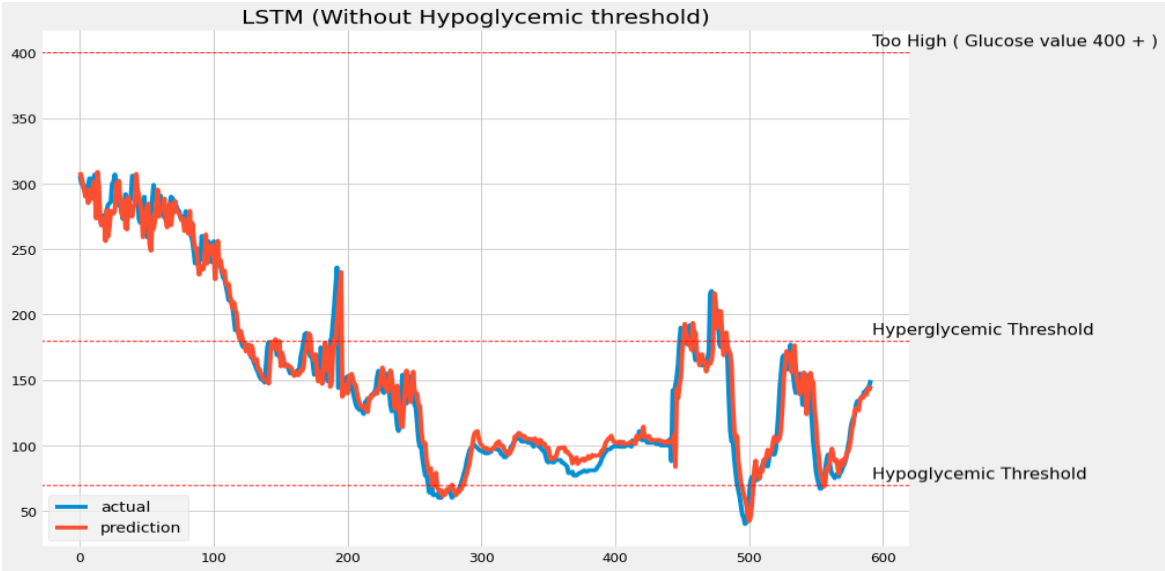

Figure 64. LSTM implementation with validation set for 15min.

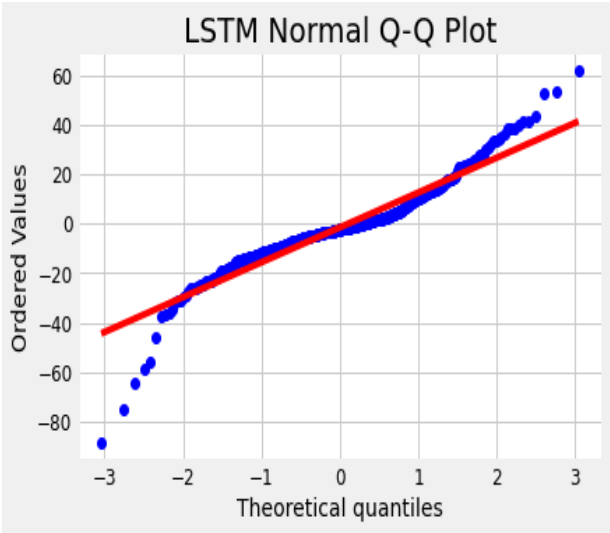

Figure 65. Q-Q plots for LSTM representation in 15 min.

Stacked LSTM model

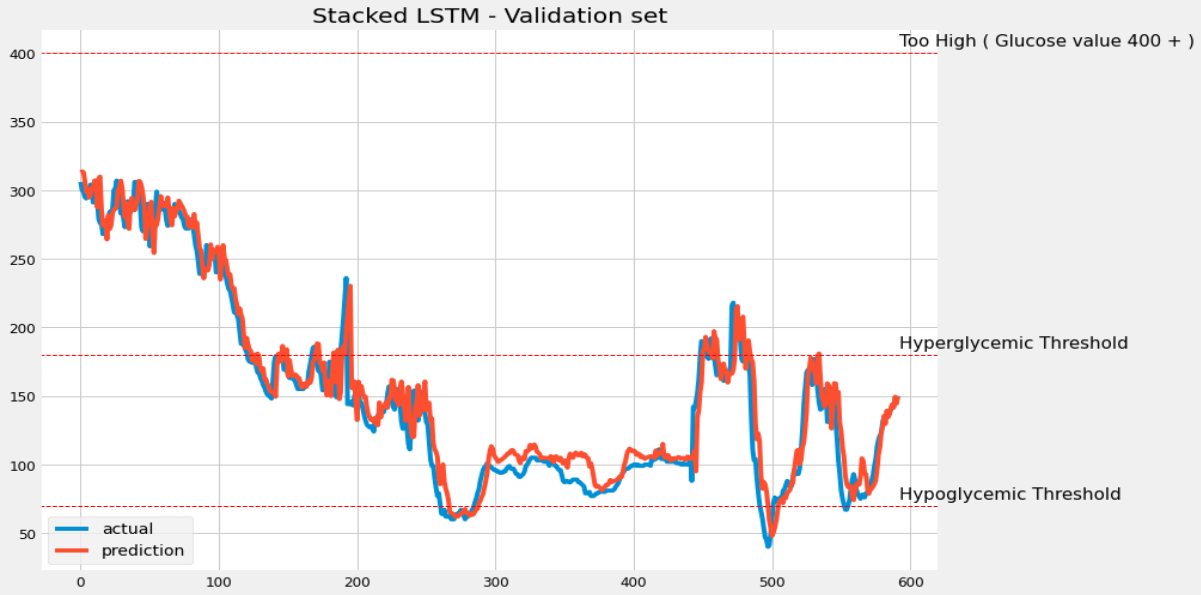

Figure 66. Stacked LSTM implementation with validation set for 15min.

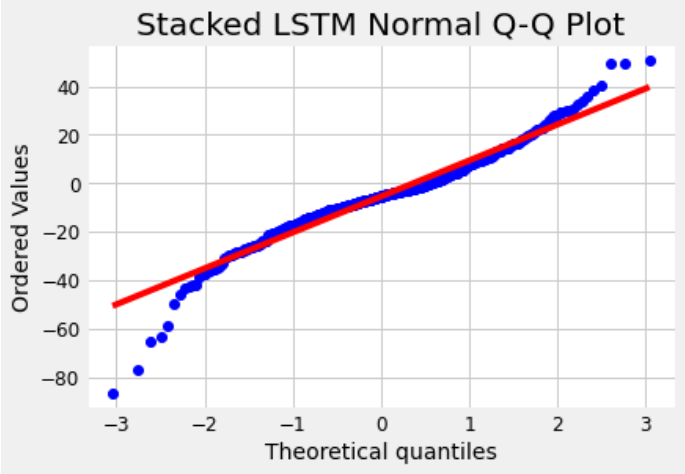

Figure 67. Q-Q plots for stacked LSTM representation in 15 min.

Bidirectional LSTM model

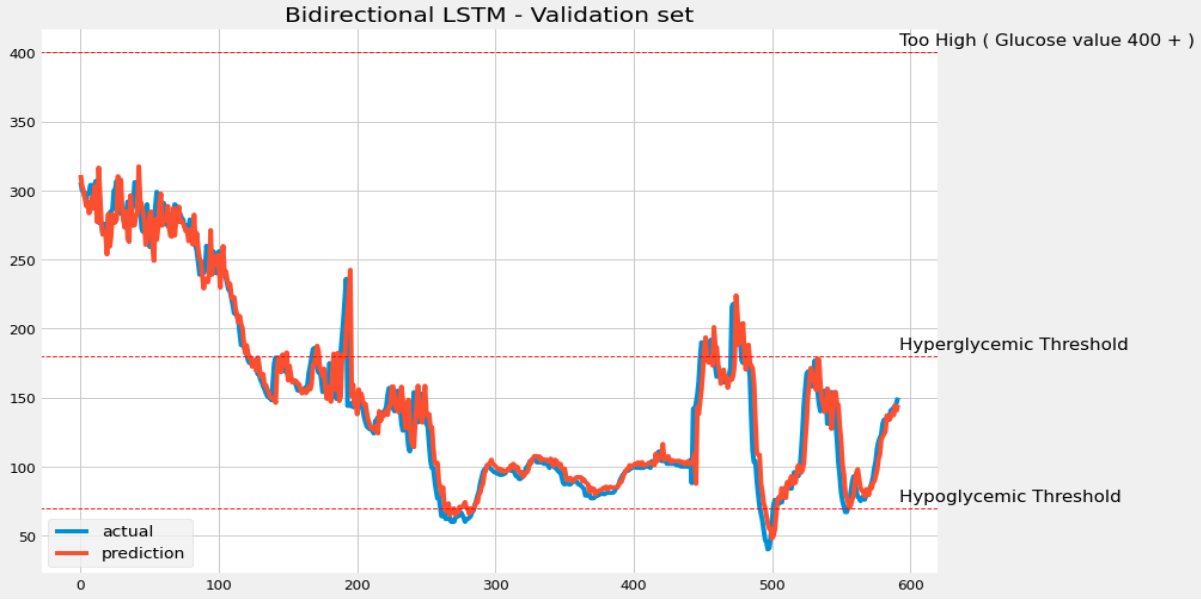

Figure 68. Bidirectional LSTM implementation with validation set for 15min.

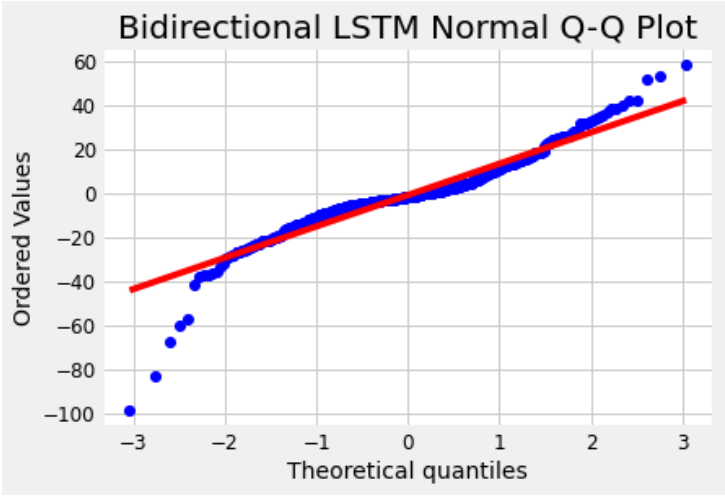

Figure 69. Q-Q plots for Bidirectional LSTM representation in 15 min.

Table 4. RMSE and MAE values for different models with 15 minute prediction horizons

Error metric	Vanilla RNN	LSTM	Stacked LSTM	Bi-LSTM
RMSE	14.74	14.80	16.08	14.93
MAE	9.63	10.03	11.77	9.86

B. 30 minutes

For the model performance shown below in Figures 70- 77, each model performed prediction based on the actual value learning. The validation-based test resulted in training to remove a residual error that was seen in the Q-Q plot with outliers seen at each iteration which could be removed using the normalization method. Better peaks were observed when compared with the actual value for the LSTM model which was also able to produce the lowest MAE and with deviation low as compared to other models.

Vanilla RNN

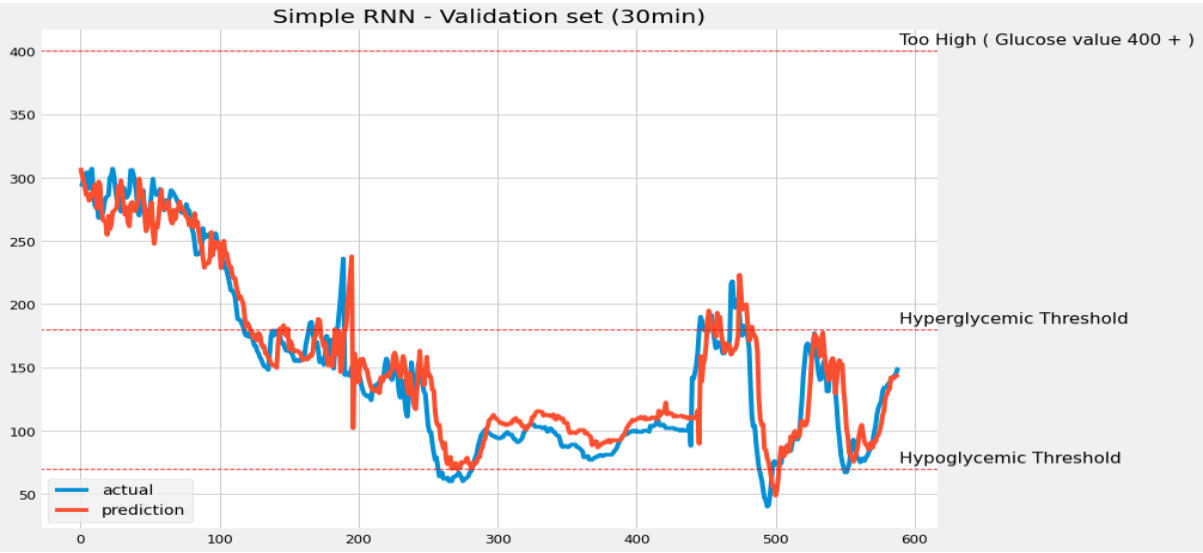

Figure 70. Vanilla RNN implementation with validation set for 30min.

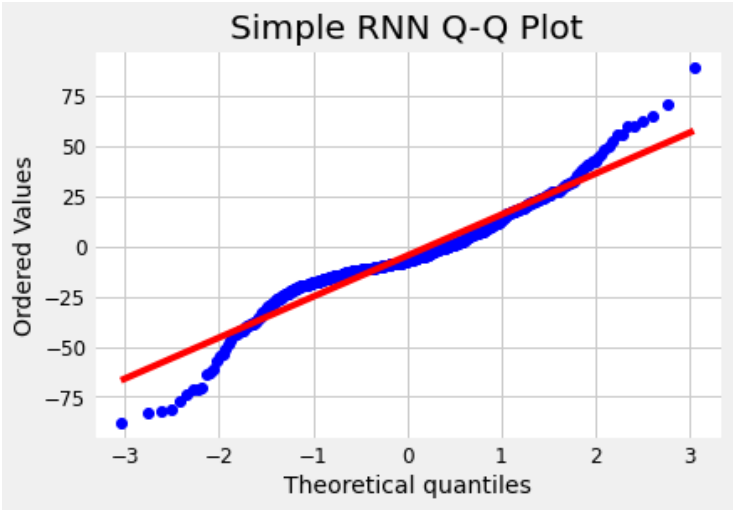

Figure 71. Q-Q plots for Vanilla RNN representation in 30 min.

LSTM model

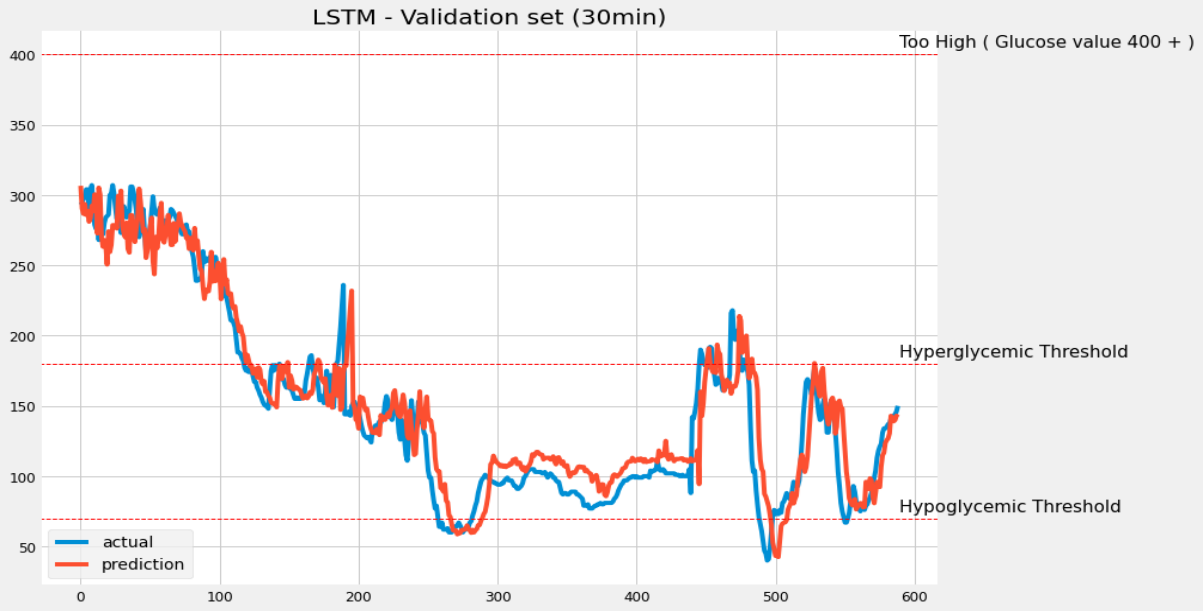

Figure 72. LSTM implementation with validation set for 30 min.

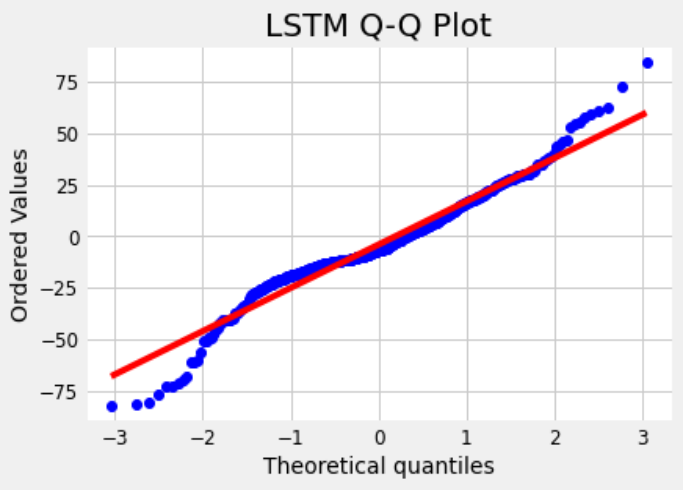

Figure 73. Q-Q plots for LSTM representation in 30 min.

Stacked LSTM model

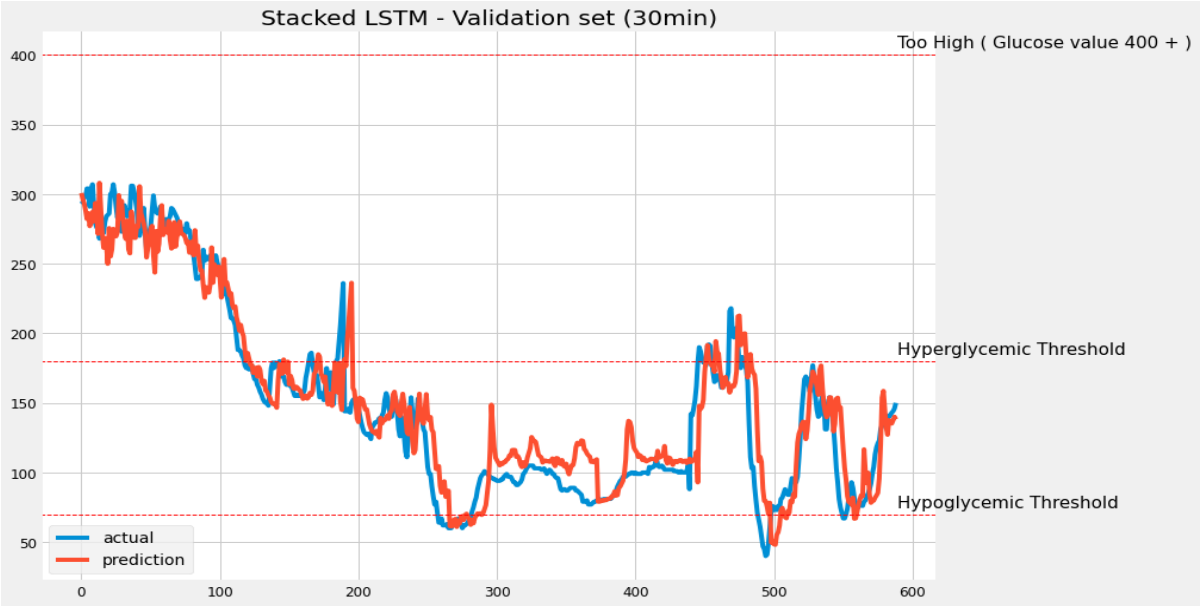

Figure 74. Stacked LSTM implementation with validation set for 30min.

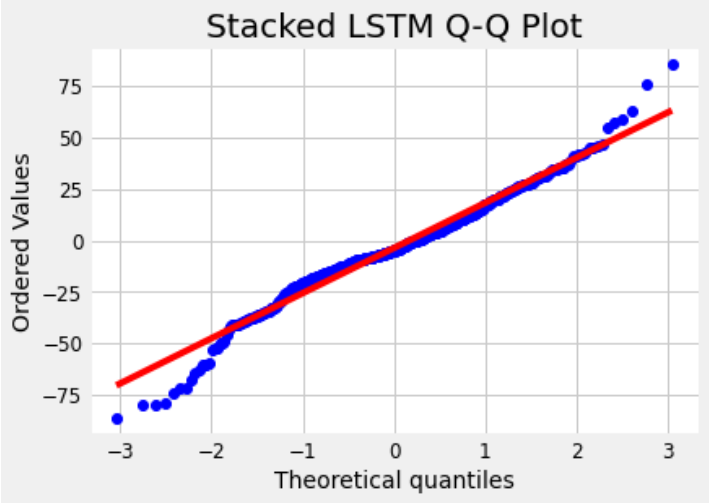

Figure 75. Q-Q plots for Stacked LSTM representation in 30min.

Bidirectional LSTM

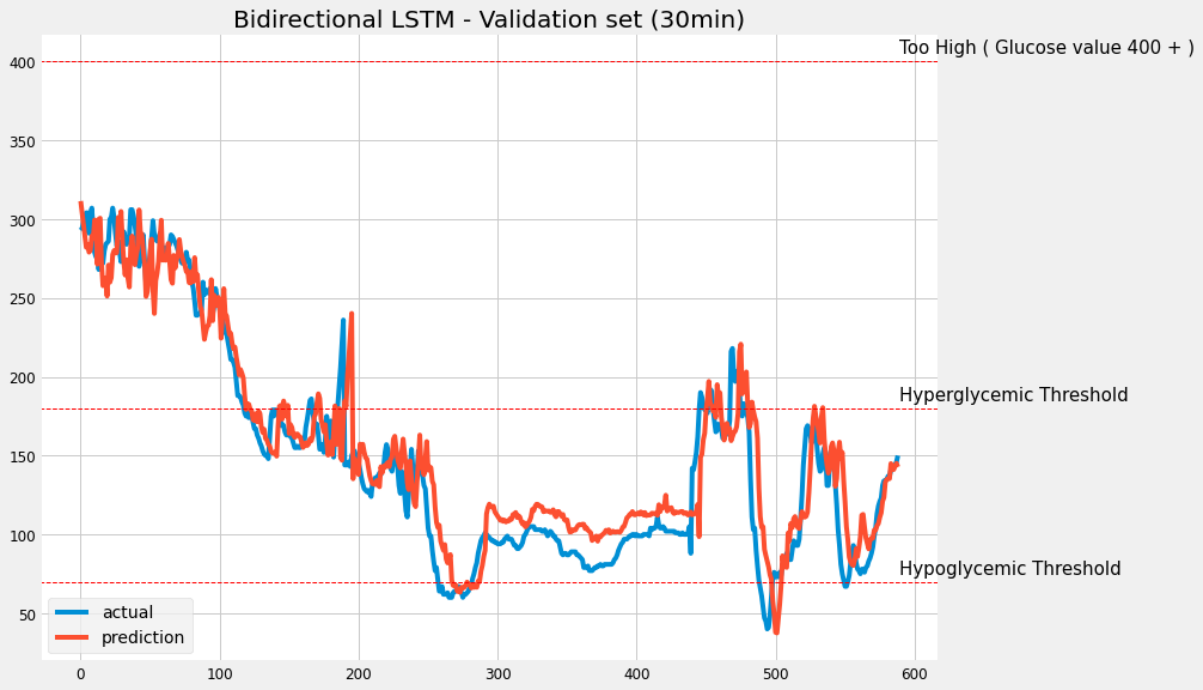

Figure 76. Bidirectional LSTM implementation with validation set for 30min.

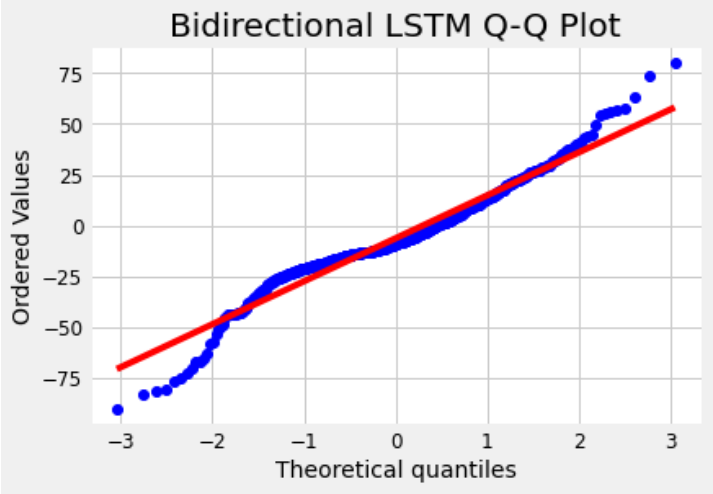

Figure 77. Q-Q plots for Bidirectional LSTM representation in 30 min.

Table 5. RMSE and MAE values for different models with 30-minute prediction horizons

Error metric	**Vanilla RNN**	**LSTM**	**Stacked LSTM**	**Bi-LSTM**
RMSE	22.57	21.74	22.49	22.51
MAE	16.66	16.35	16.69	17.15

C. 60 minutes

For the model performance shown below in Figures 78 – 85, each model deviated from the actual values. The validation-based test resulted in training to remove a residual error that was seen in the Q-Q plot with outliers seen at each iteration which could be removed using the normalization method. With better error metric based vanilla RNN was able to produce the lowest MAE and with deviation low as compared to other models.

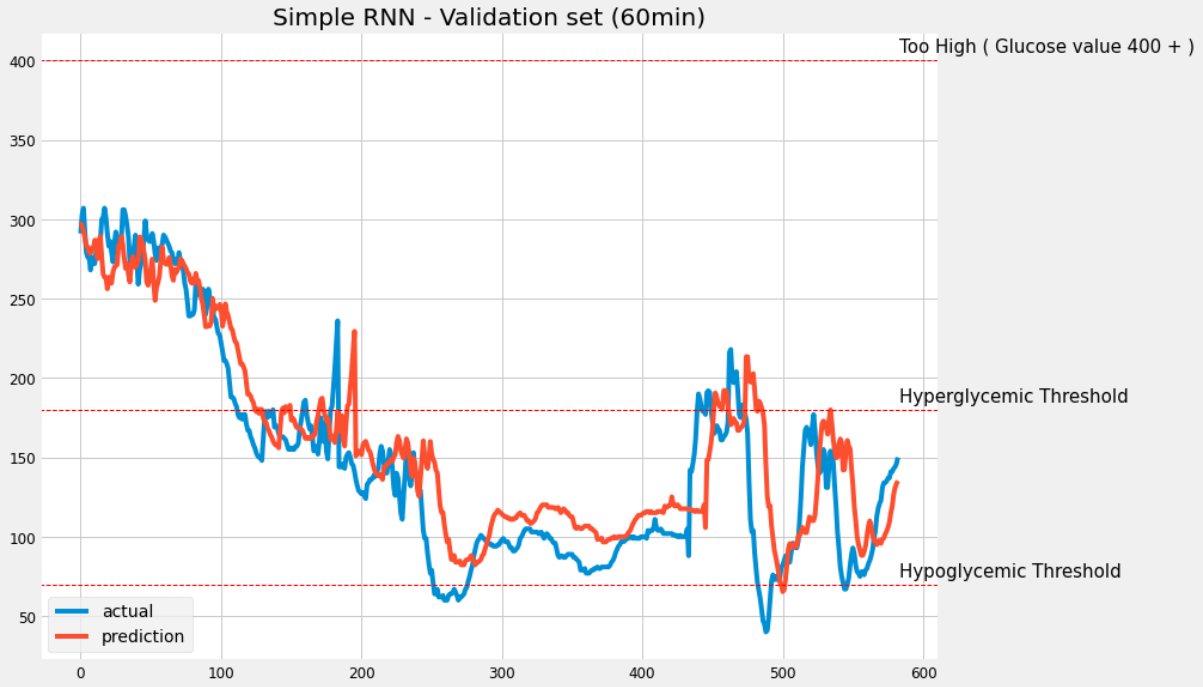

Figure 78. Vanilla RNN implementation with validation set for 60 min.

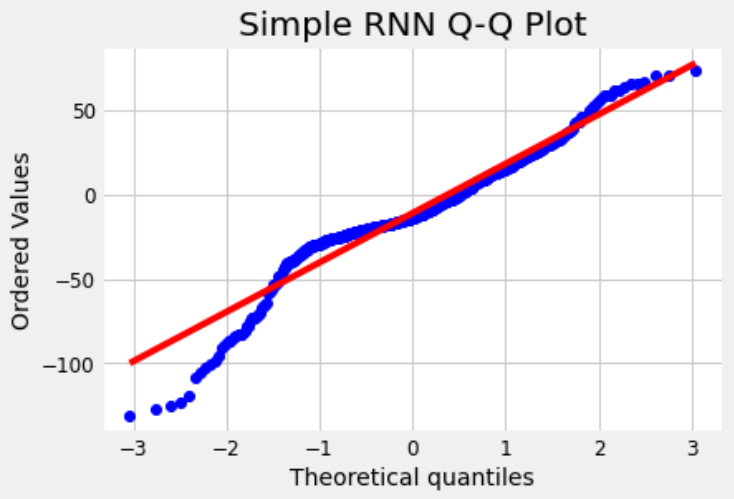

Figure 79. Q-Q plots for Vanilla RNN representation in 60 min.

LSTM model

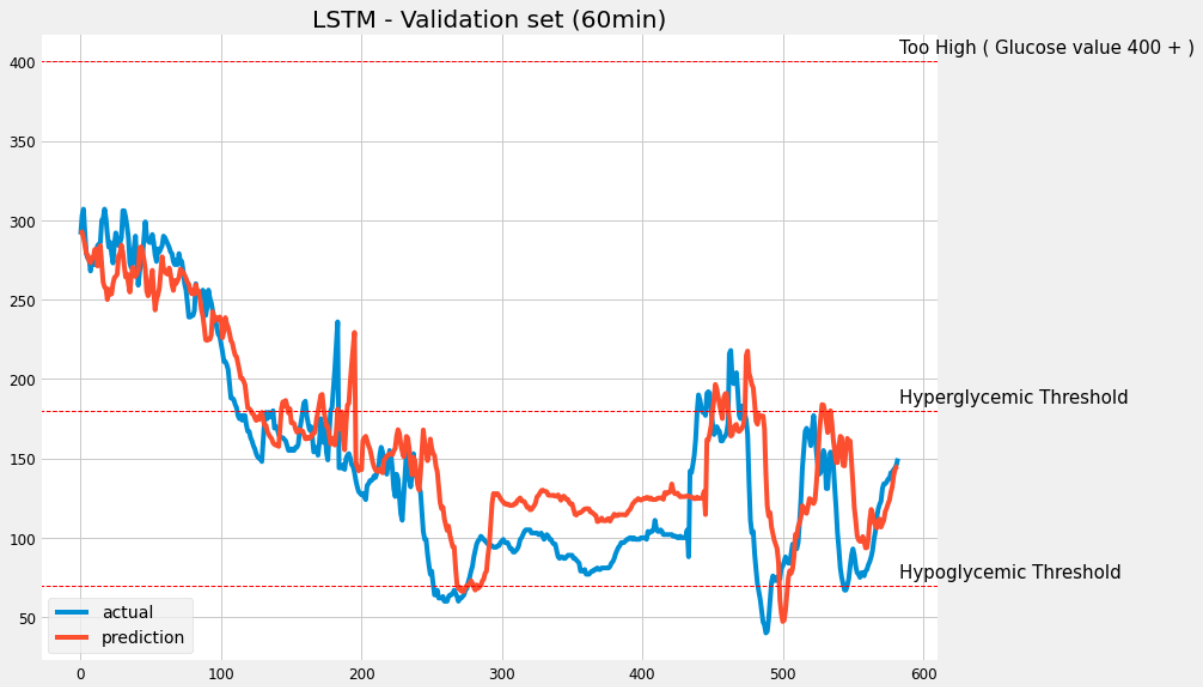

Figure 80. LSTM implementation with validation set for 60 min.

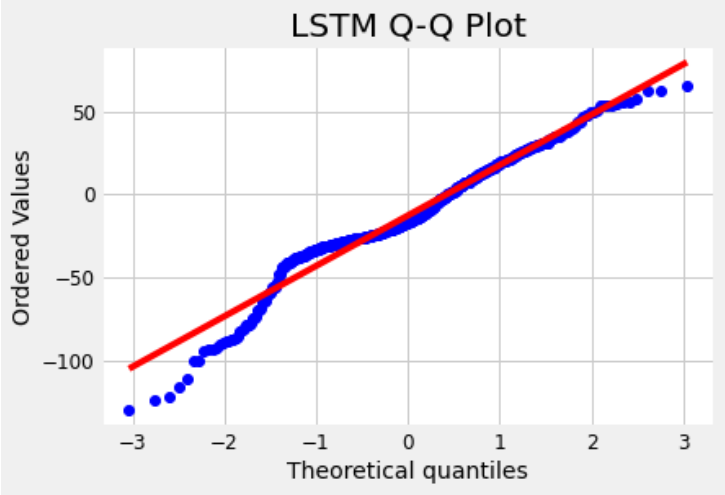

Figure 81. Q-Q plots for LSTM representation in 60 min.

Stacked LSTM

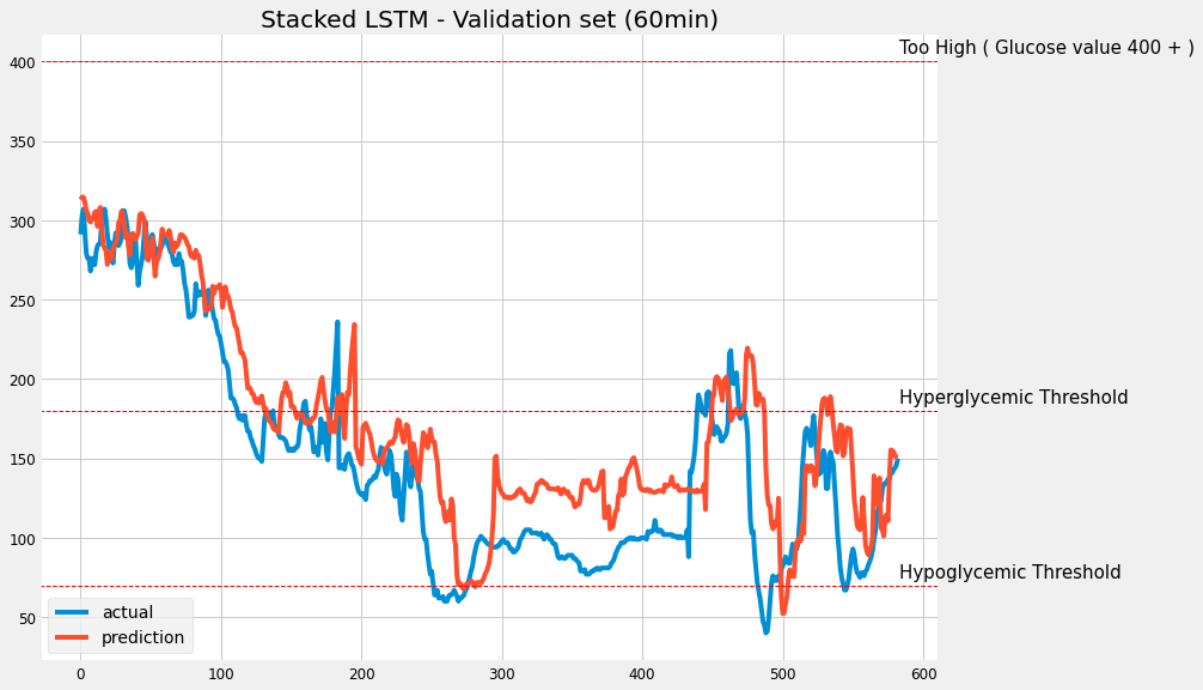

Figure 82. Stacked LSTM implementation with validation set for 60 min.

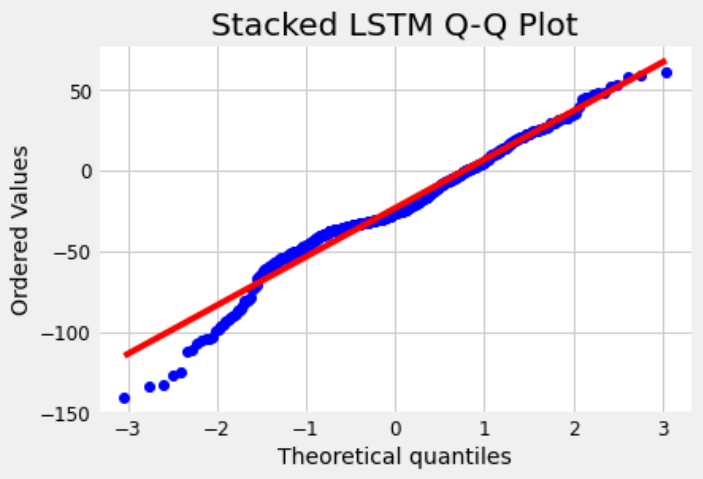

Figure 83. Q-Q plots for Stacked LSTM representation in 60 min

Bidirectional LSTM

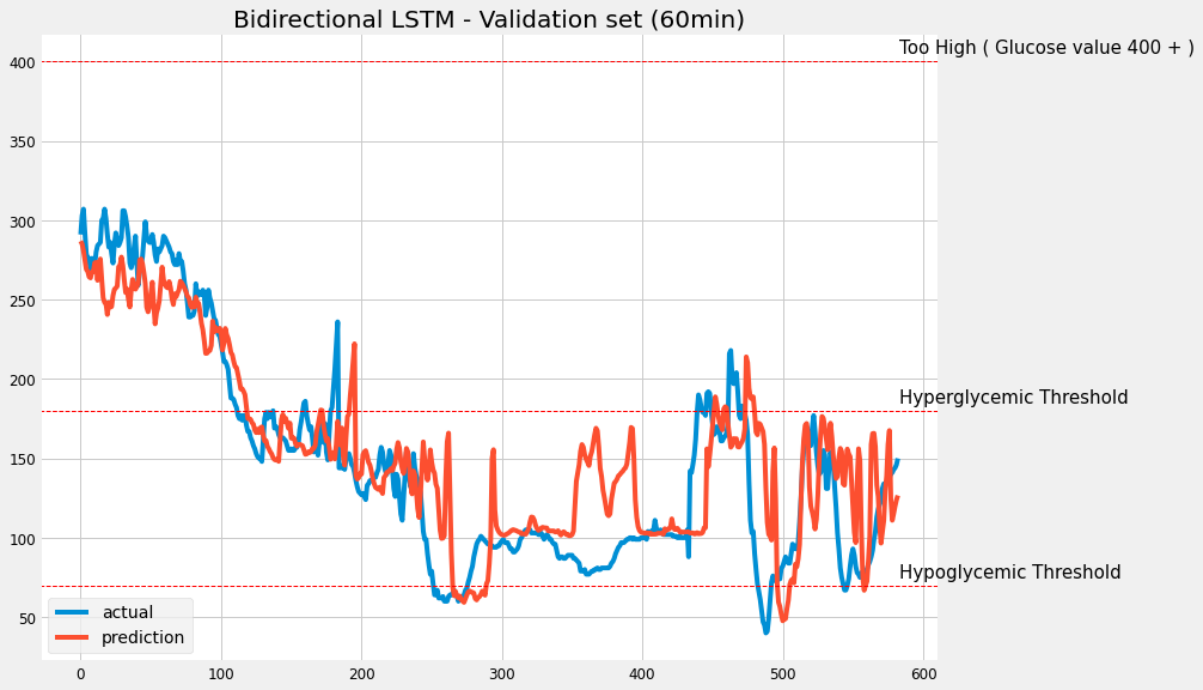

Figure 84. Bidirectional LSTM implementation with validation set for 60 min.

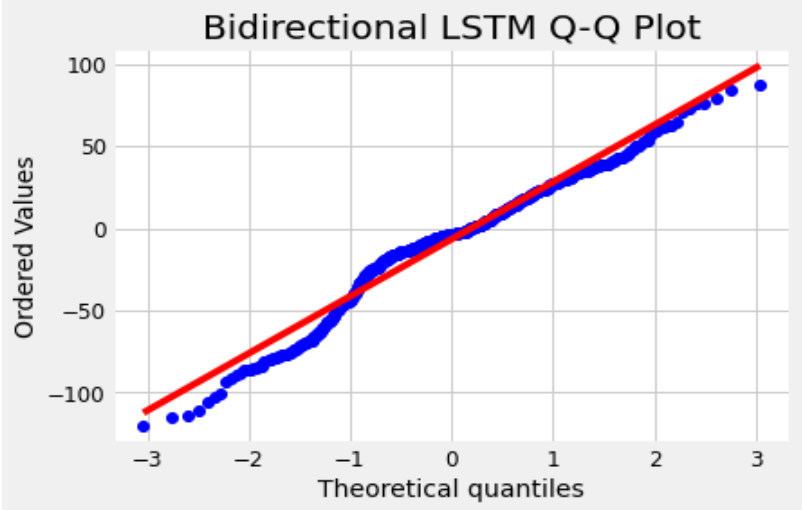

Figure 85. Q-Q plots for Bidirectional LSTM representation in 60 min.

Table 6. RMSE and MAE values for different models with 60minute prediction horizons

Error metric	Vanilla RNN	LSTM	Stacked LSTM	Bi-LSTM
RMSE	32.00	33.38	38.33	35.80
MAE	23.86	26.37	30.76	26.25

VITA

Saikat Banerjee
Norfolk, 23508

EDUCATION

Old Dominion University, Norfolk, VA — May 2022
Doctor of Philosophy in Electrical and Computer Engineering

University of Maryland, Baltimore County — August 2019
Master of Science in Computer Engineering

PUBLICATION

Peer-Reviewed Journals

- Banerjee, Saikat, and Gymama Slaughter. "Flexible Battery-less Wireless Glucose Monitoring System" Nature Scientific Reports. 2022 Submitted

- Banerjee, Saikat, and Gymama Slaughter. "A tattoo-like glucose abiotic biofuel cell." Journal of Electroanalytical Chemistry 904 (2022): 115941.

- Banerjee, Saikat, et al. "Electrochemical detection of neurotransmitters." Biosensors 10.8 (2020): 101.

Peer-Reviewed Conference Proceedings (appeared/ to appear)

- Banerjee, Saikat, Mathew Nguyen, and Gymama Slaughter. "Gold and silver oxide conducting nanocomposite cathode for glucose biofuel cell." 2021 IEEE Sensors. IEEE.

- Banerjee, Saikat, Md Faruk Hossain, and Gymama Slaughter. "A Highly Sensitive Non-Enzymatic Hydrogen Peroxide Sensor based on Palladium-Gold Nanoparticles." 2020 IEEE 15th International Conference on Nano/Micro Engineered and Molecular System (NEMS). IEEE 2020